Appendix to Final Report to

COMPOSITION VARIATION DURING FLOW OF GAS-CONDENSATE WELLS

Project Number 07122-29.FINAL

September 2011

Authors: Hai Xuan Vo and Roland N. Horne

PI: Roland N. Horne (horne@stanford.edu)
Department of Energy Resources Engineering
367 Panama Street
Stanford University, CA 94305-2220
(650)723-4744

LEGAL NOTICE

This report was prepared by Stanford University as an account of work sponsored by the Research Partnership to Secure Energy for America, RPSEA. Neither RPSEA members of RPSEA, the National Energy Technology Laboratory, the U.S. Department of Energy, nor any person acting on behalf of any of the entities:

a. MAKES ANY WARRANTY OR REPRESENTATION, EXPRESS OR IMPLIED WITH RESPECT TO ACCURACY, COMPLETENESS, OR USEFULNESS OF THE INFORMATION CONTAINED IN THIS DOCUMENT, OR THAT THE USE OF ANY INFORMATION, APPARATUS, METHOD, OR PROCESS DISCLOSED IN THIS DOCUMENT MAY NOT INFRINGE PRIVATELY OWNED RIGHTS, OR

b. ASSUMES ANY LIABILITY WITH RESPECT TO THE USE OF, OR FOR ANY AND ALL DAMAGES RESULTING FROM THE USE OF, ANY INFORMATION, APPARATUS, METHOD, OR PROCESS DISCLOSED IN THIS DOCUMENT.

THIS IS A FINAL REPORT. THE DATA, CALCULATIONS, INFORMATION, CONCLUSIONS, AND/OR RECOMMENDATIONS REPORTED HEREIN ARE THE PROPERTY OF THE U.S. DEPARTMENT OF ENERGY.

REFERENCE TO TRADE NAMES OR SPECIFIC COMMERCIAL PRODUCTS, COMMODITIES, OR SERVICES IN THIS REPORT DOES NOT REPRESENT OR CONSTIITUTE AND ENDORSEMENT, RECOMMENDATION, OR FAVORING BY RPSEA OR ITS CONTRACTORS OF THE SPECIFIC COMMERCIAL PRODUCT, COMMODITY, OR SERVICE.

Abstract

Gas-condensate wells experience a significant decrease in gas productivity once the flowing bottom-hole pressure drops below the dew-point pressure. However, there is still a lack of understanding how the condensate bank affects the deliverability because of the complex phase and flow behaviors. The difficulty of understanding the phase and flow behaviors lies in the variation of the composition due to the existence of two-phase flow and the relative permeability effect (each phase has different mobility). The change of composition will also bring about a large change in saturation and phase properties such as surface tension, viscosity, etc. of the fluids. These effects will impact mobilities and hence productivity.

The composition variation has been observed in the field but its effects have been studied only rarely in the literature. This work studied the impact of compositional variation on the flow behavior of the gas-condensate system through numerical simulations and a series of laboratory experiments. The study verified claims made about effect of flow through porous media on the apparent phase behavior of a gas-condensate mixture, namely compositional variation during depletion, saturation profile around the well, experience on shutting in the wells in an attempt to achieve condensate revaporization, and the effect of bottom-hole pressures on condensate banking. Finally, the work was extended to the case that we normally see in the field: gas-condensate reservoirs where immobile water is present.

Results from this study show that composition varies significantly during depletion. Due to the difference in mobilities caused by relative permeability, the composition of the mixture will change locally. The overall composition near the wellbore becomes richer in heavy components. As a result, the phase envelope will shift to the right. Near-well fluids can undergo a transition from retrograde gas to a volatile oil, passing through a critical composition in the process. The condensate bank can be reduced with proper producing sequence, hence the productivity of the well can be improved, for example by raising the bottomhole flowing pressure. The study also showed that the presence of immobile water did not have any significant effect on the compositional variation of the gas-condensate mixture, at least in the cases investigated.

The ultimate objective of the research was to gain a better understanding of how the condensate blocking affects the well productivity, with the focus on the effect of compositional variation on the flow behavior. This is important for optimizing the producing strategy for gas-condensate reservoirs, reducing the impact of condensate banking, and improving the ultimate gas and condensate recovery.

Acknowledgments

Thanks are extended to Dr. Louis Castanier and Dr. Kewen Li for their useful discussions and suggestions about modifying experimental apparatus and performing experiments, to Dr. Denis V. Voskov for his discussion about gas-condensate simulations.

We wish to thank Dr. Fevang and Professor C. Whitson for their useful discussion about modeling gas-condensate flow, Professor Hamdi Tchelepi for his discussion about three-phase relative permeability, Professor Kovscek for his discussion about Constant Composition Expansion, Constant Volume Depletion experiments of gas condensate.

Last but not least, the support from RPSEA is highly appreciated. Through monthly interaction with RPSEA, we have thought more deeply on the topic and understood it better. Above all, this work would not have been possible without the financial support of RPSEA under contract 07122-29.

Contents

Abstract iii

Acknowledgments v

Contents vii

List of Tables ix

List of Figures xi

1. Introduction 3

1.1. Overview 3
1.2. Scope of this Work 9
2. Physical Behaviors of Gas Condensate 11

2.1. Hydrocarbon Reservoir Fluids 11
2.1.1. Dry Gas 12
2.1.2. Wet Gas 13
2.1.3. Gas Condensate 13
2.1.4. Volatile Oil 14
2.1.5. Black Oil 14
2.2. Phase Behavior of Gas Condensate 15
2.2.1. Constant Composition Expansion (CCE) 16
2.2.2. Constant Volume Depletion (CVD) 17
2.3. Flow Behavior of Gas Condensate 18
2.3.1. Drawdown Behavior 18
2.3.2. Buildup Behavior 20
3. Experimental Investigation 23

3.1. Experimental Design 23
3.1.1. Difference between Static and Flowing Values 23
3.1.2. Synthetic Gas-Condensate Mixture 24
3.1.3. Numerical Simulation for Experiments 25
3.2. Experimental Apparatus 30
3.2.1. Gas Supply and Exhaust 32
3.2.2. Core Flooding System 32
3.2.3. Fluid Sampling System 33
3.2.4. Gas Chromatography (GC) 33
3.2.5. Computerized Tomography (CT) Scanner 37
3.3. Experimental Procedures 40
3.3.1. Gas Mixing 40
3.3.2. Absolute Permeability Measurement 45
3.3.3. Porosity Measurement 45

3.3.4. Gas-condensate Core Flooding Experiments 46
3.3.5. Gas-condensate, Immobile Water Core Flooding Experiments 48
3.3.6. Compositional Measurement 48
3.3.7. Saturation Measurement 48
4. Results and Discussions 51
4.1. Absolute Permeability Measurement 51
4.2. Porosity Measurement 51
4.3. Composition 51
4.3.1. Gas-Condensate Core Flooding Experiments 51
4.3.2. Gas-Condensate-immobile Water Core Flooding Experiments 58
4.4. Saturation 60
5. Theoretical Modeling of Compositional Variation 64
6. Optimization of Gas-Condensate Reservoir 77
6.1. Production Enhancement of Gas-Condensate Reservoir Using Production Strategies 77
6.1.1. Binary System 77
6.1.2. Multicomponent System 82
6.2. Production Enhancement of Gas-Condensate Reservoir Using Hydraulic Fracturing and Gas Injection 94
6.2.1. Hydraulic Fracturing 94
6.2.2. Gas Cycling 95
6.2.3. Different Injection Gases 97
6.3. Optimization of Gas-Condensate Reservoirs 98
7. Conclusion 103
7.1. General Conclusions 103
7.2. Suggestions for Future Work 103
Nomenclature 105
References 107
A. Gas-condensate Simulation Input File for Experiments 111
B. Gas-condensate with Immobile Water Simulation Input File for Experiments.. 119
C. Simulation Input File for Binary Gas-Condensate System at Field Scale 127
D. Simulation Input File for Multicomponent Gas-Condensate System at Field Scale 135
E. Simulation Input File for Multicomponent Hydraulically Fractured Gas-Condensate Reservoir 145
F. Simulation Input File for Multicomponent Gas-Condensate Reservoirs with Gas Cycling 157
G. Simulation Input File for Multicomponent Gas-Condensate Reservoirs with Injection Gas 167
H. Optimization of Condensate Reservoirs with Gas Injection 177

List of Tables

Table 2-1: Typical molar compositions of petroleum fluids (from Pedersen et al., 1989). 11

Table 2-2: Summary of guidelines for determining fluid type from field data (from McCain, 1994). 15

Table 3-1: Agilent 3000 Micro GC parameter setting 36

Table 3-2: GE HiSpeed CT/i scanner settings. 39

Table 3-3: Scanning positions..... 49

List of Figures

Figure 1-1: Phase diagram of a typical gas condensate with line of isothermal reduction of reservoir pressure..... 3
Figure 1-2: Illustration of pressure profile and liquid dropout in the near wellbore region. 4
Figure 1-3: An example of very poor performance of a gas-condensate well (from Barnum et al., 1995)..... 5
Figure 1-4: Shift of phase envelope with compositional change on depletion (from Roussennac, 2001). 7
Figure 1-5: Compositional variation from two wells in Kekeya gas field (from Shi, 2009). 7
Figure 1-6: Surface tension variation (from McCain and El-Banbi, 2000). 8
Figure 1-7: Gas viscosity variation (from El-Banbi and McCain, 2000). 8
Figure 2-1: Phase diagram for reservoir fluids. 12
Figure 2-2: Phase diagram of dry gas. 12
Figure 2-3: Phase diagram with line of isothermal reduction of reservoir pressure of wet gas. 13
Figure 2-4: Phase diagram with line of isothermal reduction of reservoir pressure of gas condensate..... 13
Figure 2-5: Phase diagram with line of isothermal reduction of reservoir pressure of volatile oil. 14
Figure 2-6: Phase diagram with line of isothermal reduction of reservoir pressure of black oil. 14
Figure 2-7: Phase diagram with isovolume line of gas condensate..... 15
Figure 2-8: Liquid dropout behavior of gas condensate. 16
Figure 2-9: Schematic of *CCE* experiment..... 17
Figure 2-10: Schematic of *CVD* experiment..... 18

Figure 2-11: Three regions of flow behavior in a well condensate well (from Fevang and Whitson, 1996). 19
Figure 2-12: Evolution of fluid compositions in the innermost grid block for a lean gas condensate at dew-point pressure (from Novosad, 1996)..... 21
Figure 3-1: Difference between static and flowing values. 23
Figure 3-2: Phase diagram of the synthetic gas-condensate mixture used for experiments (85% C_1 and 15% nC_4 in mole fraction). 24
Figure 3-3: Condensate dropout of the synthetic gas-condensate mixture used for experiments (85% C_1 and 15% nC_4 in mole fraction) at 70 °*F* from the simulation of *CCE* and *CVD* tests..... 25
Figure 3-4: Core used for experiments. 26
Figure 3-5: Gridding for numerical simulation of the core. 26
Figure 3-6: Two-phase (gas–condensate) simulation: (a) Condensate saturation profile. (b) nC_4 mole fraction in the liquid phase. (c) nC_4 mole fraction in the vapor phase. 27
Figure 3-7: Numerical simulation of *nC4* composition history with different *BHP* control cases (from Shi, 2009). 28
Figure 3-8: Three-phase simulation result with $S_{wi} = 0$: (a) Condensate saturation profile. (b) nC_4 mole fraction in the liquid phase. (c) nC_4 mole fraction in the vapor phase. 29
Figure 3-9: Three- phase simulation result with $S_{wi} = 0.16$: (a) Condensate saturation profile. (b) nC_4 mole fraction in the liquid phase. (c) nC_4 mole fraction in the vapor phase 30
Figure 3-10: Original experiment apparatus (from Shi, 2009). 31
Figure 3-11: Modified experiment apparatus to minimize sample tube volume. 32
Figure 3-12: Principle of Gas Chromatography (from Perry, 1981) 34
Figure 3-13: Agilent 3000 Micro *GC*. 35
Figure 3-14: *GC* calibration (from Agilent Cerity Tutorial)..... 36
Figure 3-15: A typical gas chromatogram of gas samples taken during experiments. 37
Figure 3-16: Principle of *CT* scanner (from Vinegar and Wellington, 1987)..... 38
Figure 3-17: GE HiSpeed *CT*/i. 39

Figure 3-18: Vapor pressure of n-butane (from Kay, 1940). 41
Figure 3-19: Schematics of gas-condensate mixing (modified from Shi, 2009). 43
Figure 3-20: Gas-condensate mixing. 44
Figure 3-21: Performing experiments in the *CT* scanning room. 49
Figure 3-22: Core holder set up for *CT* scanning. 49
Figure 4-1: Absolute permeability measurement using nitrogen..... 51
Figure 4-2: Gas-condensate noncapture experiment 1: nC_4 in the flowing mixture. 52
Figure 4-3: Gas-condensate noncapture experiment 2: nC_4 in the flowing mixture. 53
Figure 4-4: Gas-condensate noncapture experiment 3: nC_4 in the flowing mixture. 53
Figure 4-5: Gas-condensate noncapture experiment: nC_4 in the flowing mixture with different BHP control cases. 54
Figure 4-6: Condensate revaporization after noncapture experiment for gas-condensate system 1. 55
Figure 4-7: Condensate revaporization after noncapture experiment for gas-condensate system 2. 55
Figure 4-8: Condensate revaporization after noncapture experiment for gas-condensate system 3. 56
Figure 4-9: Gas-condensate capture experiment 1. 56
Figure 4-10: Gas-condensate capture experiment 2. 57
Figure 4-11: Gas-condensate capture experiment 3. 57
Figure 4-12: Gas-condensate-immobile water noncapture experiment 1: nC_4 in the flowing mixture. 58
Figure 4-13: Gas-condensate-immobile water noncapture experiment 2: nC_4 in the flowing mixture. 59
Figure 4-14: Gas-condensate-immobile water capture experiment 1. 60
Figure 4-15: Gas-condensate-immobile water capture experiment 2. 60
Figure 4-16: Gas-condensate noncapture experiment 3: (a) nC_4 in the flowing phases. (b) condensate saturation profile. 61
Figure 4-17: *CT* scanning of the empty titanium core holder: (a) with air inside. (n) with a water bottle inside. 62

Figure 4-18: *CT* scanning of an aluminum tube: (a) with air inside. (b) with a water bottle inside. 63
Figure 5-1: Phase diagram of the C_1- nC_4 systems. 65
Figure 5-2: *CCE* liquid dropout of the C_1- nC_4 systems. 66
Figure 5-3: Component mole fractions of 85%-15% C_1- nC_4 mixture at 70°F. 66
Figure 5-4: Phase molar density of 85%-15% C_1- nC_4 mixture at 70°F. 67
Figure 5-5: Phase viscosity of 85%-15% C_1- nC_4 mixture at 70°F. 67
Figure 5-6: *IFT* versus pressure. 69
Figure 5-7: Different relative permeability models. 69
Figure 5-8: m_{c4}/m *vs.* p for z_{C4} = 0.15 with different relative permeability models. 70
Figure 5-9: m_{c4}/m *vs.* p for z_{C4} = 0.20 with different relative permeability models. 71
Figure 5-10: m_{c4}/m *vs.* p for z_{C4} = 0.25 with different relative permeability models. 71
Figure 5-11: G *vs.* p for z_{C4} = 0.15. 72
Figure 5-12: G *vs.* p for z_{C4} = 0.20. 72
Figure 5-13: G *vs.* p for z_{C4} = 0.25. 73
Figure 5-14: A_{C4} *vs.* p for z_{C4} = 0.15 with different relative permeability models. 73
Figure 5-15: A_{C4} *vs.* p for z_{C4} = 0.20 with different relative permeability models. 74
Figure 5-16: A_{C4} *vs.* p for z_{C4} = 0.25 with different relative permeability models. 74
Figure 5-17: B_{C4} *vs.* p for z_{C4} = 0.15 with different relative permeability models. 75
Figure 5-18: B_{C4} *vs.* p for z_{C4} = 0.20 with different relative permeability models. 75
Figure 5-19: B_{C4} *vs.* p for z_{C4} = 0.25 with different relative permeability models. 76
Figure 6-1: Well bottom-hole pressure history with different minimum bottom-hole pressure. 77
Figure 6-2: Gas production rate history. 78
Figure 6-3: Accumulated gas production history. 78
Figure 6-4: Overall nC_4 mole fraction produced versus well bottom-hole pressure. 79
Figure 6-5: History of nC_4 mole fraction in the liquid phase in the well block 79
Figure 6-6: History of overall nC_4 mole fraction produced. 80
Figure 6-7: Gas production rate history. 80
Figure 6-8: Accumulated gas production history. 81

Figure 6-9: History of nC_4 mole fraction in the liquid phase in the well block with different bottom-hole pressure settings. 81
Figure 6-10: History of overall nC_4 mole fraction produced. 82
Figure 6-11: Reservoir model. 83
Figure 6-12: Phase diagram of the gas-condensate reservoir fluid. 83
Figure 6-13: Condensate production rate with different bottom-hole pressures for the case with capillary pressure. 84
Figure 6-14: Gas production rate with different bottom-hole pressures for the case with capillary pressure. 84
Figure 6-15: Condensate production rate with different bottom-hole pressures for the case without capillary pressure. 85
Figure 6-16: Gas production rate with different bottom-hole pressures for the case without capillary pressure. 85
Figure 6-17: Condensate production rate with different bottom-hole pressures for one-layer model. 86
Figure 6-18: Gas production rate with different bottom-hole pressures for one-layer model. 87
Figure 6-19: Condensate saturation (BSOIL) and C_{7+} mole fractions (liquid BXMF9, and gas BYMF9) versus time at the well block with 500 psi bottom-hole pressure. 88
Figure 6-20: Spatial distribution of condensate saturation with 500 psi bottom-hole pressure. 88
Figure 6-21: Spatial distribution of C_{7+} mole fraction in liquid with 500 psi bottom-hole pressure. 89
Figure 6-22: Condensate saturation with different bottom-hole pressures at 1600 days. 89
Figure 6-23: of C_{7+} mole fraction in liquid with different bottom-hole pressures at 1600 days. 90
Figure 6-24: Condensate production rate WOPR with different bottom-hole pressures for a tight reservoir. 90
Figure 6-25: Gas production rate WGPR with different bottom-hole pressures for a tight reservoir. 91

Figure 6-26: Saturation (BSOIL) and C_{7+} mole fractions (liquid BXMF9 and gas BYMF9) versus time at the well block with 500 psi bottom-hole pressure for a tight reservoir. 91
Figure 6-27: Spatial distribution of condensate saturation with 500 psi bottom-hole pressure for a tight reservoir. 92
Figure 6-28: Spatial distribution of C_{7+} mole fraction (BXMF9) with 500 psi bottom-hole pressure for a tight reservoir. 92
Figure 6-29: Condensate saturation with different bottom-hole pressures at 1600 days for a tight reservoir. 93
Figure 6-30: C_{7+} mole fraction (BXMF9) with different bottom-hole pressures at 1600 days for a tight reservoir. 93
Figure 6-31: Effect of fracture on condensate production rate (WOPR). 94
Figure 6-32: Effect of fracture on gas production rate (WGPR). 95
Figure 6-33: Effect of fracture on condensate saturation profile. 95
Figure 6-34: Condensate field production rate (FOPR) with different lean gas injection rates. 96
Figure 6-35: Condensate field production total (FOPT) with different lean gas injection rates. 96
Figure 6-36: Condensate saturation in the production well block with different lean gas injection rates. 97
Figure 6-37: Condensate field production rate (FOPR) with different injection gases. ... 97
Figure 6-38: Condensate field production total (FOPT) with different injection gases. .. 98
Figure 6-39: Condensate saturation in the production well block with different injection gases. 98
Figure 6-40: Optimization of a gas-condensate reservoir. 99
Figure 6-41: Cumulative condensate production of the optimization problem. 100
Figure 6-42: Cumulative gas production of the optimization problem. 100
Figure 6-43: Cumulative gas injection of the optimization problem. 101
Figure 6-44: Condensate production rate of the optimization problem. 101
Figure 6-45: Gas injection rate of the optimization problem. 102

Executive Summary

One of the most significant and unique factors associated with tight gas reservoirs is their low productivity, which is especially exacerbated in the case of gas-condensate fluids. Gas-condensates fluids exhibit complex phase and flow behaviors due to the appearance of condensate banking in the near-well region, and differ essentially in their behavior from conventional gas reservoirs, especially for low permeability high yield condensate systems, which have more severe condensate banking problems. A good understanding of how the condensate accumulation influences the productivity and the composition configuration in the liquid phase is very important to optimize the producing strategy for tight gas sands, to reduce the impact of condensate banking, and to improve the ultimate gas recovery.

This study addressed several issues related to the behavior of the composition variation, condensate saturation build-up and condensate recovery during the gas-condensate producing process in tight gas reservoirs. A key factor that controls the gas-condensate well deliverability is the relative permeability, which is influenced directly by the condensate accumulation. The accumulated condensate bank not only reduces both the gas and liquid relative permeability, but also changes the phase composition of the reservoir fluid, hence reshapes the phase diagram of reservoir fluid and varies the fluid properties. The study found that different producing strategies impact the composition configuration for both flowing and static phases and the amount of the liquid trapped in the reservoir, which in turn influence the well productivity and hence the ultimate gas and liquid recovery from the reservoir. Changing the manner in which the well is brought into flowing condition was found to affect the liquid dropout composition and can therefore change the degree of productivity loss.

Experiments using a binary synthetic mixture at laboratory scale were conducted to measure the compositional variation and to test the contributing factors for composition variation and condensate banking effect. Full compositional simulations of binary-component and multicomponent gas-condensate fluids were conducted at field scale to investigate the composition and condensate saturation variations. Different producing strategies were tested to find out the optimum producing sequences for maximum gas recovery. By taking account of the new understanding of the impact of compositional changes, the composition of the liquid dropout can be "controlled" by the production strategy (for example by dropping a lighter liquid in preference to a heavier one) and hence the recovery from tight gas reservoirs with condensate fluids can be improved.

As a primary result, it was determined that increasing the bottomhole flowing pressure of wells producing gas-condensate fluids can (depending on the composition) result in a more valuable flow stream (in terms of net present value, NPV). One important consequence of the composition variation examined in this work is that the reservoir fluid progressively changes from a gas condensate to a volatile oil because the heavier components are left in the formation due to relative permeability effects. This means that

producing companies are not able to revaporize the condensate by repressurizing the wells.

Another way for producing companies to improve the productivity by adjusting the compositional behavior of the reservoir fluid is to inject lean gas, for example by partial gas recycling.

Chapter 1

1. Introduction

1.1. Overview

Gas-condensate reservoirs are encountered more frequently as exploration is now targeted at greater depth and hence higher pressure and temperature. The high temperature and pressure lead to a higher degree of degradation of complex organic molecules. As a result, the deeper the burial of an organic material, the higher tendency the organic material will be converted to gas or gas condensate. The gas condensate usually consists mainly of methane and other light hydrocarbons with a small portion of heavier components.

Gas condensate has a phase diagram as in Figure 1-1. In this case, the reservoir temperature lies between the critical temperature and the cricondentherm, the maximum temperature at which two phases can coexist in equilibrium. Initially, the reservoir pressure is at a point that is above the dew-point curve so the reservoir is in the gaseous state only. During production, the pressure declines isothermally from the reservoir boundary to the well. If the well flowing bottom-hole pressure (*BHP*) drops below the dew-point pressure (p_d), the condensate drops out of the gas and forms a bank of liquid around the well (Figure 1-2). The gas condensate is special in the sense that when the pressure decreases isothermally, instead of having gas evolution from liquid, we have liquid condensation from the gas. Hence, sometimes, gas condensate is also called "retrograde gas".

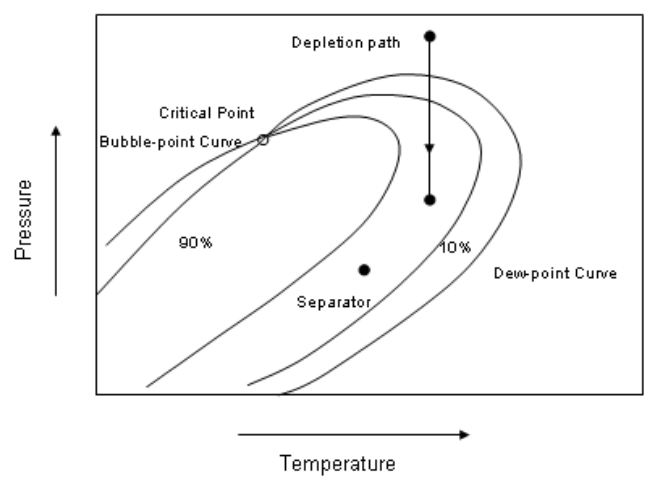

Figure 1-1: Phase diagram of a typical gas condensate with line of isothermal reduction of reservoir pressure.

When the condensate drops out in the reservoir, at first, due to relative permeability behavior, the condensate liquid will not flow until the accumulated condensate saturation exceeds the critical condensate saturation. This leads to a loss of valuable hydrocarbons because the condensate contains most of the heavy components. Besides that, near the wellbore where the condensate bank appears, there will be a multiphase flow so the gas relative permeability is reduced. The reduction of gas permeability due to the condensate bank is called condensate blocking. The condensate blocking effect leads to a reduction of gas productivity of the well.

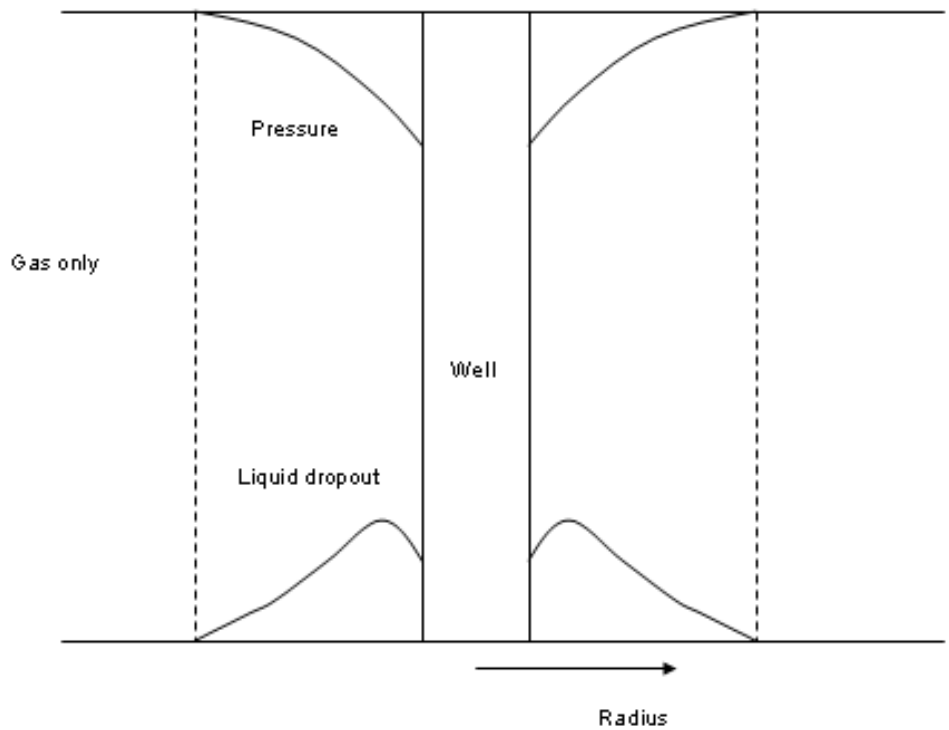

Figure 1-2: Illustration of pressure profile and liquid dropout in the near wellbore region.

The productivity loss due to condensate build up is large in some cases, especially in tight reservoirs. Afidick et al. (1994) reported that liquid accumulation had occurred around the wellbore in the Arun field and that it had reduced individual well productivity by 50% even though the retrograde-liquid condensation in laboratory *PVT* experiments was less than 2%. Barnum at al. (1995) conducted a study using data from 17 fields and concluded that the condensation of hydrocarbon liquids in gas-condensate reservoirs can restrict gas productivity severely. However, gas recovery factors below 50% are limited to reservoirs with a permeability-thickness less than 1,000 md-ft. For more permeable reservoirs, the productivity loss is not as severe. Barnum at al. (1995) also presented one example of poor well performance (Figure 1-3). This is a moderately rich gas-condensate field with an initial condensate-gas ratio of 73 bbl/Mscf. The well produced at initial rates over 1 Mscf/day. When the flowing bottom-hole pressure reached the dew-point, gas production declined rapidly and the well died. Pressure surveys indicated that the well was full of liquid hydrocarbons. Attempts to swab the well were unsuccessful, even though data from surrounding wells indicated the average reservoir pressure was still

over 2,000 psi above the dew-point pressure. The well appeared to have "locked up" and ceased production shortly after flowing bottom-hole pressure fell below the dew-point pressure. Eventually the well was stimulated successfully by hydraulic fracturing, and it returned to the initial production rates.

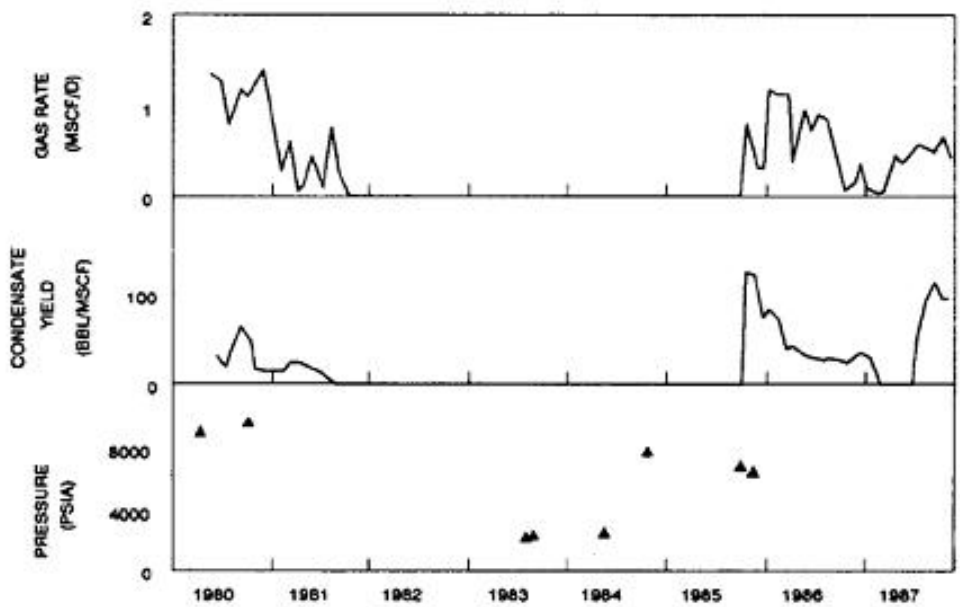

Figure 1-3: An example of very poor performance of a gas-condensate well (from Barnum et al., 1995).

When the entire reservoir pressure drops below the dew point, the condensation will occur throughout the whole reservoir. If the condensate saturation exceeds the critical condensate saturation, both gas and condensate will flow. In the case when the condensate saturation is below the critical condensate saturation, the gas flowing into the well will become leaner and the liquid in the condensate ring will become heavier in composition. According to El-Banbi and McCain (2000), lightening the produced gas can increase the gas effective permeability hence the gas productivity of the well (however the liquid productivity decreases). The productivity above the dew-point pressure is controlled by the permeability-thickness and the viscosity of the gas whereas the productivity below the dew-point pressure is determined by the critical condensate saturation and the shape of the relative permeability curves.

Understanding how the condensate bank affects the deliverability is important to improve the productivity of gas-condensate reservoirs.

The study of productivity loss in gas-condensate well started back in the 1930s but due to the complex compositional variation, phase and flow behaviors, it is still an outstanding problem.

The problem of condensate banking was addressed early on by Muskat (1949) in his discussion of gas cycling. Muskat (1949) estimated the radius of the condensate blockage

as a function of time, gas rate, rock and fluid properties. Kniazeff and Naville (1965), and Eilerts et al. (1965) independently developed numerical models to estimate the saturation and pressure in the vicinity of the wellbore. Later, O'Dell and Miller (1967) presented a method for calculating the volume of retrograde liquid around the producing wellbore and its effect on the producing rate based on the steady-state flow concept. Roebuck et al. (1968a), and Roebuck et al. (1968b) developed the first models for individual components and considered the component mass transfer between phases. Fussell (1973) used a modified version of the models developed by Roebuck et al. and concluded that the productivity of the well could be reduced due to condensate accumulation by a factor of three compared to that predicted by the method of O'Dell and Miller (1967). Jones et al. (1985), and Jones et al. (1986) analyzed the pressure transient response of the gas-condensate system. Fevang and Whitson (1996) addressed the physics of the condensate banking and came up with the three flow region theory. According to this theory, a gas-condensate reservoir with an initial pressure above the dew-point pressure is divided into three flow regions. In the outer region (region 3) the pressure is above the dew-point pressure, and only gas exists. In an intermediate region (region 2) the pressure is below the dew-point pressure but the condensate saturation is still below the critical saturation, so only gas flows in this region. Region 2 is the region of net accumulation of the gas condensate. Finally there is an inner region (region 1) where the pressure is decreased further, hence the condensate saturation exceeds the critical condensate saturation, and both condensate and gas flow in this region.

The difficulty of understanding the phase and flow behaviors lies in the variation of the composition. Zhang and Wheaton (2000) showed in their theoretical model that composition varies with time around the well. Numerical simulation (Roussennac, 2001) also shows that during depletion, if the reservoir pressure drops below the dew point, the liquid will condense in the reservoir. Due to the difference in mobilities of the gas and condensate phase and the relative permeability effects, the composition of the liquid will change locally. The overall composition near the wellbore becomes richer in heavy components. As a result, the phase envelope will shift to the right (Figure 1-4). Compositional variation has also been observed in the field. Figure 1-5 shows the variation of composition at wellhead from two wells in Kekeya gas field in China (Shi, 2009). As we can see, during production, pressure dropped, the heavy components dropped out in the condensate, the methane (C_1) composition at the wellhead increased and the butane (C_4) composition at the wellhead decreased. Novosad (1996) used compositional simulation and proved that near-well fluids can undergo transition from retrograde gas to a volatile oil early in the depletion, passing through a critical composition in the process. This brings about a large change in phase properties and saturation, and thus their flow behavior. El-Banbi and McCain (2000) stated that composition change will affect the surface tension (Figure 1-6) and viscosity (Figure 1-7) of the fluids. These effects will impact the mobilities and hence productivity.

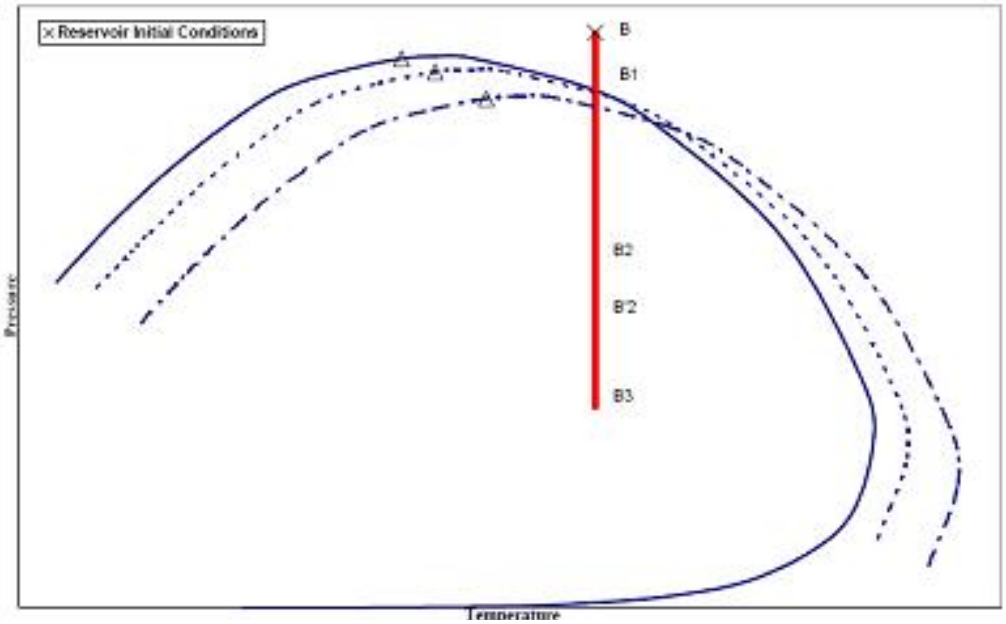

Figure 1-4: Shift of phase envelope with compositional change on depletion (from Roussennac, 2001).

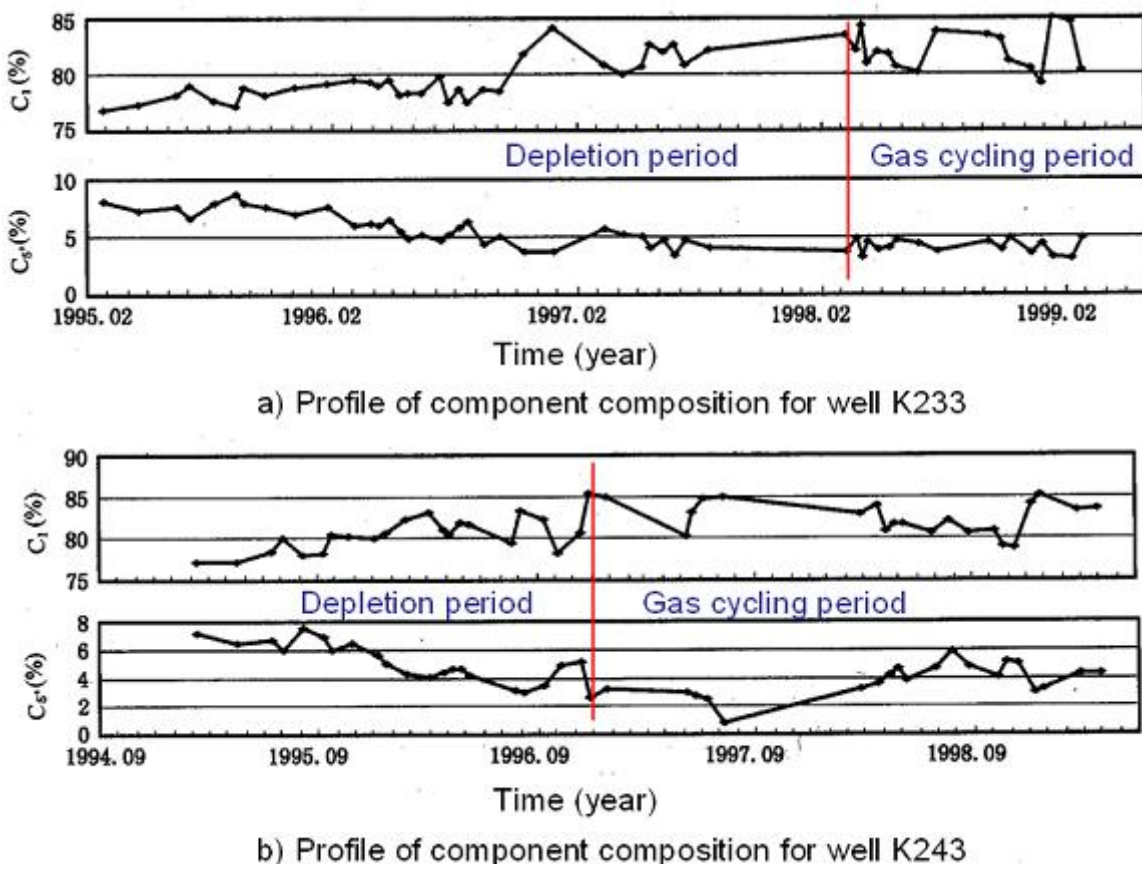

Figure 1-5: Compositional variation from two wells in Kekeya gas field (from Shi, 2009).

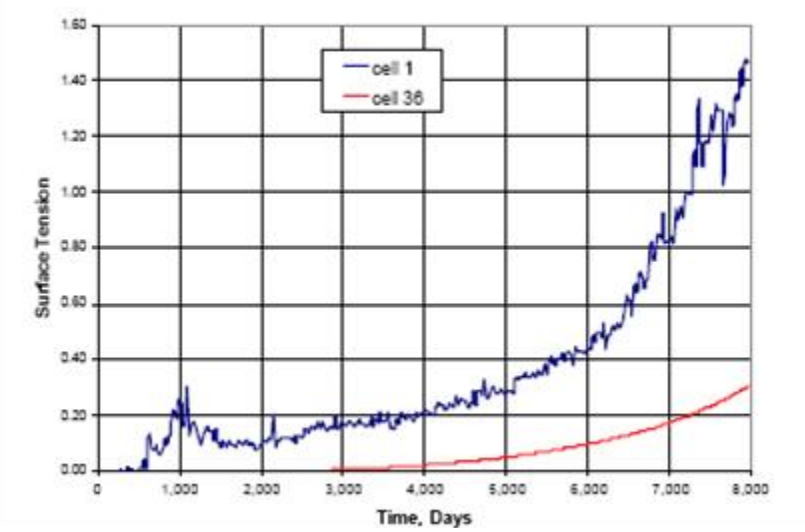

Figure 1-6: Surface tension variation (no units given) (from El-Banbi, McCain and Semmelbeck, 2000).

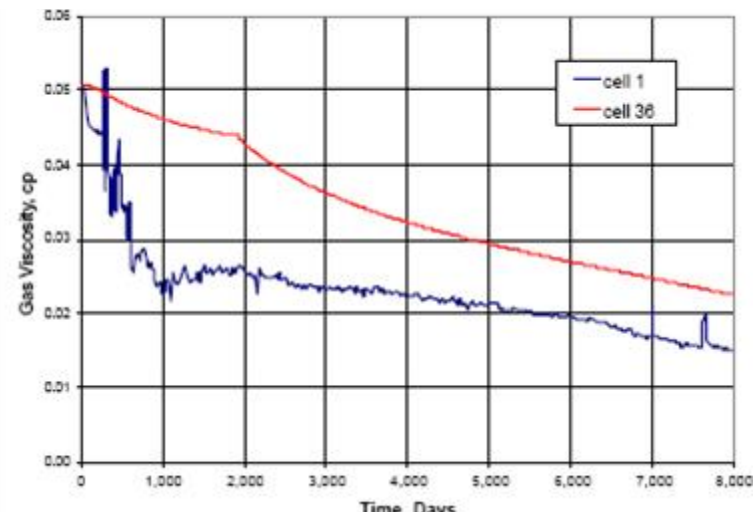

Figure 1-7: Gas viscosity variation (from El-Banbi, McCain and Semmelbeck, 2000).

The effect of interstitial water on the gas-condensate composition has been studied sparsely in the literature. Saeidi and Handy (1974) studied the flow and phase behavior of gas condensate (methane-propane) in a sandstone core. They indicated that the presence of irreducible water saturation had no significant effect on the composition of the flowing fluid for the gas-condensate system in which gas is the only flowing phase. Nikravesh and Soroush (1996) developed the basic concept relevant to the theory of gas-condensate flow behavior near the critical region. They predicted that the condensate is formed in the smaller pores, fills these pores and then continues into the larger pores. In the presence of interstitial water saturation, the condensate is formed at the water surfaces in the early stages of condensate formation.

1.2. Scope of this Work

This work is an extension of the previous work of Shi (2009). Shi (2009) investigated the flow behavior of the gas-condensate well in the case without the presence of immobile water through a series of laboratory core flood experiments. Although achieving some solid conclusions, the lack of repeatability of the experimental results was a concern. As repeatability is essential for scientific validity, the first part of this work was to replicate the previous experiments and try to achieve repeated results. Shi (2009) also ran numerical simulations and concluded that shutting the well after the formation of the condensate bank is not a good strategy, because the condensate will not revaporize due to the local compositional change. Besides that, Shi (2009) simulated the behavior of flow under different well flowing bottom-hole pressure (*BHP)* controls. However, there were no experiments to back up these simulations. So the second part of this work was to check these simulated predictions through experiments. Then, the whole work was extended to the case that we normally see in the field, namely gas-condensate reservoirs where mobile or immobile water is present. Finally, the effects of production strategies, hydraulic fracturing, gas injection on the performance of gas-condensate reservoirs were investigated.

The ultimate objective of the research was to gain a better understanding of how condensate blocking affects the well productivity, with a focus on the effect of compositional variation on flow behavior. This is important for optimizing the performance of gas-condensate reservoirs, reducing the impact of condensate banking, and improving the ultimate gas and condensate recovery.

Chapter 2

2. Physical Behaviors of Gas Condensate

2.1. Hydrocarbon Reservoir Fluids

Hydrocarbon reservoir fluids contain methane and a wide variety of intermediate and large molecules. The physical state of a hydrocarbon reservoir fluid depends on its composition, reservoir pressure and temperature. If a hydrocarbon reservoir fluid contains small molecules, its critical temperature may be below the reservoir temperature and the fluid would be in a gaseous state. However, when the hydrocarbon reservoir fluid contains heavy molecules, its critical temperature may be higher than the reservoir temperature and the fluid would be in liquid state.

Generally, the deeper the reservoir the higher proportion of light hydrocarbons due to degradation of complex organic molecules.

The most common classification of hydrocarbon reservoir fluids is based on the degree of volatility. According to this classification, reservoir hydrocarbon fluids are classified as gas, gas condensate, volatile and black oil. Gas is classified further as dry gas or wet gas depending on whether or not there will be liquid condensation at the surface.

Table 2-1: Typical molar compositions of petroleum fluids (from Pedersen et al., 1989).

Component	Gas	Gas Condensate	Volatile Oil	Black Oil
N_2	0.3	0.71	1.67	0.67
CO_2	1.1	8.65	2.18	2.11
C_1	90.0	70.86	60.51	34.93
C_2	4.9	8.53	7.52	7.00
C_3	1.9	4.95	4.74	7.82
C_4 $(i+n)$	1.1	2.00	4.12	5.48
C_5 $(i+n)$	0.4	0.81	2.97	3.80
C_6 $(i+n)$	6+: 0.3	0.46	1.99	3.04
C_7		0.61	2.45	4.39
C_8		0.71	2.41	4.71
C_9		0.39	1.69	3.21
C_{10}		0.28	1.42	1.79
C_{11}		0.20	1.02	1.72
C_{12}		0.15	12+: 5.31	1.74
C_{13}		0.11		1.74
C_{14}		0.10		1.35
C_{15}		0.07		1.34
C_{16}		0.05		1.06
C_{17}		17+: 0.37		1.02
C_{18}				1.00
C_{19}				0.90
C_{20}				20+: 9.18

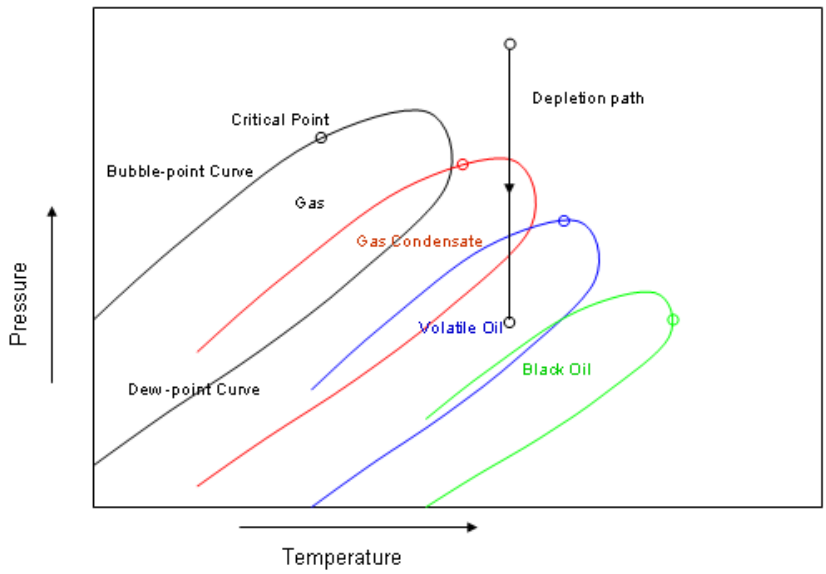

Figure 2-1: Phase diagram for reservoir fluids.

Typical molar compositions of gas, gas condensate, volatile oil and black oil are shown in Table 2-1. Phase envelopes of the petroleum reservoir fluids are shown in Figure 2-1 where "C" indicates the critical point of the fluid.

2.1.1. Dry Gas

Dry gas is composed of mainly methane and nonhydrocarbons such as N_2 and CO_2. Figure 2-2 shows a phase diagram of a dry gas. Due to the lack of heavy components, the two-phase envelope is located mostly below the surface temperature. The hydrocarbon mixture is solely gas from reservoir to the surface.

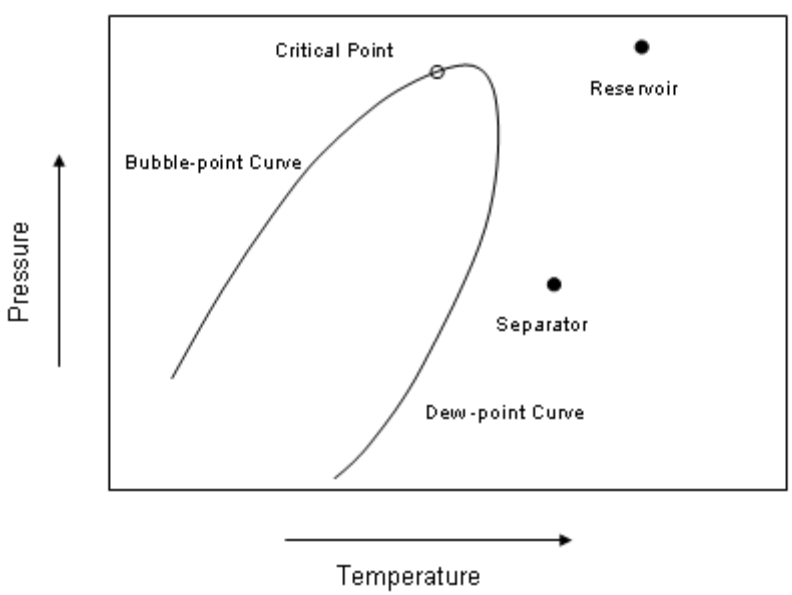

Figure 2-2: Phase diagram of dry gas.

2.1.2. Wet Gas

Wet gas is composed of mainly methane and other light hydrocarbons with a phase diagram as in Figure 2-3. A wet-gas reservoir exists solely as gas through the isothermal reduction of pressure in the reservoir. However, the separator conditions lie within the two-phase envelope causing liquid formation at the surface.

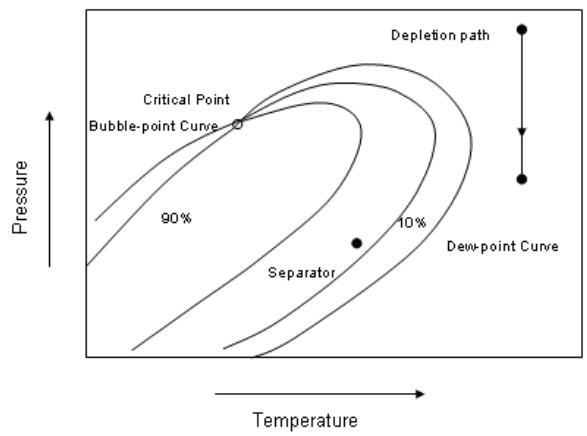

Figure 2-3: Phase diagram with line of isothermal reduction of reservoir pressure of wet gas.

2.1.3. Gas Condensate

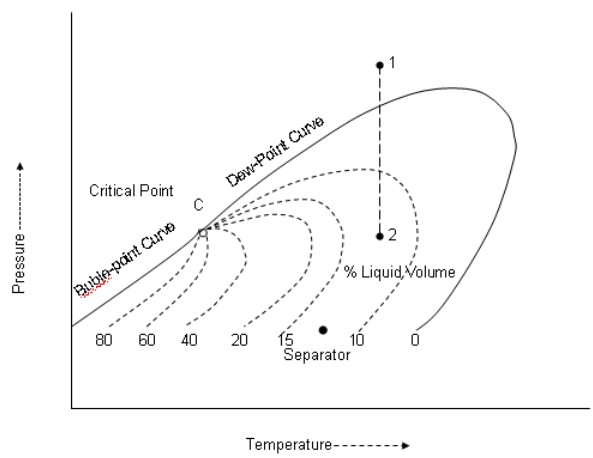

Figure 2-4: Phase diagram with line of isothermal reduction of reservoir pressure of gas condensate.

Gas condensate contains a small fraction of heavy components. The presence of the heavy components expands the two-phase envelope of the fluid mixture to the right (Figure 2-4) compared to that of wet gas (Figure 2-3), hence the reservoir temperature lies between the critical temperature and the cricondentherm. The liquid will drop out of the gas when the pressure falls below the dew-point pressure in the reservoir. Further liquid condensation will occur on the surface.

2.1.4. Volatile Oil

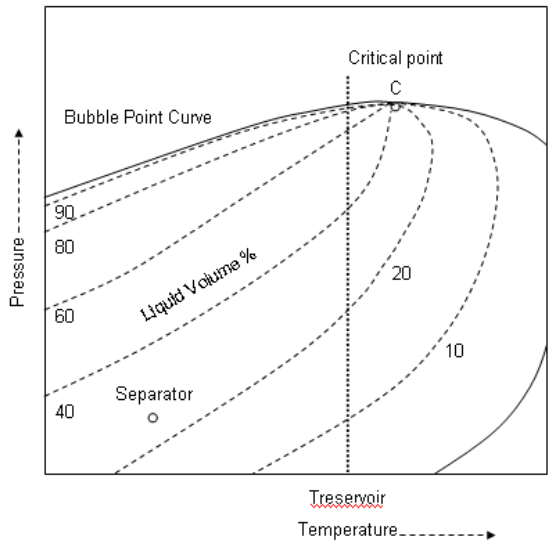

Figure 2-5: Phase diagram with line of isothermal reduction of reservoir pressure of volatile oil.

Volatile oil contains more heavy components (heptanes plus) than gas condensate so it behaves like liquid at reservoir conditions. A two-phase envelope of volatile oil is shown in Figure 2-5. The reservoir temperature is lower but near critical temperature. The isovolume lines are closer and tighter near the critical point so a small isothermal reduction of the pressure below the bubble-point pressure result in a large portion of liquid volume vaporized. Hence the oil is called "volatile" oil.

2.1.5. Black Oil

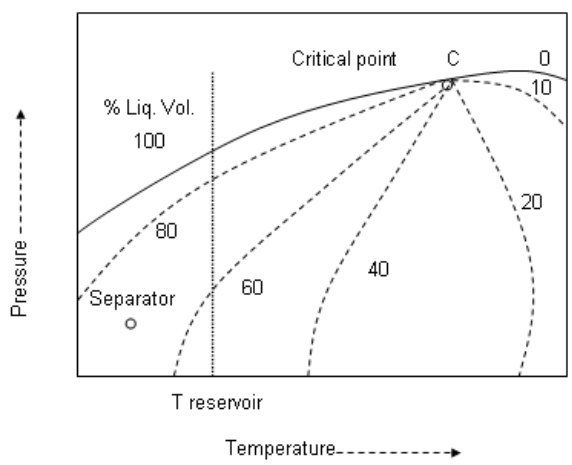

Figure 2-6: Phase diagram with line of isothermal reduction of reservoir pressure of black oil.

Black oil (also called "low shrinkage" oil) contains a large fraction of heavy components. The two-phase envelope is widest of all hydrocarbon reservoir fluids. The critical temperature is much higher than the reservoir temperature. The bubble-point pressure of the black oil is low. The isovolume lines are broadly spaced at reservoir conditions and

the separator condition lies on a relatively high isovolume line so a large reduction of the pressure below the bubble-point pressure (at constant temperature) results in vaporization of only a small amount of liquid. Hence, the oil is called "low shrinkage" (Figure 2-6).

Another type of classification which is based on the surface-determined properties is listed in Table 2-2. Gas-condensate reservoirs produce condensate and gas both in the reservoir and at the surface with producing gas-liquid ratio from 3,200 to 150,000 SCF/STB, and the stock tank oil density changes throughout the life of the reservoir. This is different from the wet-gas reservoir where the liquid is formed only at the surface and the density of the stock tank oil does not change. McCain (1994) further distinguished the difference between volatile oil and gas condensate based on a cut-off composition of 12.5% C_{7+}.

Table 2-2: Summary of guidelines for determining fluid type from field data (from McCain, 1994).

	Black Oil	Volatile Oil	Retrograde Gas	Wet Gas	Dry Gas
Initial producing gas/liquid ratio (scf/STB)	<1,750	1,750 to 3,200	>3,200	>15,000	1000,000
Initial stock-tank liquid gravity (°API)	<45	>40	>40	Up to 70	No liquid
Color of stock-tank liquid	Dark	Colored	Lightly colored	Water white	No liquid

2.2. Phase Behavior of Gas Condensate

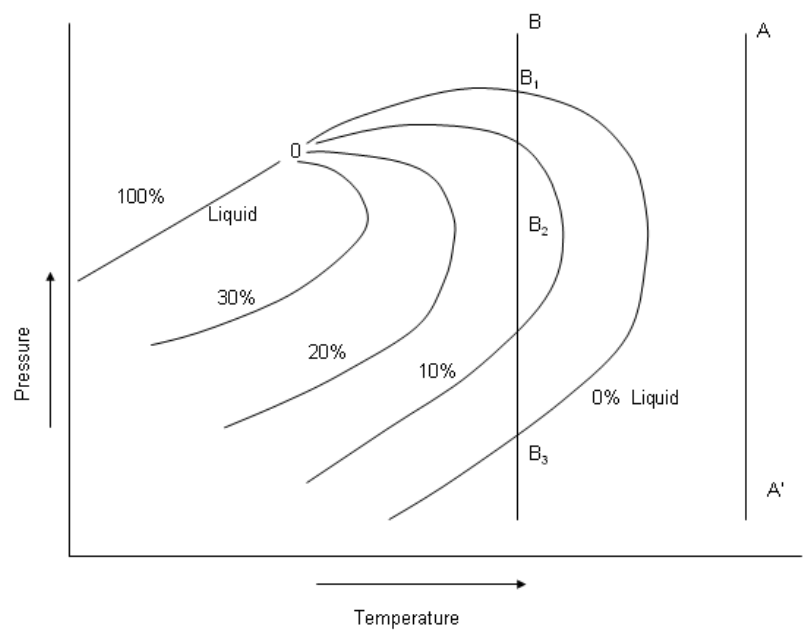

Figure 2-7: Phase diagram with isovolume line of gas condensate.

Figure 2-7 shows a phase diagram with isovolume lines of the gas condensate. When the pressure is above the dew point (B_1) the fluid is single-phase gas. Isothermal depletion leads to the dew point where the first drop of condensate occurs. If the pressure is reduced further to abandonment pressure ($B_1 \rightarrow B_2 \rightarrow B_3$), the amount of condensate dropout will increase to a maximum value, then decrease due to revaporization. This characteristic is shown in the Figure 2-8. However, this process assumes that liquid and gas remain immobile in the reservoir and hence that the composition is constant. In reality, due to the fact that the gas is produced more from the reservoir than liquid condensate because of its higher mobility, the overall composition will change and the two-phase envelope will shift. The critical point moves to higher temperature and the two-phase envelope move right and downwards as shown earlier in Figure 1-4.

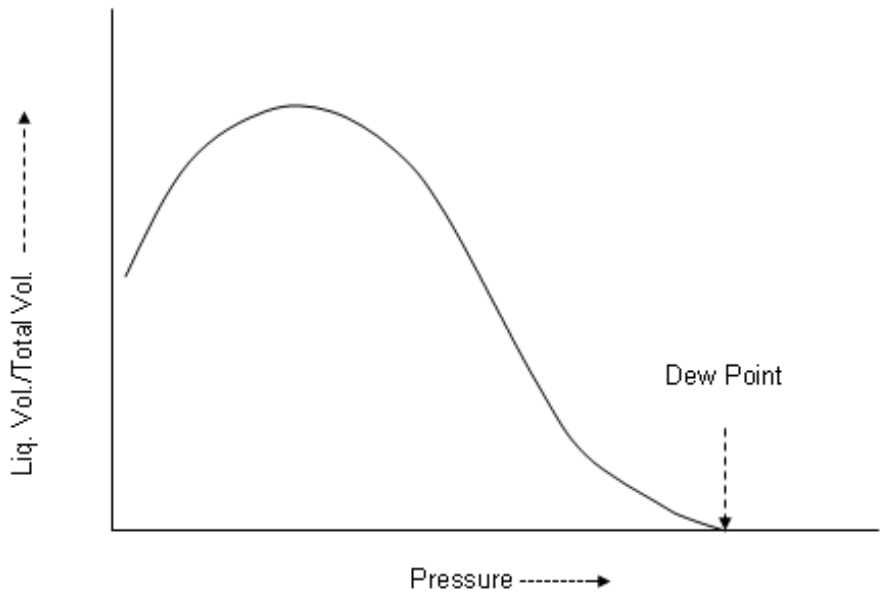

Figure 2-8: Liquid dropout behavior of gas condensate.

In order to quantify the phase behavior and properties of gas condensate at reservoir conditions, two *PVT* tests normally used are Constant Composition Expansion (*CCE*) and Constant Volume Expansion (*CVD*).

2.2.1. Constant Composition Expansion (CCE)

The schematic of a *CCE* experiment is shown in Figure 2-9. In this experiment, a known amount of gas condensate is loaded in a visual cell at a pressure above the initial reservoir pressure. The system is normally left overnight for equilibration. The pressure is then reduced stepwise by increasing the cell volume while maintaining the temperature constant. The volume at each pressure level is recorded after the system reaches equilibrium. During the experiment, the overall composition of the system is kept constant and no condensate or gas is removed from the cell. This experiment is applicable

for gas-condensate reservoirs if the pressure is above the dew-point pressure, hence the composition is constant. The experiment is also applicable to conditions near the producer within the condensate ring where a steady state can be assumed in which the composition is constant.

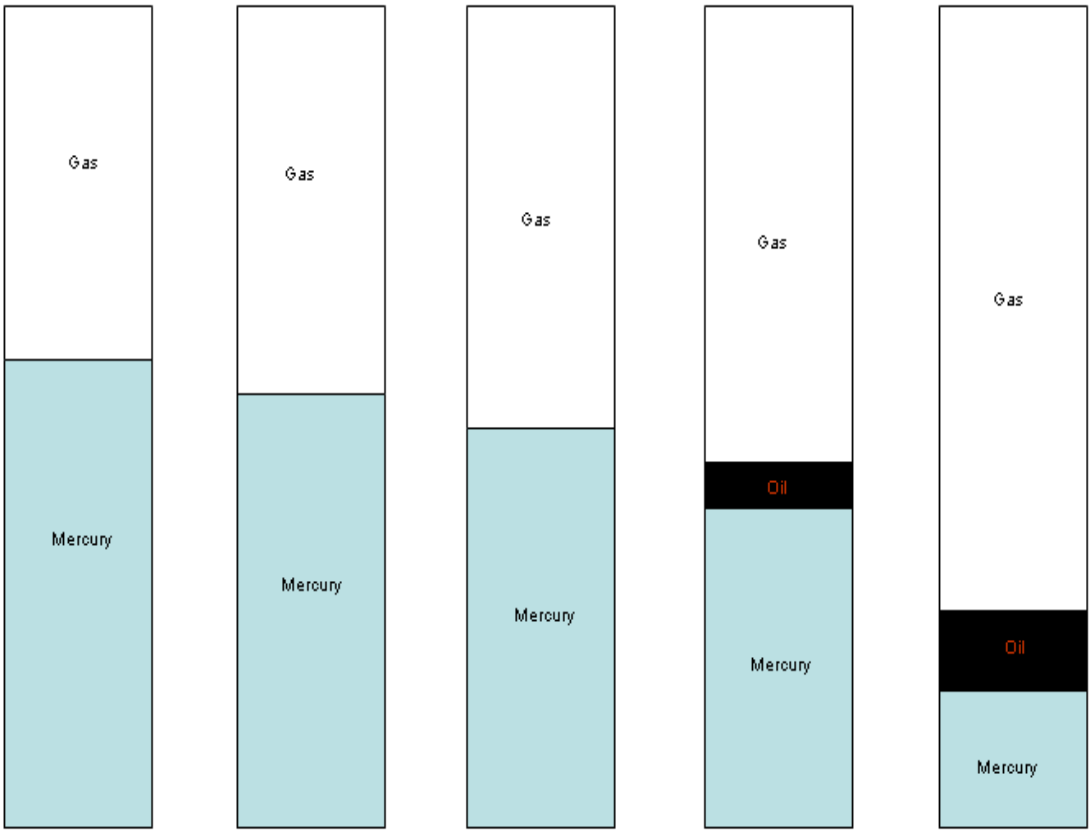

Figure 2-9: Schematic of *CCE* experiment.

2.2.2. Constant Volume Depletion (CVD)

A *CVD* is an experiment where the overall compositions vary during the process. The *CVD* experiment on a gas-condensate system is based on the assumption that the condensate is immobile. Figure 2-10 shows a schematic of the *CVD* experiment. The system is brought just to its dew point which is normally found from the *CCE* experiment, after which a series of expansions are conducted by expelling gas at constant pressure until the cell volume equal to the volume at the dew point. At each stage, the pressure, liquid and gas volumes are recorded. The expelled gas is collected and determined in terms of composition then the new overall composition is calculated based on material balance. The temperature is kept constant during the whole process. The assumption that the condensate phase is immobile is only valid if the condensate saturation is below the critical condensate saturation. Also, the *CVD* experiment does not take into account the net accumulation of the gas condensate due to relative permeability effect.

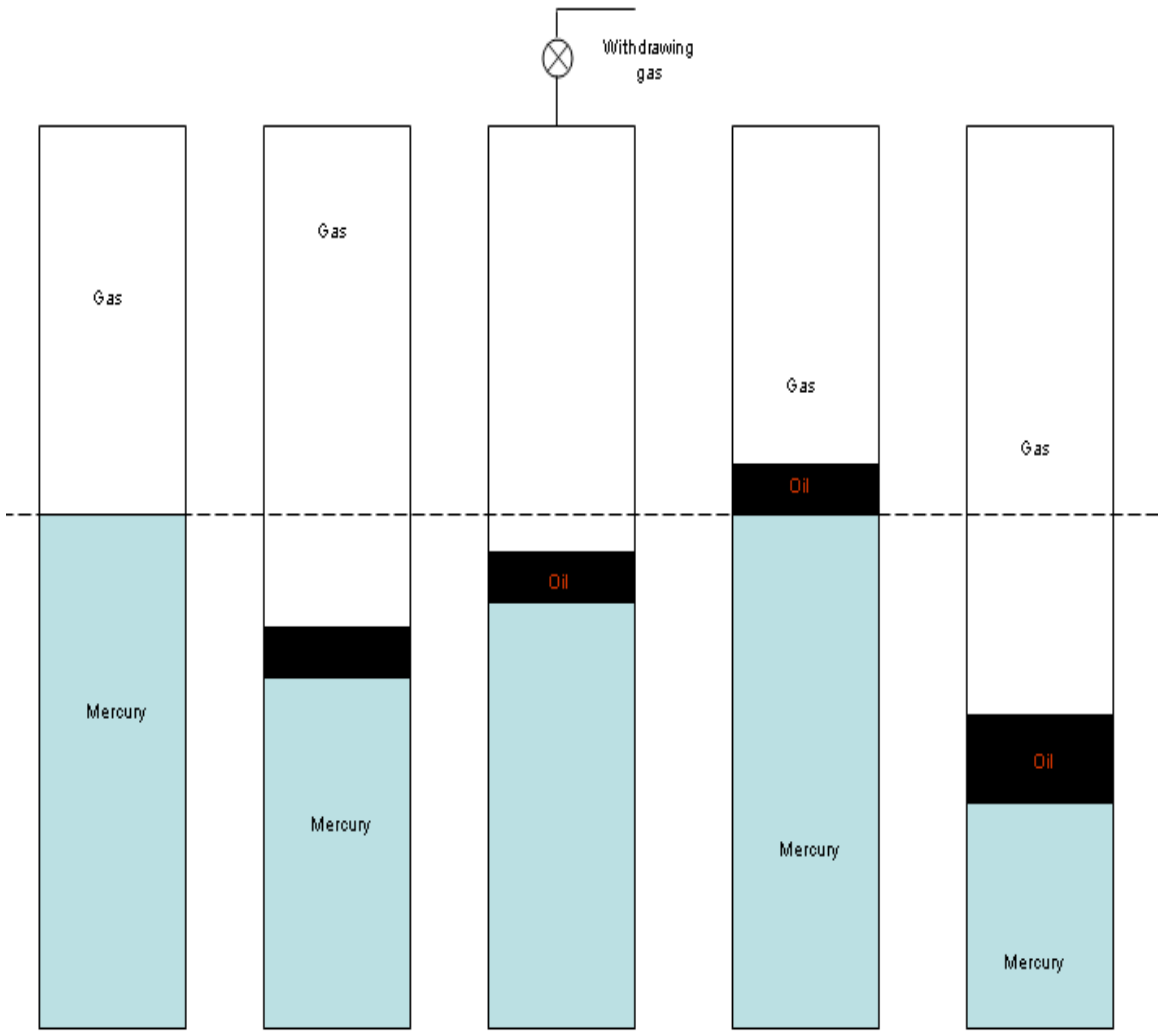

Figure 2-10: Schematic of *CVD* experiment.

2.3. Flow Behavior of Gas Condensate

2.3.1. Drawdown Behavior

Reservoir performance during production of a condensate well can be described as (Economides et al., 1987 and Ali et al., 1997):

Stage 1: Single-phase gas reservoir

For $BHP > p_d$, the reservoir fluid exists as single-phase gas.

Stage 2: Mobile gas, immobile liquid

As *BHP* declines below p_d, a condensate bank develops around the wellbore with the saturation below the critical saturation, hence the liquid is immobile.

Stage 3: Mobile gas and liquid

As production continues, condensate accumulates until the condensate saturation exceeds the critical condensate saturation in the zone near the well. Condensate liquid will flow in the reservoir.

As the liquid saturation profile continues to increase in magnitude and radial distance, eventually a steady state is reached in which liquid dropout is equal to the liquid production.

Stage 4: Both reservoir pressure and *BHP* are below the dew point.

The liquid condensation will occur throughout the whole reservoir.

Based on previous studies, Fevang and Whitson (1996) proposed a simple but accurate model for the flow of gas condensate into a producing well from a reservoir undergoing depletion once steady-state flow is reached. Based on this model, the fluids flow can be divided into three main flow regions (Figure 2-11):

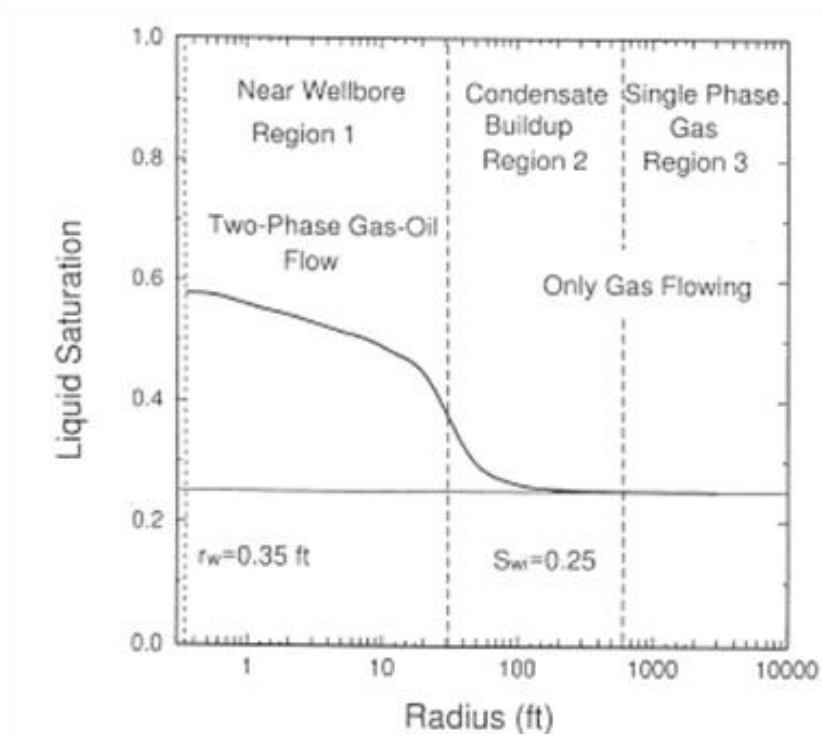

Figure 2-11: Three regions of flow behavior in a well condensate well (from Fevang and Whitson, 1996).

Region 1: An inner near-well region where the condensate saturation exceeds the critical condensate saturation hence both gas and condensate flow (although with different velocities). In this region, the flowing composition is constant, hence the fluid properties can be approximated by the *CCE*. Region 1 is the main source of deliverability loss in a gas-condensate well. Gas permeability is reduced due to the liquid blockage. The size of

region 1 increases with time. Region 1 exists only if the *BHP* is below the dew-point pressure p_d.

Region 2: A region of condensate buildup where only gas is flowing. In this region the pressure is below the dew-point pressure but the condensate saturation is below the critical condensate saturation hence only gas flows in region 2. In other words, region 2 is the region of net condensate accumulation. Due to the condensate drop-out, the flowing gas phase becomes leaner. Condensate drop-out in region 2 can be approximated by the *CVD* experiment corrected for water saturation. The consequence of region 2 is that the producing wellstream is leaner than calculated by the *CVD* experiment. The size of region 2 decreases with time as region 1 expands over time. Region 2 always exists together with region 1.

Region 3: An outer region where pressure is above the dew point. Only the original gas phase is contained in this region. The composition is constant in region 3 and equal to the composition of the original reservoir gas. The fluid properties in this region can be calculated by the *CCE* experiment. Region 3 can only exist if the pressure is above the dew-point pressure.

2.3.2. Buildup Behavior

During production, as we mentioned previously, the overall composition of the gas condensate changes, as it becomes richer in heavier components. If the well is shut in, the liquid bank that is formed around the production well may not revaporize to the gas phase. In a theoretical derivation, Economides et al. (1987) determined conditions under which a hysteresis in condensate saturation will occur. Although a pressure buildup would indicate a revaporization based on the original gas-condensate *PVT* properties, condensate accumulation in the reservoir may preclude the reverse process. Roussennac (2001) showed by simulation that if the production period is longer than a certain threshold, the fluid near the well can switch from gas-condensate behavior to a volatile oil behavior. Novosad (1996) also showed in numerical simulations that during depletion of a lean gas condensate, the fluid near the wellbore changes from gas condensate to near critical retrograde gas and later to volatile oil (Figure 2-12). For a rich gas-condensate fluid, the fluid will change from a retrograde gas to near critical retrograde gas, a volatile oil, black oil then reverse to near critical oil and finally a dry gas. Furthermore, if the gas-condensate system is near critical, the behavior during the pressure depletion is even more complicated. Double retrograde condensation, with two liquids rather than the usual single liquid phase, can occur (Shen et al., 2001). In short, the thermodynamic and flow behaviors of the gas condensate during the buildup period depend on the overall composition, condensate saturation and pressure at the moment of well shut in. Hence shutting in the well after having condensate banking is not a good strategy to mitigate the condensate blockage effect because the saturation of a volatile oil will increase with pressure increase.

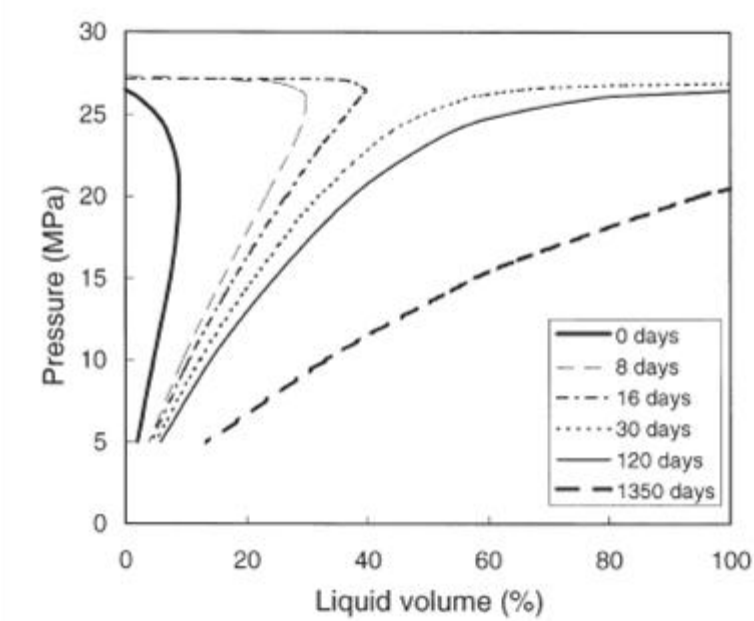

Figure 2-12: Evolution of fluid compositions in the innermost grid block for a lean gas condensate at dew-point pressure (from Novosad, 1996).

Chapter 3

3. Experimental Investigation

3.1. Experimental Design

3.1.1. Difference between Static and Flowing Values

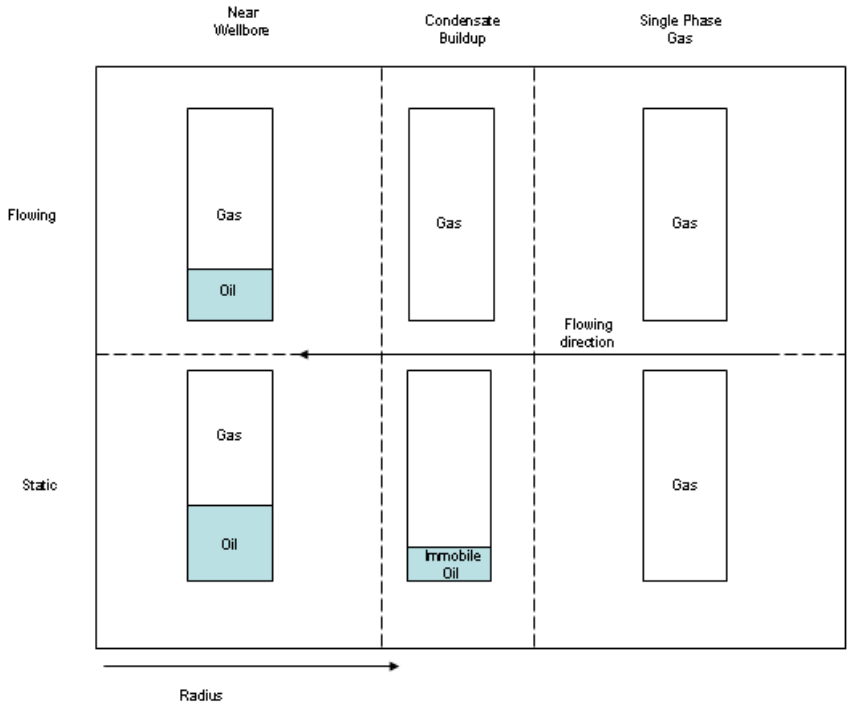

Figure 3-1: Difference between static and flowing values.

Before running numerical simulations and doing experiments for the gas-condensate system, it is important to understand the difference between the static value and flowing value of a property (such as density, viscosity, composition). Static value is the value at a given location at a given time. This would be the value of the property in a grid block of a numerical simulation. Due to relative permeability and the difference in mobilities of condensate and gas phases, the value of a property of the flowing mixture in a given grid block will be different from the static value. During experiments, samples taken are from the flowing phases. Figure 3-1 illustrates the difference between static value and flowing value for the three flow regions based on Fevang's model (Fevang and Whitson, 1996). In region 3 only gas exists, so the static value and the flowing values will be the same. However, in the region 2, there are two phases but the liquid phase is immobile and only the gas flows, so the static value and the flowing value will be different. In region 1, both

liquid and gas will flow but with different velocities hence again the static and flowing values will be different.

3.1.2. Synthetic Gas-Condensate Mixture

For the purpose of replicating Shi's experiments (Shi, 2009), trying to achieve the repeatability of the experimental results and extending her work, the synthetic gas-condensate mixture for this study was the same as the one she used. The mixture consists of 85% C_1 and 15% nC_4 by mole fraction. This gas-condensate mixture was selected based on the following criteria:

- The binary mixture is easy to mix in the laboratory, from commercial high quality pure component gases.
- The critical temperature of the mixture is below the laboratory temperature so the experiments can be performed at room temperature, which eliminates the need to heat the flammable gases hence improving safety.
- The gas has a broad two-phase region in order to achieve condensate dropout during the experiment.

The phase diagram of the synthetic gas-condensate mixture used for the experiments is shown in Figure 3-2. The critical point of the mixture is T_c= 10 °F, p_c= 1,844 psia. At room temperature of 70°F and pressure range from 2,200 – 1,000 psia, this mixture has a broad two-phase region.

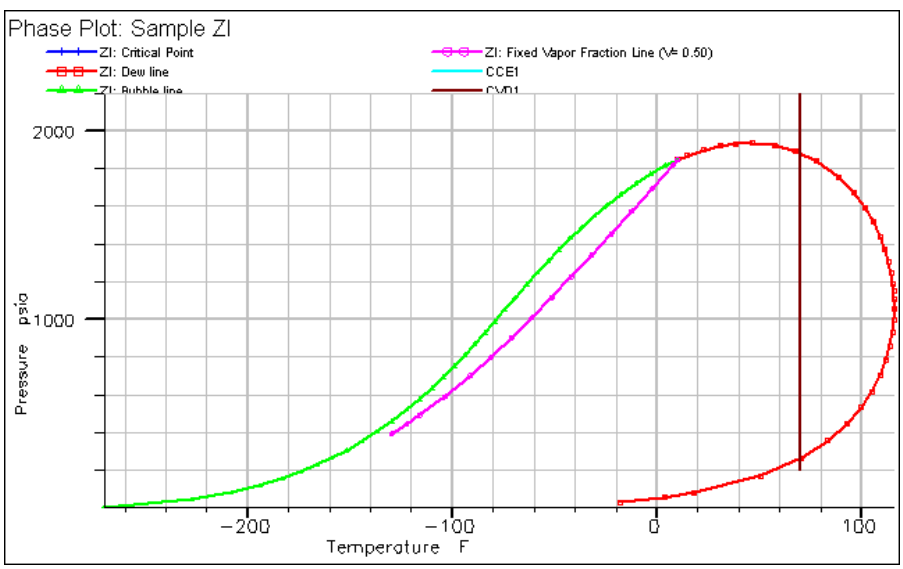

Figure 3-2: Phase diagram of the synthetic gas-condensate mixture used for experiments (85% C_1 and 15% nC_4 in mole fraction).

Figure 3-3 shows the condensate dropout volumes in *CVD* and *CCE* tests. The accumulated condensate volumes from both tests are almost the same in the condensing region. Both tests also show that the condensate revaporizes into the gas phase at lower

pressure. As mentioned in Section 2.2, these tests do not account for the condensate buildup hence they do not indicate the maximum possible condensate accumulation in the reservoir. The maximum liquid dropout volumes from these simple PVT tests are less than 12%. However, as we will see in Section 3.1.3, reservoir simulation shows that the condensate saturation during actual flowcan be as high as 47%.

Next, the effect of curved interfaces in the porous medium on the phase behavior of the gas-condensate mixture needed to be investigated. This effect has been studied by several authors. Sigmund et al. (1971) investigated the effect of porous media on phase behavior of C_1/nC_4 and C_1/nC_5 and concluded that the porous medium has no effect on dew-point and bubble-point pressures, or on equilibrium compositions in pore spaces with moderate surface curvature and pore size larger than several microns. As the core plug used here was Berea sandstone, the curvature is low, so the rock would not be expected to affect the phase behavior of the gas-condensate mixture.

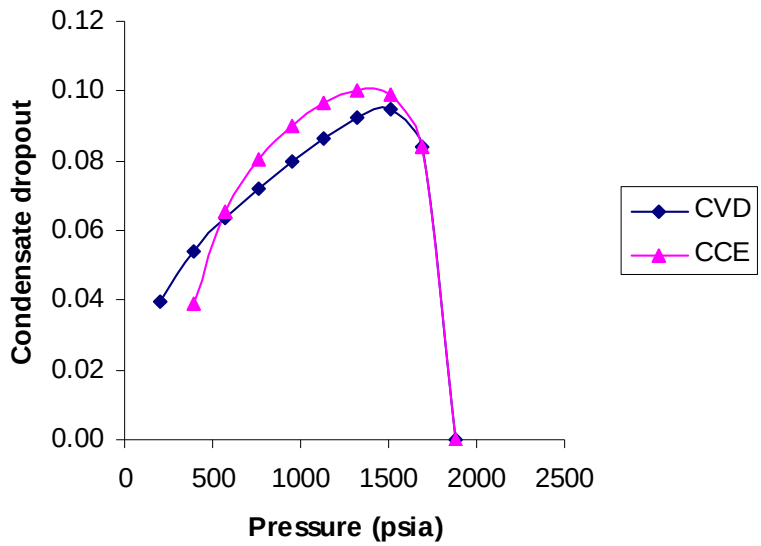

Figure 3-3: Condensate dropout of the synthetic gas-condensate mixture used for experiments (85% C_1 and 15% nC_4 in mole fraction) at 70 °*F* from the simulation of *CCE* and *CVD* tests.

3.1.3. Numerical Simulation for Experiments

The core used for experiment is cylindrical (Figure 3-4). The synthetic gas-condensate mixture is injected at one end and comes out at the other end of the core, so the flow is one-dimensional linear flow. The simulation for this linear flow can be done in a one-dimensional Cartesian coordinate system (Figure 3-5). The core is divided into 51 grid blocks in the *x* direction only. The cross-section of the grid block is a square whose area is equal to the cross-sectional area of the cylindrical core. The reason to do this is to maintain the same pore volume, hence the same volume of condensate dropout compared to reality.

Figure 3-4: Core used for experiments.

Figure 3-5: Gridding for numerical simulation of the core.

Numerical simulations were conducted in this study to define the experimental parameters such as duration. Simulation was also used to check the flow pressures and to have an idea how composition and saturation were distributed along the core. In the simulation model, two wells, one gas injection and one producing, were used. Both wells were controlled by constant bottom-hole pressures. The bottom-hole pressure of the injection well was set above the dew-point pressure while the bottom-hole pressure of the producing well was set below the dew-point pressure of the gas-condensate mixture. So the fluid at the upstream end was always in gas phase, and the fluid at the downstream end was always in the two-phase region.

Simulation for Two-phase Gas-Condensate System

First, based on the phase diagram in Figure 3-2, we set the bottom-hole pressure for the injection well at 130 atm (1,911 psi) and for the producing well at 70 atm (1,029 psi). Figure 3-6(a) shows that liquid saturation builds up quickly once the pressure drops below the dew-point pressure. After two minutes the system reaches steady state (curves do not change versus time). Hence if the experiments last three minutes, the flow will be stable and gas samples taken will be representative. It is also shown in Figure 3-6(a) that the maximum condensate accumulation at the steady state can be as high as 47% whereas the critical condensate saturation from the input relative permeability curve is only 24% and the maximum liquid dropout from the *CCE* and *CVD* experiments are only about 9%. This is because the numerical simulation takes into account the condensate accumulation due to relative permeability effects. Obviously, the liquid saturation at the upstream end will be zero as the upstream pressure was still above the dew-point pressure.

Figure 3-6(b) and Figure 3-6(c) show that the nC_4 compositions in the liquid phase and in the vapor phase change dramatically along the core once the condensate has dropped out. The vapor phase becomes lighter (more C_1) hence the concentration of nC_4 in the vapor phase decreases in the direction of flow. Along the core, the pressure drop is higher going from left to right.

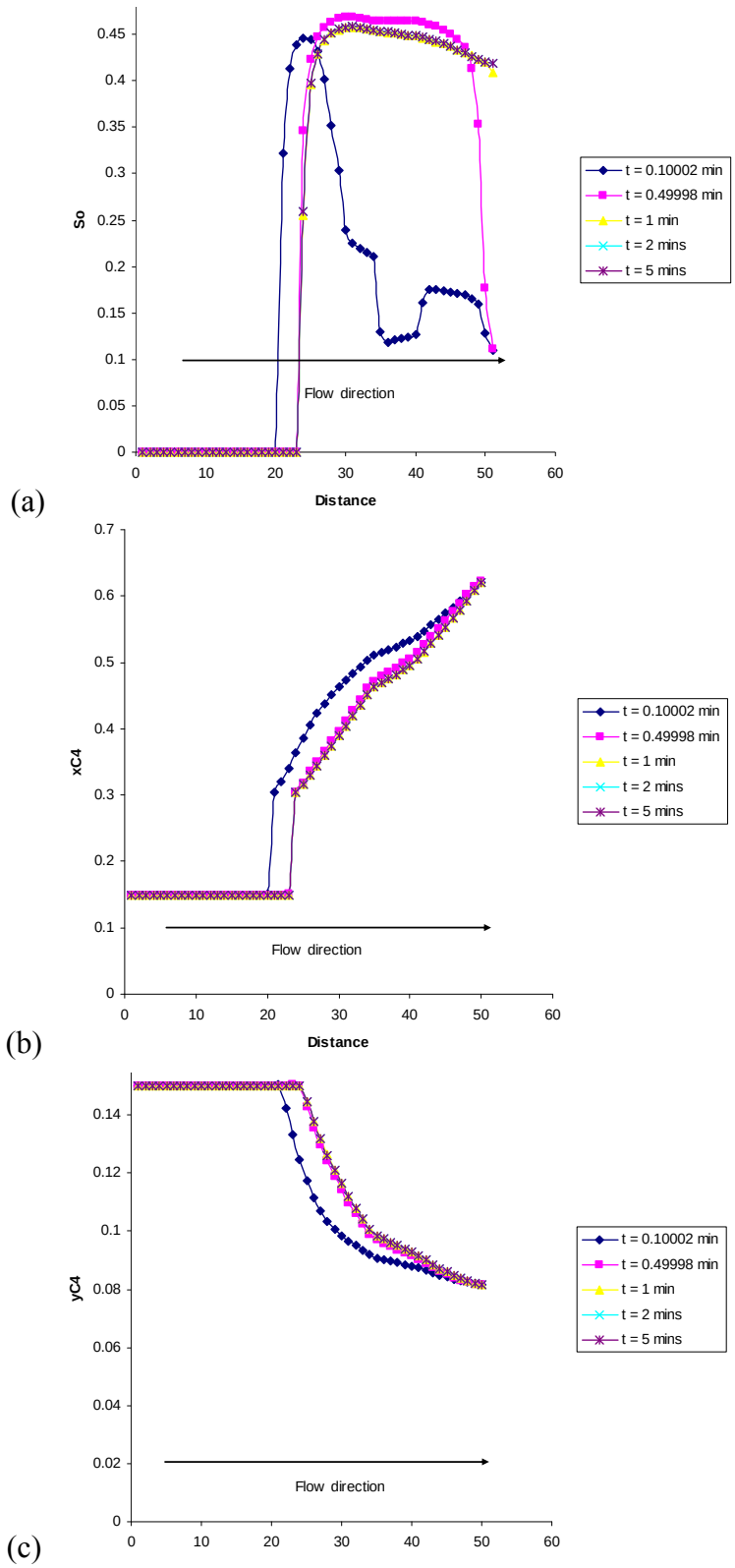

Figure 3-6: Two-phase (gas–condensate) simulation: (a) Condensate saturation profile. (b) nC_4 mole fraction in the liquid phase. (c) nC_4 mole fraction in the vapor phase. Distance indicated as grid block number – the core is 30 cm long.

Shi (2009) also looked into the behavior of flow under different downstream bottom hole pressure controls. She performed simulations with the same upstream pressure of 130 atm (1911 psia), but with different downstream pressures (Figure 3-7). She concluded that the higher the *BHP* at the producer, the larger the single-phase region, hence the liquid accumulates in a smaller region around the production well.

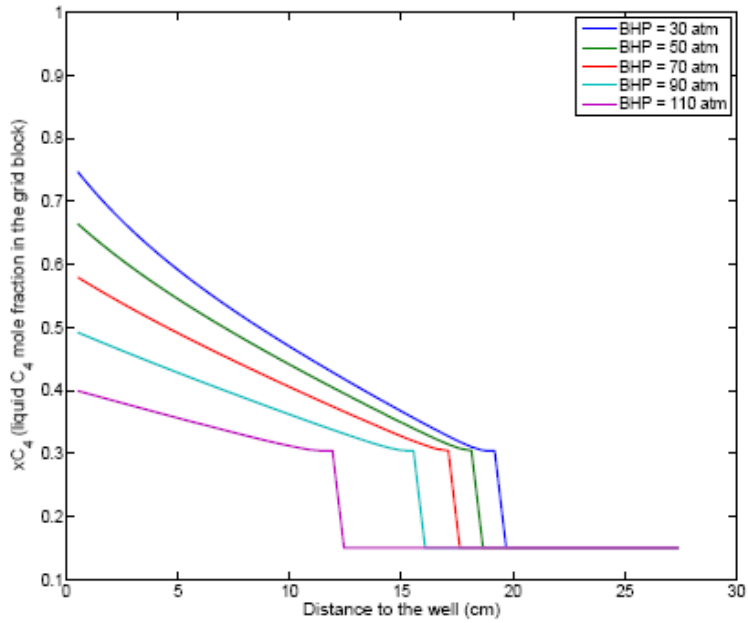

Figure 3-7: Numerical simulation of *nC4* composition history with different *BHP* control cases (from Shi, 2009).

Simulation for Three-phase System (Gas-Condensate and Immobile Water)

We extended the simulation study to investigate gas condensate flowing through a core in the presence of immobile water. The segregation model in Eclipse was used for the oil relative permeability. The mutual solubilities of water and hydrocarbons are small, so to simplify the problem the hydrocarbon phase behavior can be studied independently of the water phase. To model the water-hydrocarbon compositional effects properly (assuming any exist because of initial nonequilibrium of injected mixture and connate water), we would need to use a simulator that uses a nontraditional (not van der Waals) mixing rule (e.g. Huron-Vidal mixing rule).

Using this assumption, first we wanted to check our three-phase model by setting the immobile water saturation S_{wi} to zero and comparing the results with the results from the two-phase case. Figure 3-8 shows that the results of the two-phase system and the three-phase system with immobile water saturation equal to zero are the same, which demonstrated that the three-phase model for the simulator was correct.

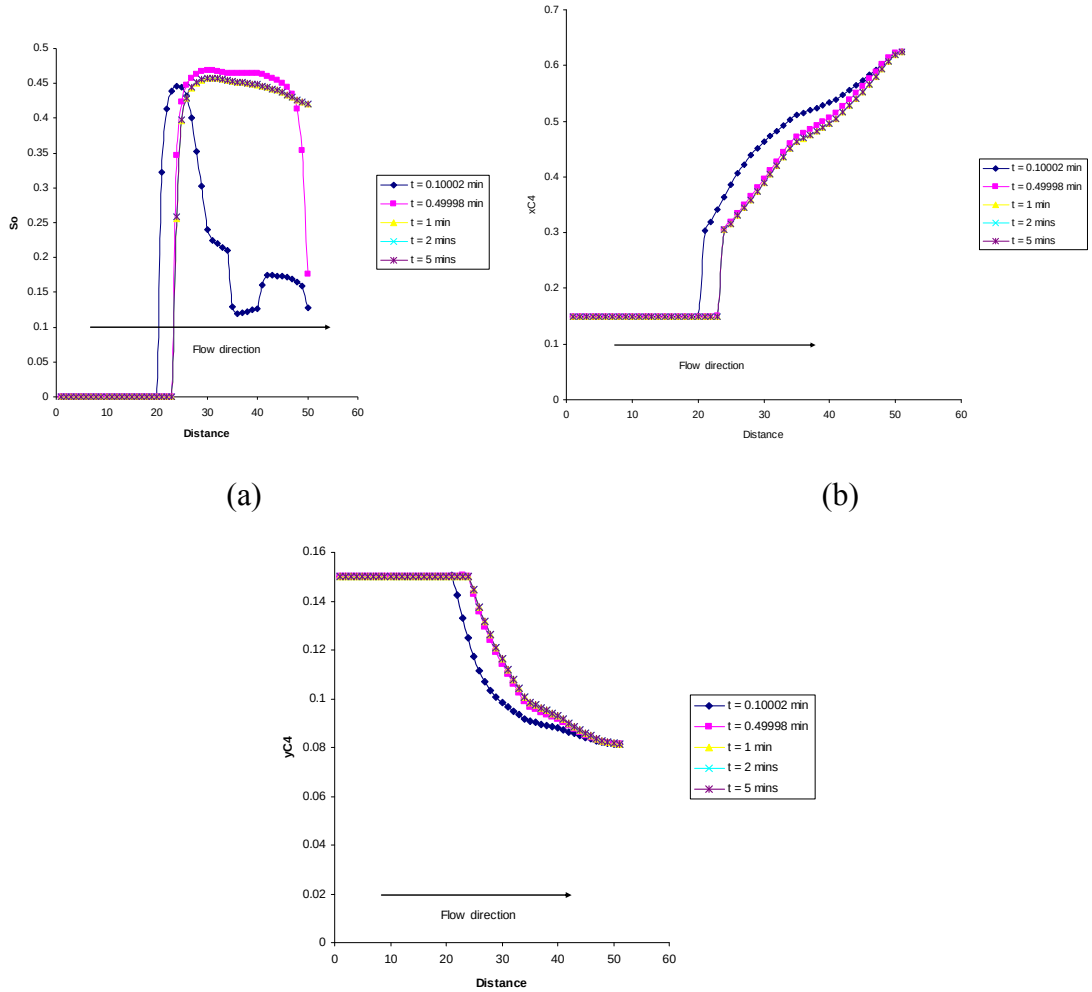

Figure 3-8: Three-phase simulation result with $S_{wi} = 0$: (a) Condensate saturation profile. (b) nC_4 mole fraction in the liquid phase. (c) nC_4 mole fraction in the vapor phase.

The simulation results for the gas-condensate mixture flowing in the presence of immobile water are shown in Figure 3-9. As we can see, there is some difference in composition between two-phase system (gas-condensate) and the three-phase system (gas-condensate-water) during the transient period. However, after the flow reaches steady state, the composition is the same for both systems.

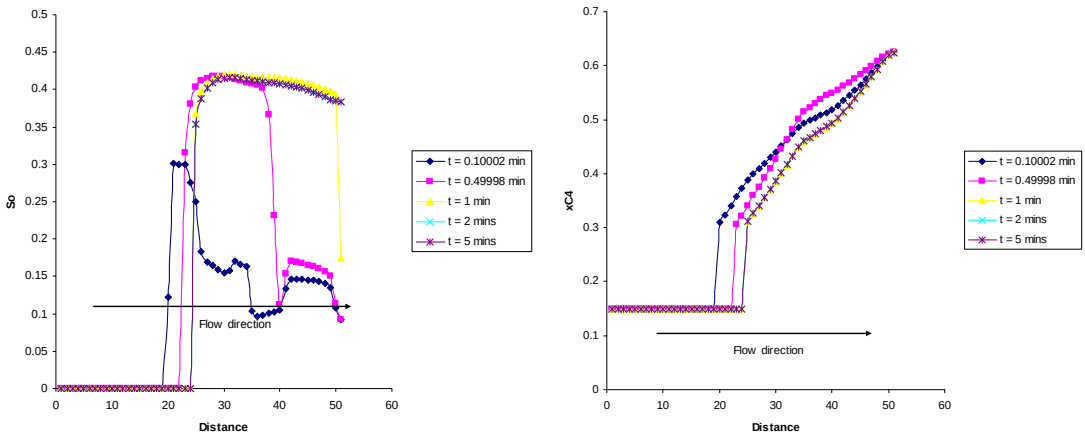

(a) (b)

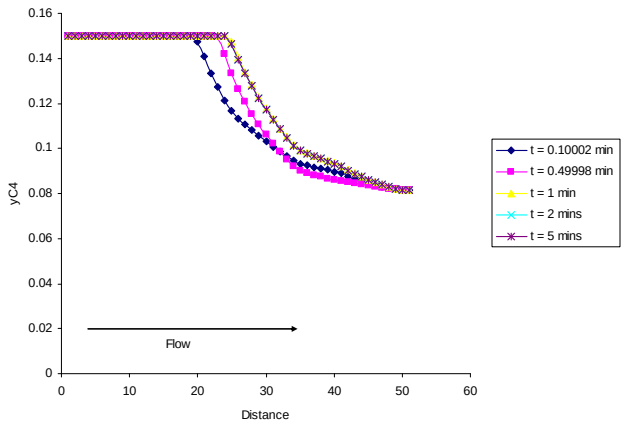

(c)

Figure 3-9: Three- phase simulation result with S_{wi} = 0.16: (a) Condensate saturation profile. (b) nC_4 mole fraction in the liquid phase. (c) nC_4 mole fraction in the vapor phase

3.2. Experimental Apparatus

The apparatus was modified from the previous design of Shi (Shi, 2009) to achieve repeatability of the experimental results. Figure 3-10 shows the original design of the apparatus. As we can see, the tubing volumes between the sample ports and the collecting bags are quite large. During the flow, the residual gas in these volumes was not flushed away so the samples taken during flow were contaminated by the residual gas.

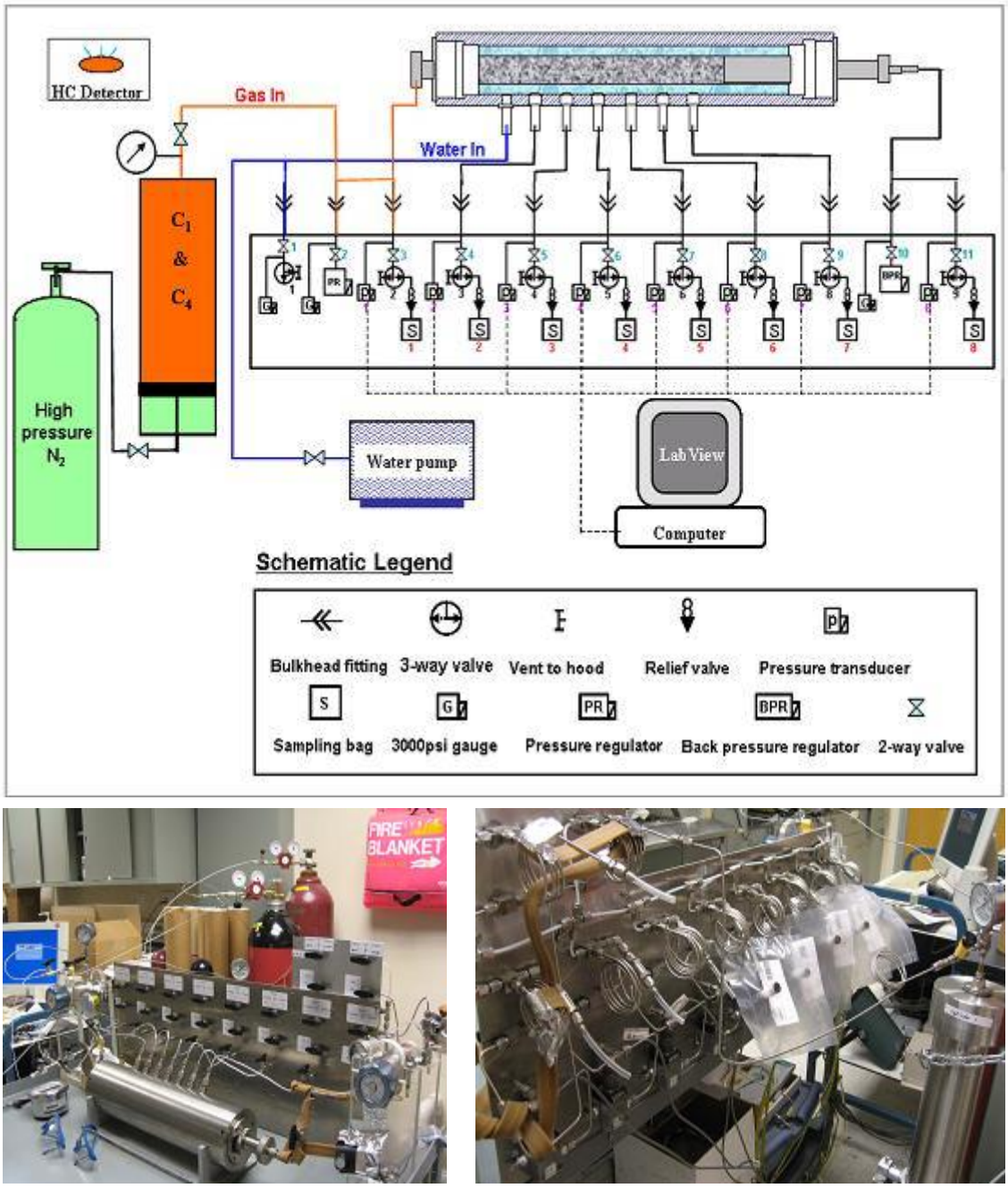

Figure 3-10: Original experiment apparatus (from Shi, 2009).

The apparatus was modified by fitting valves directly onto the core holder to minimize the volume in the sample tubes. The modification is shown in Figure 3-11. The modified experimental apparatus consists of the three main subsystems: gas supply and exhaust, core flooding system and fluid sampling system.

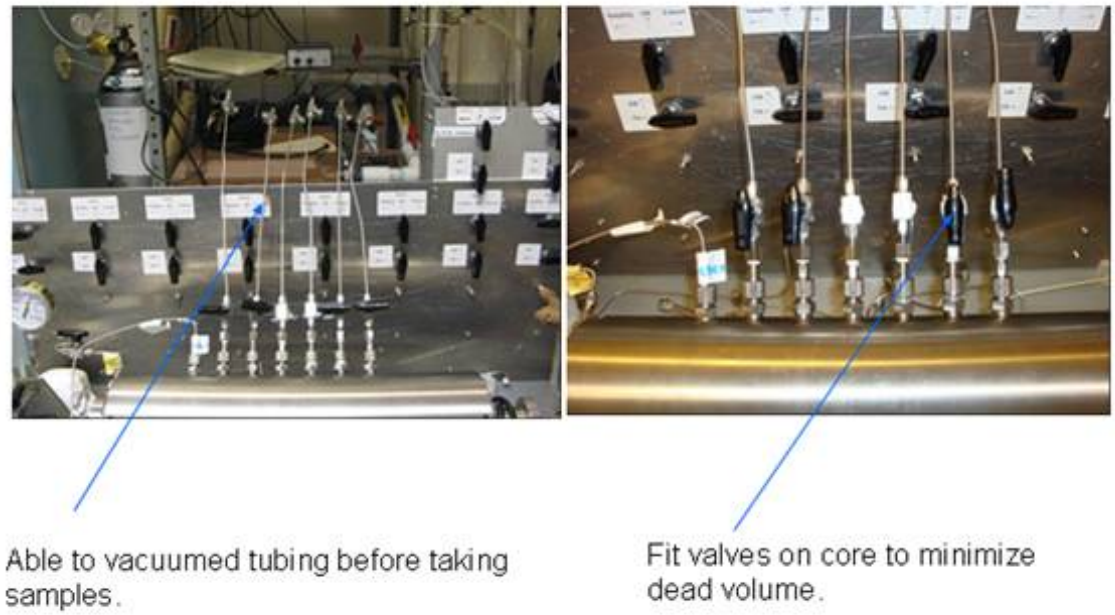

Figure 3-11: Modified experiment apparatus to minimize sample tube volume.

3.2.1. Gas Supply and Exhaust

The synthetic gas-condensate mixture was mixed in a piston cylinder. This piston cylinder has an internal volume of 3,920 ml and pressure rating of 4,641 psi. During the experiments, the pressure of the gas mixture was maintained about 200 psi above its dew-point pressure by pushing the back of the piston using a 6,000 psi N_2 gas bottle. O-rings in the piston prevent the gases on both sides from mixing together hence a high constant pressure gas mixture supply is achieved without affecting the gas composition. Two types of experiments were conducted: capture and noncapture. During the noncapture experiments, the downstream exhaust gas was discharged directly to the ventilated cabinet because the exhausted gas volume is small. During the capture experiments or during noncapture experiments in the CT scanner room (where the ventilated cabinet was not available), the exhaust gas was discharged into an empty piston cylinder.

3.2.2. Core Flooding System

The core flooding system consists of a titanium core holder, Berea sandstone core plug, valves and pressure regulators. The core holder can support a maximum confining pressure of 5,800 psi while maintaining the pore pressure at 5,366 psi. There were six ports (P_2 to P_7) to allow pressure monitoring and fluid sampling, but these ports were modified to fit shut-off valves. Adding the valves minimizes the dead volumes. These and other hardware modifications allowed us to achieve repeatable results, as will be discussed in Chapter 4. The same core as the one used previously by Shi (2009) was used for the experiments. The Berea sandstone core has a length of 30 cm and diameter of 4.9 cm. The permeability of the core is 9 md and its porosity is 16%. Upstream and downstream pressures were regulated using a pressure regulator and a back-pressure regulator.

3.2.3. Fluid Sampling System

One of the key modifications to achieve repeatability in the experiments was to make sure that the whole volume of gas sample captured at each port during the experiments was transferred completely to the plastic gas sample bag. This is because if the volume of the gas sample captured is bigger than the volume of the plastic sample bag, when we transfer the gas the pressure drops below the dew point and condensate drops out in the fluid sampling tubing. However, the gas is moving faster than the condensate so the gas in the plastic sample bag may not be the same as the captured gas. For this reason, a 0.4 m long tubing was connected to the valve on each port. The other end of the tubing was fitted with another valve. Before taking samples, the tubings were vacuumed and the valves were closed. A sample was taken by opening the valve on the core holder, waiting for 30 seconds and closing it. The sample could be then transferred to the plastic sample bag. The pressure transducers were not connected to the tubing at this stage, to simplify the hardware configuration.

3.2.4. Gas Chromatography (GC)

The composition was determined by Gas Chromatography (GC).

> "Chromatography is a separation process that is achieved by distributing the substances to be separated between a moving and a stationary phase. Those substances distributed preferentially in the moving phase pass through the chromatographic system faster than those that are distributed preferentially in the stationary phase. Thus the substances are eluted from the column in the reverse order of the magnitude of their distribution coefficients with respect to the stationary phase" (Scott, 1998).

If the moving phase is gas, then the process is called gas chromatography. Conversely, if the moving phase is liquid then the process is called liquid chromatography. Evidently, the moving phase has to be an inert material that serves only to move the substances.

A block diagram representing the principle of gas chromatography is shown in the Figure 3-12. A sample of mixture that needs to be analyzed is injected into a heated inlet, vaporized and swept by an inert carrier gas into a column packed or internally coated with a stationary liquid or solid phase, resulting in partitioning of the injected substances. The partitioning is normally achieved mostly based on the boiling points hence it is similar to distillation. Different components are moved along the column at different rates. The eluted components are then carried by the carrier gas into the detector. The concentration is normally related to the area under the detector time response curve.

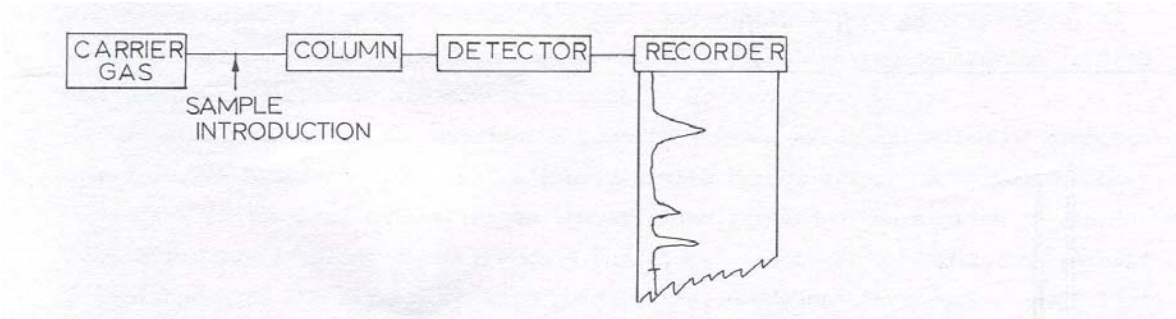

Figure 3-12: Principle of Gas Chromatography (from Perry, 1981)

The GC used for this study was an Agilent 3000 Micro GC (Figure 3-13). According to Agilent 3000 Micro Gas Chromatograph User Information, this device can be used to analyze natural gas, refinery gases, vent gas, landfill gas, water and soil headspace samples, mine gas, and furnace gas. The instrument uses self-contained *GC* modules, each consisting of an injector, columns, flow control valve, and a thermal conductivity detector (*TCD*). Samples are introduced through a 1/16 inch Swagelok connection to the inlet(s) on the front panel. This design eliminates the need for traditional hypodermic syringe injection through septa. The inlet pressure can be nearly atmospheric because an internal vacuum pump connected to the column exit eliminates column back pressure. The heart of the instrument is the *GC* module, which includes a heated injector, sample column, reference column, thermal conductivity detector (*TCD*), electronic pressure control hardware, gas flow solenoids, and control board. Operation can be better understood by examining what takes place during an analysis. The major steps include:

1. Injection
2. Separation
3. Detection

Injection

The gas sample enters the *GC* heated manifold. The manifold regulates the sample temperature and directs it into the injector. The injector then drives the sample into the column, while a vacuum pump helps draw the sample through the system.

Separation

After passing through the injector, the sample gas enters the column, which separates it into its component gases typically in less than 180 seconds. Gas chromatography works because different volatile molecules have unique partitioning characteristics between the column substrate and the carrier gas. These differences allow for component separation and eventual detection. The columns built into this *GC* are Molecular Sieves and Porous Layer Open Tubular. The Molecular Sieve is used for separation of small molecular weight gases by an exclusion process. Porous Layer Open Tubular (*PLOT*) columns are capillary columns where the stationary phase is based on an adsorbent or a porous polymer.

Detection

After separation in the column, the sample gas flows through a thermal conductivity detector (*TCD*). Carrier and sample gases separately feed into this detector, each passing over different hot filaments. The varying thermal conductivity of sample molecules causes a change in the electrical resistance of the filaments when compared to the reference or carrier filaments.

Electronic Pressure Control

The instrument controls the temperature, pressure, and flow electronically during the run and between runs, without operator intervention.

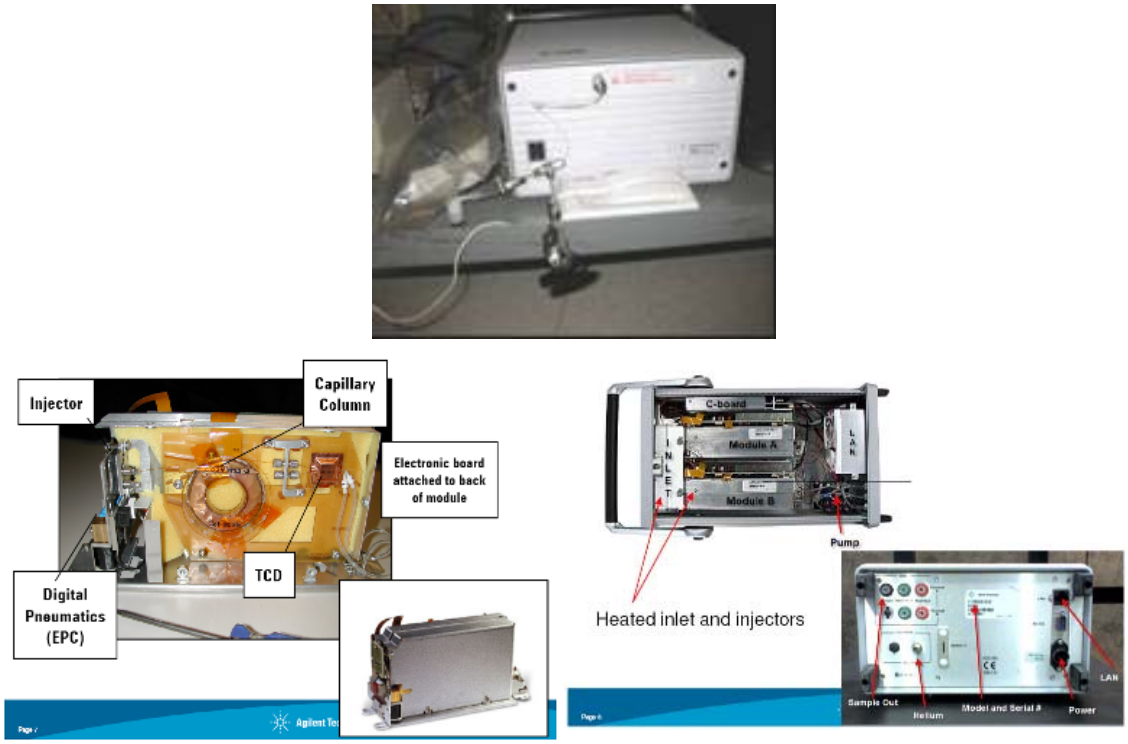

Figure 3-13: Agilent 3000 Micro *GC*.

The carrier gas used for this *GC* is Helium with an input pressure of 80-82 psi.

Before being used for compositional analysis, the *GC* needs be calibrated. Calibration is the process of relating detector response to the amount of material that produces that response by analyzing specially prepared calibration mixtures with known concentrations (Figure 3-14). Response factors calculated from the calibration are then used to convert the detector response area to the concentration to the gas mixture that needs to be analyzed. Calibration is also used for peak identification. As the gas mixture we analyzed consists of around 85% C_1 and 15% nC_4 in moles, a gas mixture standard with the mole composition of 85%-15% C_1-nC_4 was used to calibrate the *GC*. A single-level calibration and linear calibration curve fitting are sufficient. C_1 is detected in detector A

(Molecular Sieve). nC_4 is detected in detector B (*PLOT*). Table 3.1 lists the parameter setting for the *GC* in the analysis mode.

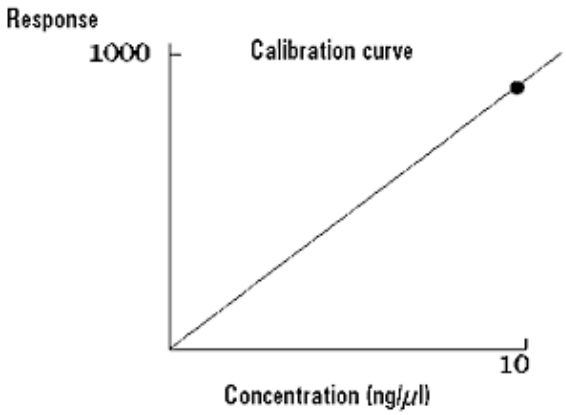

Figure 3-14: *GC* calibration (from Agilent Cerity Tutorial).

Table 3-1: Agilent 3000 Micro GC parameter setting

Parameter	Column A (Molecular Sieve)	Column B (PLOT)
Inlet Temperature	80°C	80°C
Injector Temperature	80°C	80°C
Column Temperature	100°C	125°C
Sample Pump	On, 30 s	On, 30 s
Inject Time	0 s	30 s
Backflush Time	12 s	NA
Run Time	160 s	160 s
Post Run Time	0 s	0 s
Pressure Equilibration Time	0 s	0 s
Column Pressure	On, 35 psi	On, 32 psi
Post Run Pressure	35 psi	32 psi
Detector Filament	On	On
Detector Sensitivity	Standard	Standard
Detector Data Rate	50 Hz	50 Hz
Baseline Offset	0 mV	0 mV

After being calibrated, the *GC* is ready to analyze the composition of gas samples taken during the experiments. A typical gas chromatogram of the samples is shown in Figure 3-15.

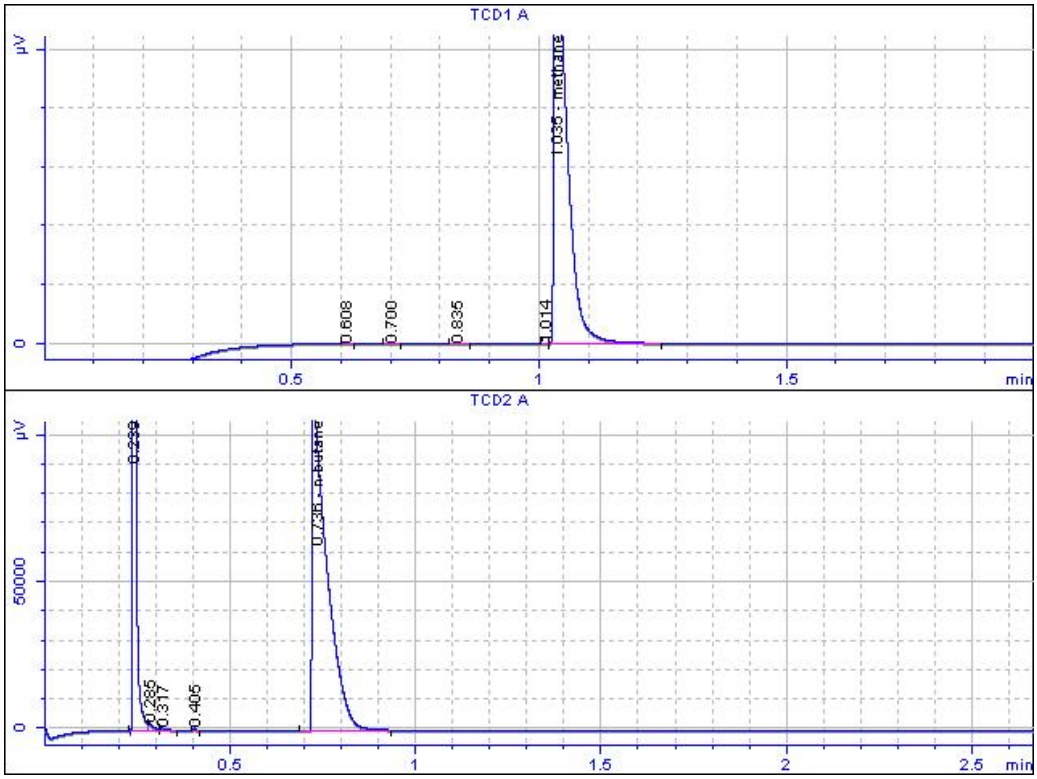

Figure 3-15: A typical gas chromatogram of gas samples taken during experiments.

3.2.5. Computerized Tomography (CT) Scanner

Computerized tomography is a nondestructive method that can be used to observe dynamic single and multiphase flow in the rock, and to measure the rock's petrophysical properties.

The basic measurement principle of the *CT* scanner is described in the following paragraphs and illustrated in Figure 3-16.

A collimated X-ray source rotates around the object and the X-ray penetrates a thin slice of the object "A" at different angles. The transmitted X-ray intensity is recorded. From the projections, a cross-sectional image is constructed. Three-dimensional *CT* images can also be reconstructed from sequential cross-sectional slices taken as the object moves through the scanner. The basic quantity measured in each volume element (voxel) is linear attenuation coefficient, μ_A as defined from the Beer's law:

$$I = I_0 e^{-\mu_A h} \tag{3-1}$$

where I_0 is the incident X-ray intensity, I is the intensity after passing through the material "A" with a thickness of h.

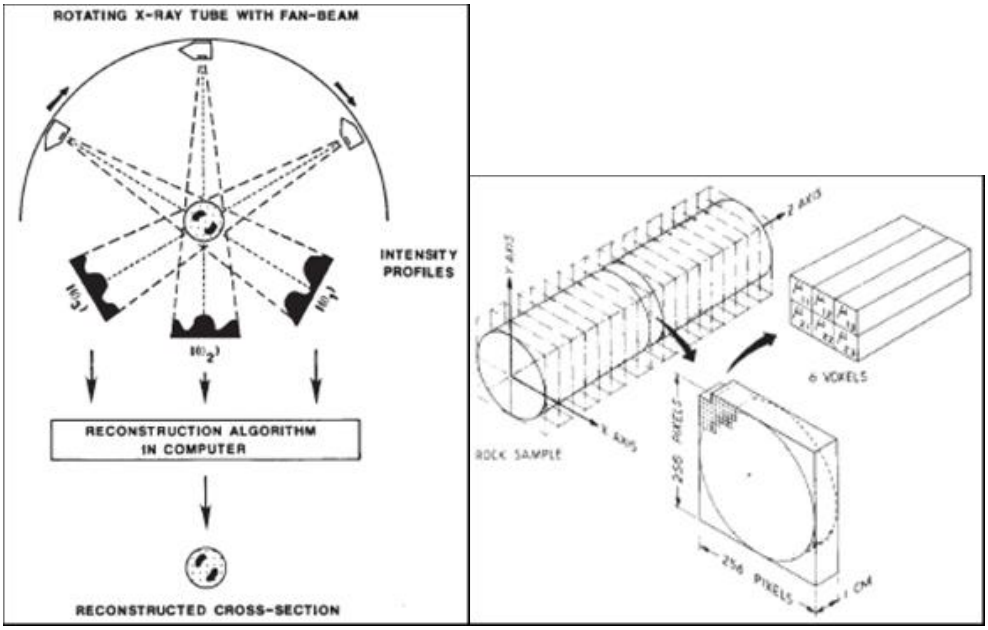

Figure 3-16: Principle of *CT* scanner (from Vinegar and Wellington, 1987).

For a heterogeneous medium, the energy transmitted along a particular ray path is:

$$\ln\left(\frac{I}{I_0}\right) = \int_o^L \mu_A h dh \tag{3-2}$$

Beer's law assumes that the X-ray beam is narrow and monochromatic. In practice, the beam is polychromatic, which can lead to image artifacts.

After image construction, the computer converts the linear attenuation coefficient into CT number by normalizing with the linear attenuation coefficient of water (μ_w):

$$CT_A = 1000\frac{\mu_A - \mu_w}{\mu_w} \tag{3-3}$$

The units of *CT* number are Hounsfield (H). Air is -1000 H and water is 0 H.

In this study, the GE HiSpeed *CT*/i scanner was used to quantify the saturation distribution along the core during the experiments (Figure 3-17). For two-phase systems and three-phase systems where the third phase is immobile, a single energy level scan is sufficient to determine the saturations. The condensate saturation (S_c) is calculated using Equation (3-4):

$$S_c = \frac{CT_{\exp} - CT_{gr}}{CT_{cr} - CT_{gr}} \tag{3-4}$$

The subscripts *exp*, *gr* and *cr* represent the *CT* number of the rock during the experiment with the C_1-nC_4 mixture, C_1-saturated and nC_4-saturated rock, respectively. The parameters used for *CT* scanning are listed in Table 3-2.

Figure 3-17: GE HiSpeed *CT*/i.

Table 3-2: GE HiSpeed CT/i scanner settings.

Anatomical Reference	SN
Scan Type	Axial, Full 1 s
Gantry tilt	0°
SFOV	Head
kV	140
mA	200
Prep Group	1 s
ISD	3 s
Smart Scan	Y
DFOV	25 cm
Matrix Size	512x512

3.3. Experimental Procedures

3.3.1. Gas Mixing

The gas mixing procedure is a revised version of the one developed by Shi (2009). In order to have component mole percentage of 85% methane and 15% n-butane in moles, 5.6 moles n-butane and 31.6 moles methane are needed to fill the 3,920 ml volume of the piston cylinder at 2,000 psi. n-butane is usually stored in the liquid state with the tank pressure at around 35 psig. According to Figure 3-18, at room temperature (70°F), n-butane is in liquid phase as long as the fluid pressure is above 30 psi. The liquid n-butane can thus be transferred to an empty piston cylinder by gravity. Methane is supplied in high pressure cylinders, so the methane can be directly transferred to the piston cylinder by the high pressure difference.

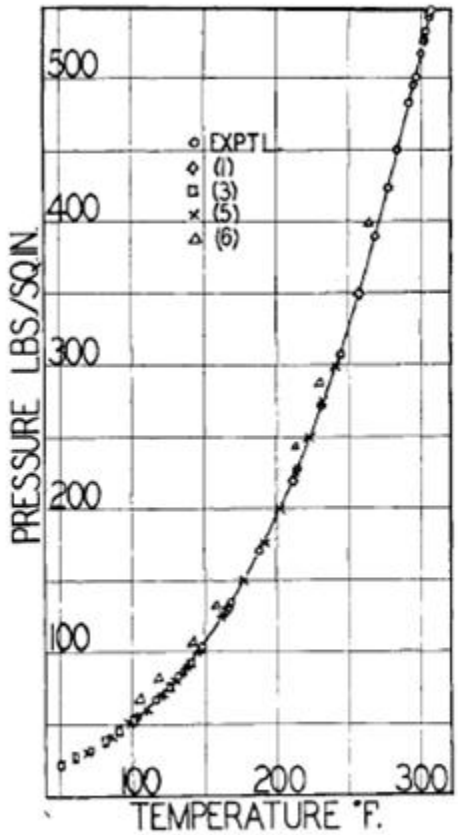

VAPOR PRESSURE OF *n*-BUTANE

Figure 3-18: Vapor pressure of n-butane (from Kay, 1940).

Figure 3-19 and Figure 3-20 show the whole process of mixing the liquid n-butane with gaseous methane. Firstly, the piston was pushed all the way down using nitrogen gas. The piston cylinder was vacuumed from the lower end as shown in Figure 3-19(a) and Figure 3-20(a). At the same time, the metal tubing connecting to the water pump was also vacuumed to eliminate the air in tubing line. The valve connected to the vacuum pump was closed and deionized water (*DI* water) was then pumped to the vacuumed cylinder. The water was pumped at a rate of 4.5 cc/minute to minimize the air dissolved in the injection water. If the piston was not pushed all the all down before vacuuming and pumping water, the water would flow in the piston cylinder by differential pressure at high rate hence air would be dissolved in the water. The volume of water pumped was measured by marking the water levels on the water bottle before and after pumping. The pump can also be set to shut down automatically if the pressure in the cylinder increases above 500 psi to make sure that the cylinder is full of water. After finishing pumping, valves were closed and the metal tubing was disconnected at the valve position. A long plastic tubing was connected to the cylinder. The piston cylinder was positioned at a 45 degree angle from horizontal such that the piston was on the low side. The long tubing connecting the piston cylinder was pulled vertically and the other end of the tubing (fitted with a valve) was put in a higher position compared to the position of the piston cylinder (Figure 3-20(b)). The valves were opened to allow overpressured water and dissolved gas

to escape from the long plastic tubing. The water-filled piston cylinder stayed in that position for about 1 hour to allow the dissolved air to escape out of the water. A wooden stick was used to hit the cylinder body gently every 10 minutes to help the gas to migrate up and come out of the water. The valve at the end of the plastic tubing was closed. The long plastic tubing was full of water.

Secondly, a space in the piston cylinder was needed for liquid n-butane transfer. 5.6 moles of liquid n-butane at room temperature has a volume of 539 ml so we needed to push to piston down to displace 539 ml of deionized water (539 g) from the piston cylinder to make space for the n-butane transfer. We injected low pressure nitrogen or shop air (90 psi) into the top of the water-filled piston cylinder. The next step was to open the valve at the end of the plastic tubing so that the nitrogen/air pushed the piston down and expelled the water out from the bottom. Water was collected in a beaker and weighed on a digital scale. The valve at the end of the long plastic tubing was closed when the amount of displaced water reached 539 g (Figure 3-19(b) and Figure 3-20(c)). The nitrogen/air source was then disconnected from the system and the nitrogen/air was allowed to escape from the top of the piston cylinder.

Thirdly, the n-butane cylinder was connected to the piston cylinder as shown in Figure 3-19(c) and Figure 3-20(d). The tubing and the top part of the piston cylinder were vacuumed. The n-butane cylinder was put upside down and in a higher position such that the liquid n-butane could flow directly into the piston cylinder by gravity. After vacuuming, the valve connected to the vacuum pump was closed and the valve on the n-butane bottle was opened for n-butane transfer. The practice was to wait about half an hour after the pressure indicated by the pressure gauge on the n-butane cylinder stopped dropping. Then the valve on the n-butane cylinder and the valve on the top of the piston cylinder were closed. 5.6 moles n-butane had therefore been transferred successfully into the piston cylinder.

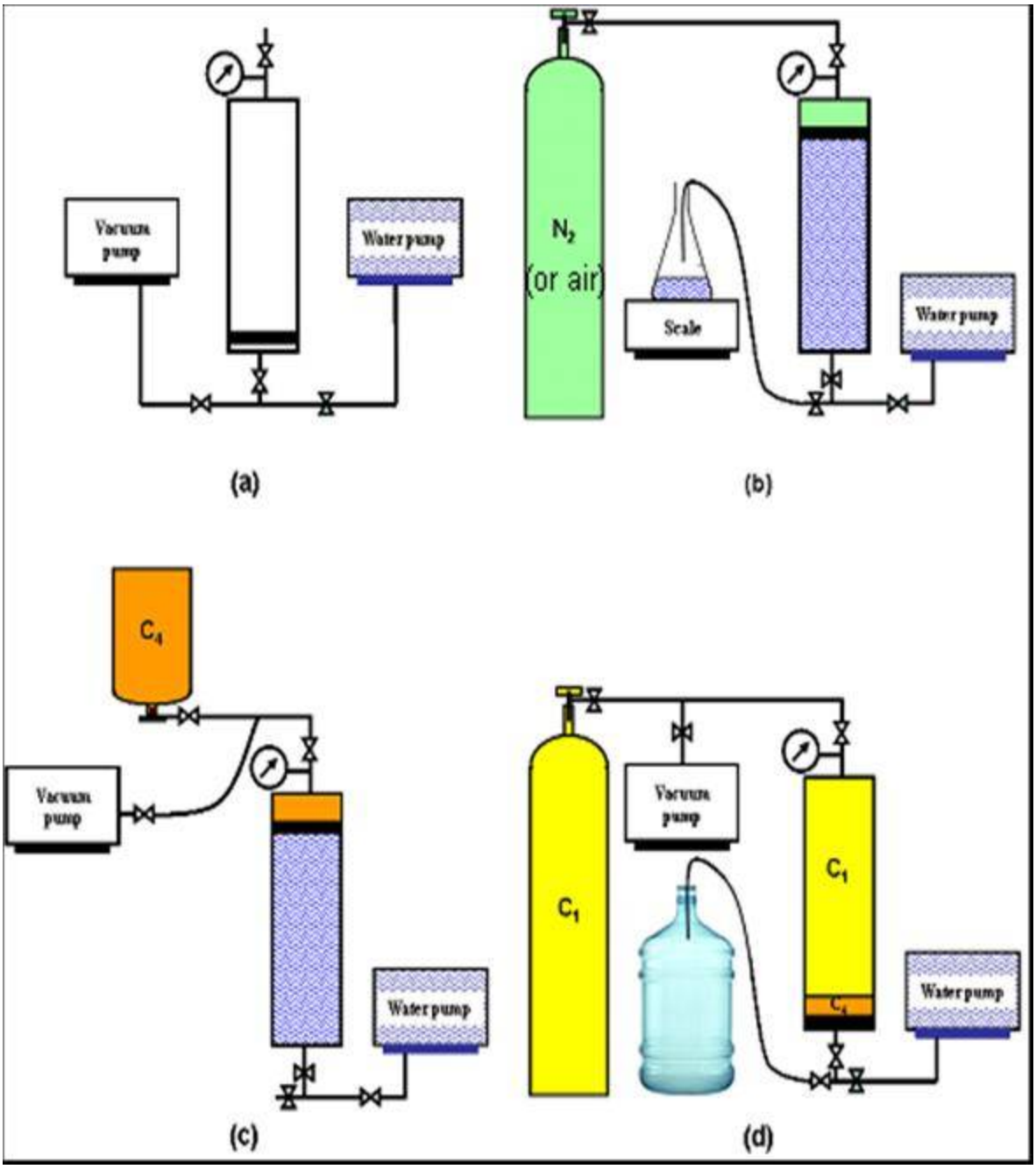

Figure 3-19: Schematics of gas-condensate mixing (modified from Shi, 2009).

(a) (b)

(c) (d)

(e)

Figure 3-20: Gas-condensate mixing.

Lastly, the n-butane cylinder was disconnected, and the methane cylinder connected to the piston cylinder partially filled with n-butane as in Figure 3.19(d) and Figure 3-20(e). The next step was to vacuum the connecting tubing and inject the methane directly into

the piston cylinder and discharge all the remaining water from the bottom of the piston cylinder to the water bottle. When the pressure was stable, the tubing connected between the methane bottle and cylinder was disconnected at the cylinder position. The cylinder was then shaken. The pressure in the cylinder would drop as liquid n-butane vaporized. The whole process of transferring methane to the cylinder was repeated until the pressure reached 2,000 psi and the pressure did not drop after shaking. Because the full methane bottle had a pressure of only 2,300 psi, to save gas a low pressure methane bottle (less than 1,800 psi) was used for displacing the water and a high pressure (more than 2,000 psi) was then used to fill the cylinder to reach the final pressure of 2,000 psi. At the final pressure of 2,000 psi, roughly 32 moles of methane were transferred to the piston cylinder at room temperature. Hence the mole percentage of the methane in the mixture is about 85%. Varying the supply pressure on the methane cylinder using a pressure regulator, the composition of the mixture can be adjusted. The piston cylinder was shaken 100 times to allow the methane and n-butane to be fully mixed. The final composition of the mixture was determined accurately by *GC* composition analysis. The mixture was ready for use when a sample taken when the cylinder was upright and a sample taken when the cylinder was upside down had the same composition. Before the experiments, as we will mention later in Section 3.3.4, the gas-condensate mixture was pressurized up to 2,200 psi using nitrogen gas pushing on the back of the piston.

3.3.2. Absolute Permeability Measurement

The absolute permeability of the core was measured using nitrogen gas. Nitrogen was injected into the core at different input pressures. The output pressure was atmospheric. Downstream gas flow rates were measured by the volume of water displaced from the upside-down glass graduated cylinder over a fixed period of time. The gas permeability was calculated using the formula:

$$k_{gas} = \frac{2\mu_{gas} p_{out} q_{out} L}{A(p_{in}^2 - p_{out}^2)} \tag{3-5}$$

The Klinkenberg effect was corrected by plotting gas permeability versus reciprocal of average pressure between the input and output pressures and reading off the permeability value at the intercept with the permeability axis.

3.3.3. Porosity Measurement

The porosity was measured using the standard mass balance method. The core was heated in an oven for 4 hours and left to cool down in a sealed container. The mass of the core was measured. After that, the core was vacuumed, and then saturated using deionized water. After 8 hours of being saturated with deionized water, the surface of the core was dried using a semiwet paper and the core was weighed again. The difference between the weights before and after saturating the rock is the mass of the deionized water occupying the pore volume. As the density of deionized water is known, we were able to calculate the pore volume hence the porosity (the core geometry is known).

3.3.4. Gas-condensate Core Flooding Experiments

Two types of experiments were performed in this study: noncapture and capture. The difference between them was that in the noncapture experiments the samples were taken while the fluid was flowing, while in the capture experiments fluid flowed through the core for a given time period then both inlet and outlet valves were closed at the same time. The samples were then taken from the "captured" fluid. At the end, the remaining fluid in the core was discharged to an empty cylinder to determine the composition of the condensate dropout left in the core. These experimental procedures were modified from the previous procedures to achieve repeatability of the results.

Noncapture Experiments

In the noncapture experiment, the whole system was vacuumed overnight and the core was presaturated with C_1 at 2,200 psi. The gas-condensate cylinder was compressed to 2,200 psi (dew-point pressure of the 85%-15% moles C_1-nC_4 is around 1,840 psi) using nitrogen pushing on the back of the piston inside the cylinder. The gas-condensate mixture was then flushed through the core to displace C_1 with the downstream pressure at 2,000 psi (about 160 psi above the dew-point pressure of the gas mixture).

The first step of the procedure was to inject C_1 directly into the vacuumed core. This was done to make sure that the gas mixture was in the gaseous state in the core and we could flush the gas mixture through to core to displace methane without dropping below the dew-point pressure of the gas mixture. The C_1-nC_4 mixture was flushed through the core for 10 minutes. Then the downstream valve was closed, and the core contents sampled through the sample tubes. The first five batches of samples were discarded to eliminate all residual methane in the dead volumes of the sampling ports. The sample tubings were vacuumed and samples were taken under no-flow conditions. After demonstrating good repeatability under no-flow conditions, the sample tubings were vacuumed again. The gas-condensate mixture was flushed through the core at 1,000 psi differential pressure for 3 minutes, and flow samples were taken. Both upstream and downstream valves were then closed. To avoid artifacts in X-ray CT images, the sample tubings were removed before scanning. The plastic handles of the valves on the core holder were also removed. The core was then scanned in the X-ray CT scanner to determine the saturation distribution.

The compositional behavior under different well flowing bottom-hole pressure (*BHP*) control was then investigated using the noncapture experiments. The experimental procedure was to keep the same upstream pressure but vary the downstream pressure and measure the composition corresponding to each downstream pressure. The core could also be scanned to determine the saturation distribution.

Finally, we studied the effect of repressurization on revaporization of the condensate. Due to the relative permeability effect and difference in mobilities of the gas and condensate phases, the overall in-situ composition changes thereby shifting the phase

envelope of the gas condensate (shown earlier in Figure 1-4). In this case, shutting in a well may not be a good strategy because the condensate may not revaporize back to gas. The procedure of the repressurization experiment was to first perform all the steps for the noncapture experiment. After taking the flow samples, we shut the downstream valve and let the pressure in the core build up to 2,200 psi. After 35 minutes, samples along the core were taken. The saturation distribution was also determined by *CT* scanning. This procedure mimics the real situation in which a well is producing in a gas-condensate reservoir: after the *BHP* drops below the dew-point pressure, and the well is shut in in an attempt to achieve condensate revaporization.

Capture Experiments

Capture experiments were designed to have flow samples under conditions in which both upstream and downstream valves were closed so the samples would be closer to static composition rather than that of the flowing gas. Furthermore, the captured condensate in the core could be discharged to an empty cylinder to determine the composition of the condensate dropout.

The whole system was vacuumed overnight and the core was presaturated with C_1 at 2,200 psi. The original procedure had been to presaturate with C_1 at 2,000 psi. The gas-condensate cylinder was compressed to 2,200 psi (dew-point pressure of 85%-15% molar C_1-nC_4 is around 1,840 psi) using nitrogen pushing on the back of the piston inside the cylinder. The gas-condensate mixture was flushed through the core for 10 minutes with the downstream pressure at 2,000 psi (about 160 psi above the dew-point pressure of the gas mixture). This was done to make sure that the gas mixture was in the gaseous state at the inlet of the core and we could flush the gas mixture through to core to displace methane without dropping below the dew-point pressure of the gas mixture (original procedure was at 2,000 – 1,950 psi differential pressure so it had been difficult to remove the methane out of the core). The C_1-nC_4 mixture was flushed through the core for 10 minutes. Then the downstream valve was closed and the fluids sampled. The first five batches of samples were discarded to eliminate all residual methane in the dead volumes of the sampling ports. The sample tubings were vacuumed and samples were taken under no-flow conditions.

After demonstrating good repeatability under no-flow conditions, the sample tubings were vacuumed and the gas-condensate mixture was flowed through the core at 1,000 psi differential pressure for 3 minutes. Then the upstream and downstream valves were closed simultaneously. Fluid samples were taken in capture mode immediately. At the end, the entire content of the core was discharged into an empty (vacuumed) cylinder for compositional analysis.

After scanning the core during noncapture experiments, we found out that the titanium core-holder had caused X-ray beam hardening which can affect the measurement results for saturation. We decided not to use the *CT* scanner for subsequent experiments.

3.3.5. Gas-condensate, Immobile Water Core Flooding Experiments

The core holder was vacuumed for 48 hours if there was some water in the core previously. The vacuum pump was connected at the outlet of the core holder, the inlet valve was closed. After that, the water pump was connected to the inlet of the core holder. The inlet valve was opened. Deionized water was pumped in while keeping the vacuum pump on. The vacuum pump was turned off and disconnected when water reached the tubing at the outlet. The estimated time was calculated based on the water pumping rate and the pore volume. Water pumping was continued to displace about four pore volumes to eliminate any air trapped in the core. The upstream of the core holder was then lifted to an angle about 30 degrees from horizontal. C_1 was injected through the core at 50-100 psi for two to three hours to drain the water to immobile water saturation S_{wi}. The sample tubings were also bled off from time to time to release trapped water. The core holder was then put back to the horizontal position, the downstream valve was closed and the core was filled with C_1 at 2,200 psi. The capture and noncapture experiments were performed in the same way as for the previous gas-condensate system without water. No *CT* scanning was used for the gas-condensate-immobile water experiments.

3.3.6. Compositional Measurement

The gas samples that needed to be analyzed were collected in Tedlar gas sample bags. The bag can be connected directly to the *GC* for analysis. A T-connector was used to vacuum the whole system before injecting the sample into the *GC* in order to protect the sample from being contaminated by air. For each gas sample, at least two runs through the GC were conducted to make sure the result was consistent. It was also noticed that to have good results the *GC* needs to be conditioned regularly to remove residuals on the detectors. This involves baking the *GC* at high temperature for a given period and calibrating the *GC* again, as outlined in the user manual.

3.3.7. Saturation Measurement

Measurements with the X-ray *CT* scanner are subject to a variety of errors and image artifacts including positioning error, beam hardening, object shape, and obstruction.

Positioning error was eliminated in this study by fixing the core holder on the table of the *CT* scanner and performing all scans without moving it, as shown in Figure 3-21.

The X-ray source of the *CT* scanner delivers a spectrum of X-ray energies rather than single-level energy. The lower energies are absorbed in the core holder, rock and at the interfaces. Beam hardening is the process of increasing the average energy level of an X-ray beam by filtering out the low-energy photons. This creates an error in the linear attenuation measurement. In analyzing the rock, beam hardening can be reduced by using special core holder designs (surrounding the core colder with a cylindrical water jacket, using an aluminum core holder, etc.), moving to higher energy levels or calibrating the *CT* scanner to a *CT* number higher than that of water using a doped water solution. In this study, we tried to minimize the beam hardening by using higher energy level (140 kV).

Figure 3-21: Performing experiments in the *CT* scanning room.

The X-shaped artifacts created by the object shape are eliminated by the cylindrical design of the core holder which has the same circular cross-sectional shape as expected by the CT inversion algorithms (which are designed for the human body).

The scanning slices were chosen carefully to be located between the sample ports. The tubing and plastic valve handles were removed to make sure the scanning slices were clear of any obstruction to achieve the best result possible (Figure 3-22 and Table 3-3). Slice #1 is on the upstream of P_1, slice #2 is between P_1 and P_2, etc., and slices #7 and #8 are on the downstream of P_7.

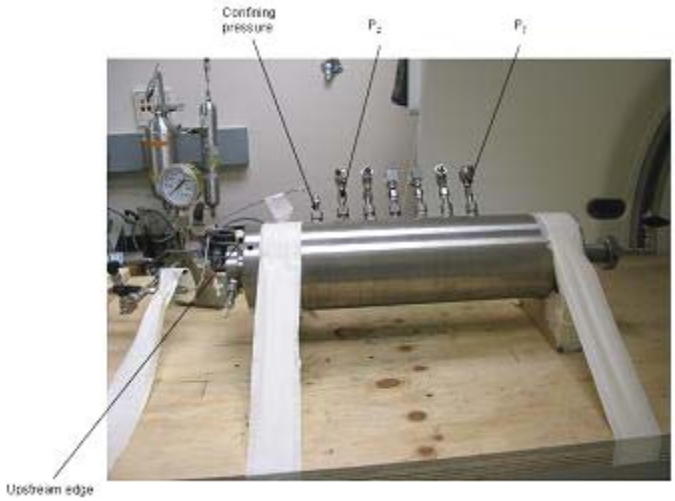

Figure 3-22: Core holder set up for *CT* scanning.

Table 3-3: Scanning positions

Slice	Distance from the upstream edge of the core holder (mm)	Thickness of the slice (mm)
1	118	3
2	158	3
3	198	3
4	238	3
5	278	3
6	318	3
7	358	3
8	370	3

In order to calculate the saturation at experimental conditions, we need CT_{gr}, CT_{cr}, CT_{exp}. CT_{gr}, CT_{cr} to be measured at a pressure of about 1,600 psi which is close to the average pressure along the core during the experiment. To saturate the core with liquid n-butane at 1,600 psi, liquid n-butane was first transferred to an empty piston cylinder then nitrogen was used to push on the back of the piston. After being saturated with methane or liquid n-butane at 1,600 psi, the core was left for 30 minutes to make sure all pores were filled.

Chapter 4

4. Results and Discussions

4.1. Absolute Permeability Measurement

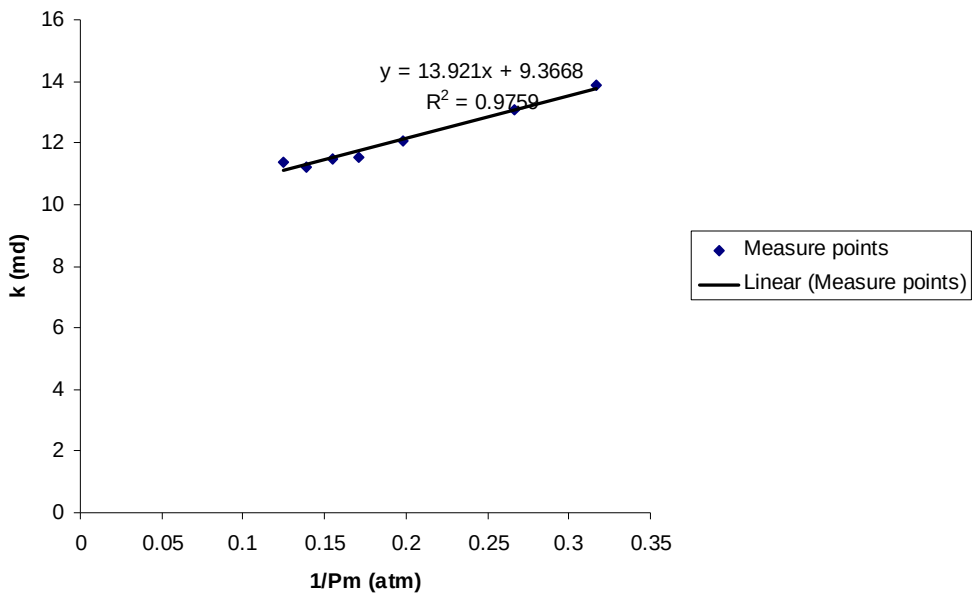

Figure 4-1: Absolute permeability measurement using nitrogen

Figure 4-1 shows a plot of nitrogen permeability versus $1/p_m$. The liquid permeability is the value of the intercept with the vertical axis, or 9.3 md in this case.

4.2. Porosity Measurement

Using the material balance method, the porosity of the core was measured to be around 16%.

4.3. Composition

4.3.1. *Gas-Condensate Core Flooding Experiments*

Noncapture Experiments

The compositional distribution along the core during a gas-condensate noncapture experiment is shown in Figure 4-2. No-flow samples were taken before the flow test when the gas mixture was above the dew-point. The no-flow compositions were repeated perfectly and were identical to the composition from the source cylinder. This

confirmation indicated that the rock does not have an effect on the (static) phase behavior of the gas mixture.

During flow through the core, going from left to right, the pressure drop was higher. Liquid dropped out in the core and accumulated in the rock. The flowing mixture became lighter (more C_1) and the concentration of nC_4 in the flowing phase along the core decreased.

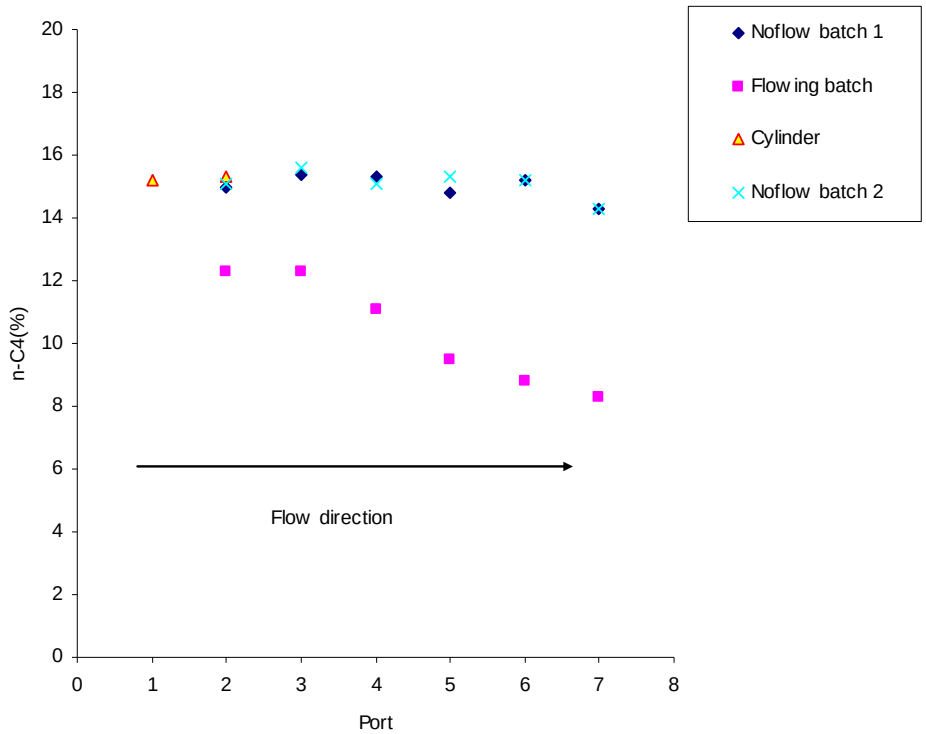

Figure 4-2: Gas-condensate noncapture experiment 1: nC_4 in the flowing mixture.

Figure 4-3 and Figure 4-4 show two more noncapture experiments following the same procedure. The compositional distributions along the core confirm the result in Figure 4-2. These results also confirm the three-region theory shown earlier in Figure 2-11 and the simulations results in Figure 3-6.

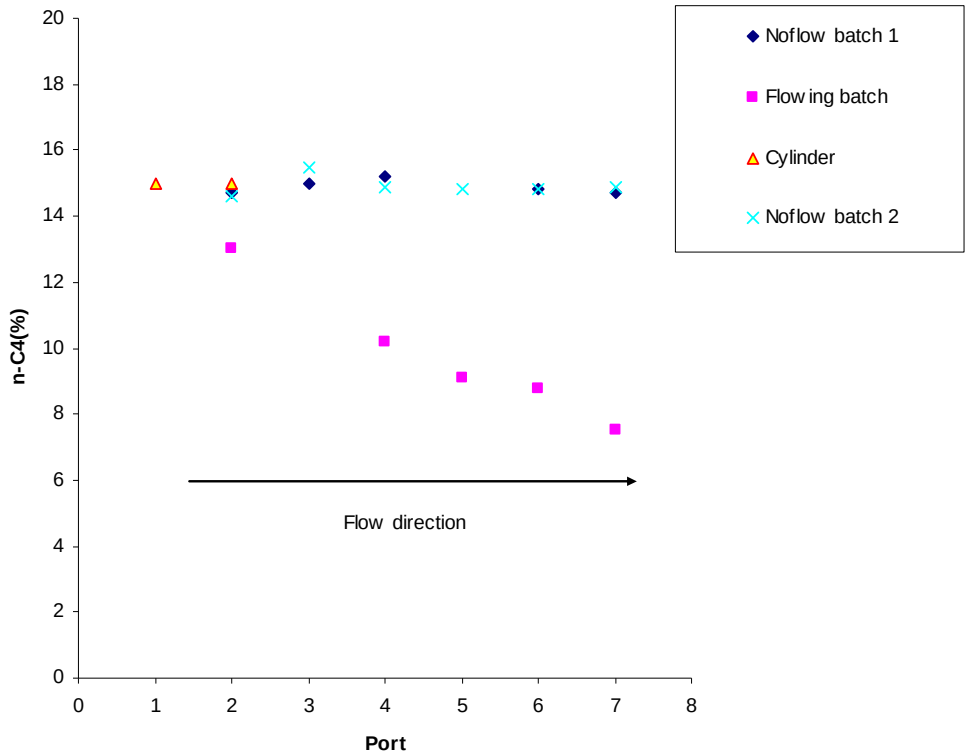

Figure 4-3: Gas-condensate noncapture experiment 2: nC_4 in the flowing mixture.

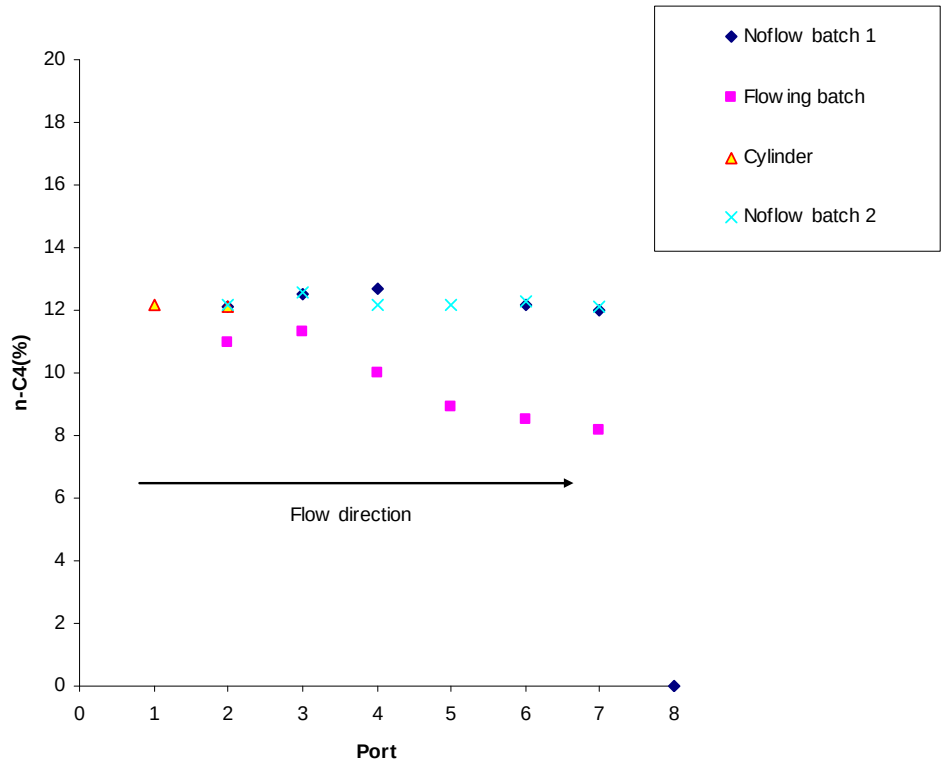

Figure 4-4: Gas-condensate noncapture experiment 3: nC_4 in the flowing mixture.

The effect of producing pressure (BHP in a real well) on the composition is shown in Figure 4-5. The result in Figure 4-5 shows that the higher the pressure drop below the dew-point the more nC_4 accumulates in the condensate, and the less nC_4 is found in the flowing mixture. This result confirms the simulation result reported previously by Shi (2009). This finding is important because it tells us a way to minimize the condensate banking by minimizing the pressure drop below the dew-point by either producing the well at higher pressure or applying partial pressure maintenance (using gas cycling for example).

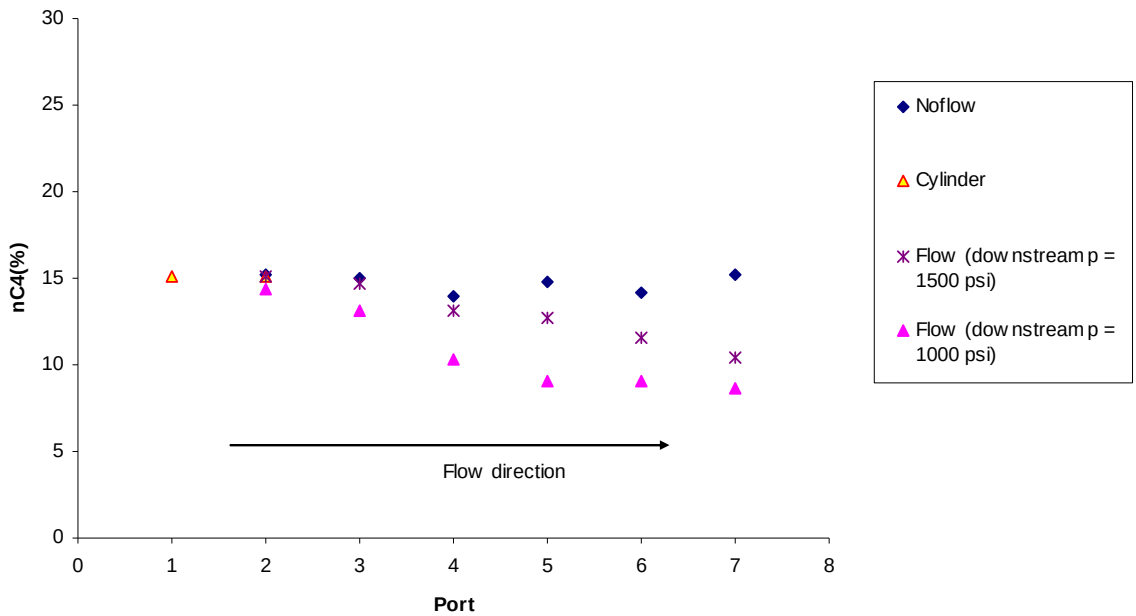

Figure 4-5: Gas-condensate noncapture experiment: nC_4 in the flowing mixture with different BHP control cases.

The results of revaporization experiments are shown in Figure 4-6 to Figure 4-8 in three different experiments. In the first experiment (Figure 4-6), composition during flow was not registered. However in the other two experiments (Figure 4-7 and Figure 4-8) it is clear that the composition changes after flow stops, but not all the way back to the original gas composition. Hence we can see that after 35 minutes the condensate does not revaporize fully back into gas. This confirms the shift of the phase envelope and hence that shutting the well is not an effective strategy to remove the condensate bank.

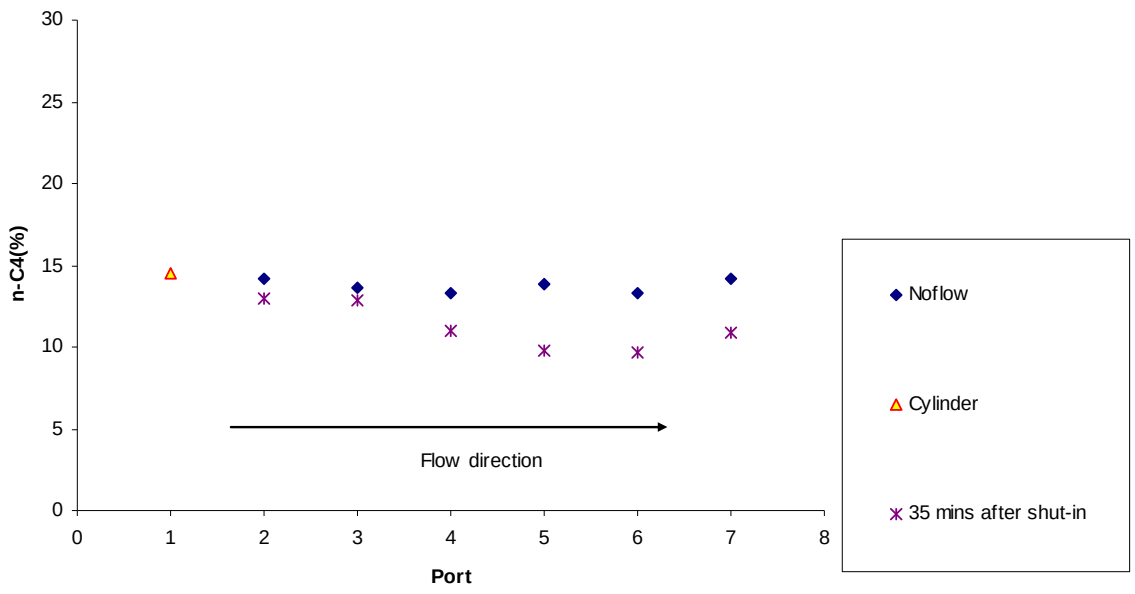

Figure 4-6: Condensate revaporization after noncapture experiment for gas-condensate system 1.

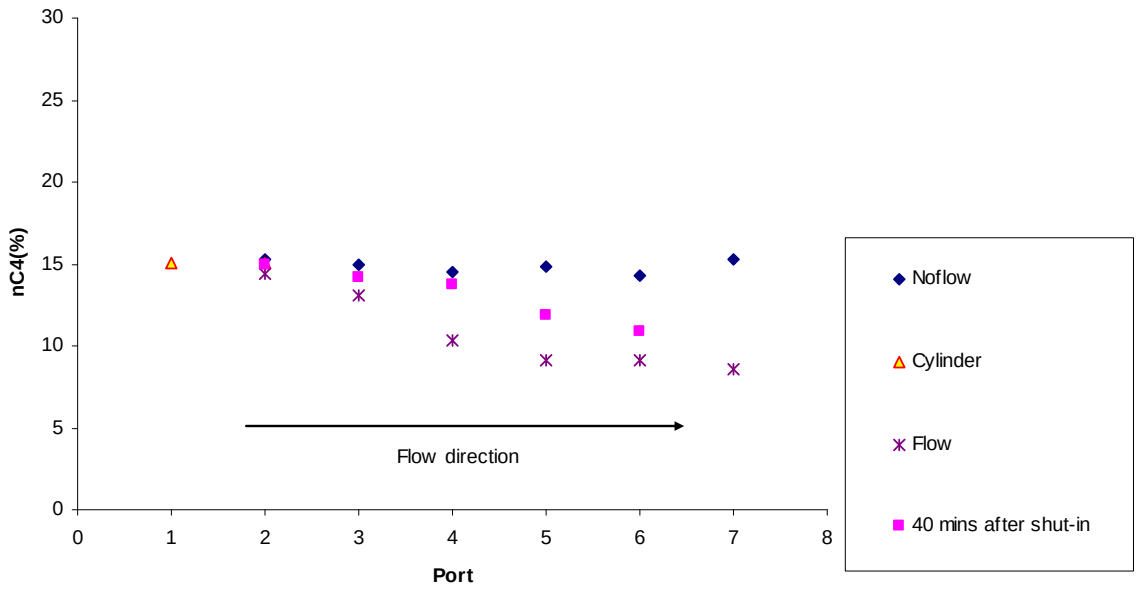

Figure 4-7: Condensate revaporization after noncapture experiment for gas-condensate system 2.

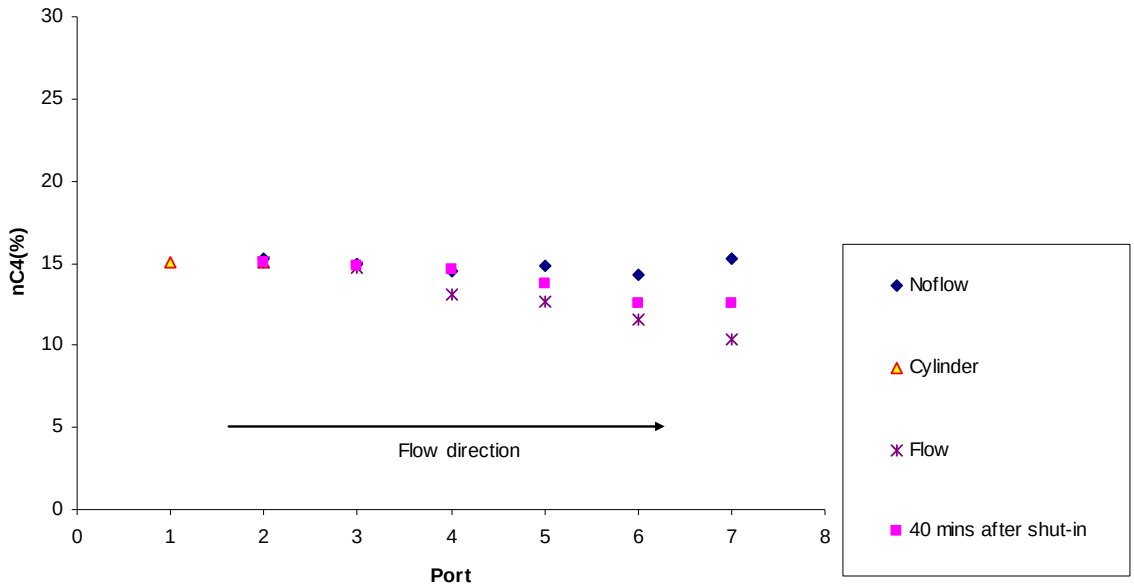

Figure 4-8: Condensate revaporization after noncapture experiment for gas-condensate system 3.

Capture Experiments

The results of a capture experiment are shown in Figure 4-9. Good repeatability was achieved under both static conditions and flowing conditions. The compositional distribution along the core shows a similar trend of liquid dropout as the trend seen during noncapture experiments. A second capture experiment also confirmed the result (Figure 4-10).

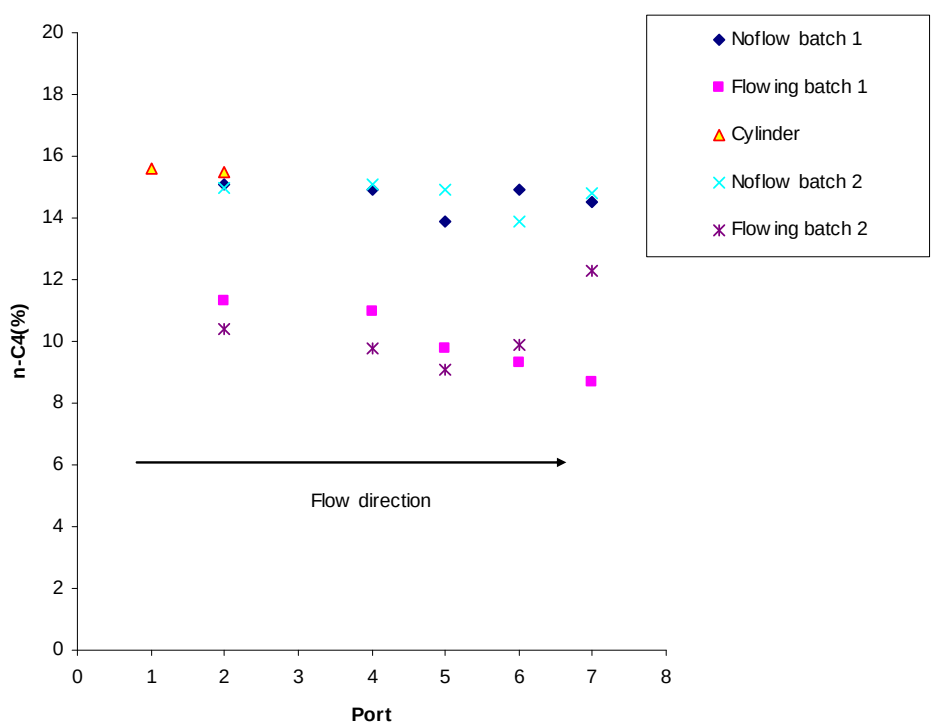

Figure 4-9: Gas-condensate capture experiment 1.

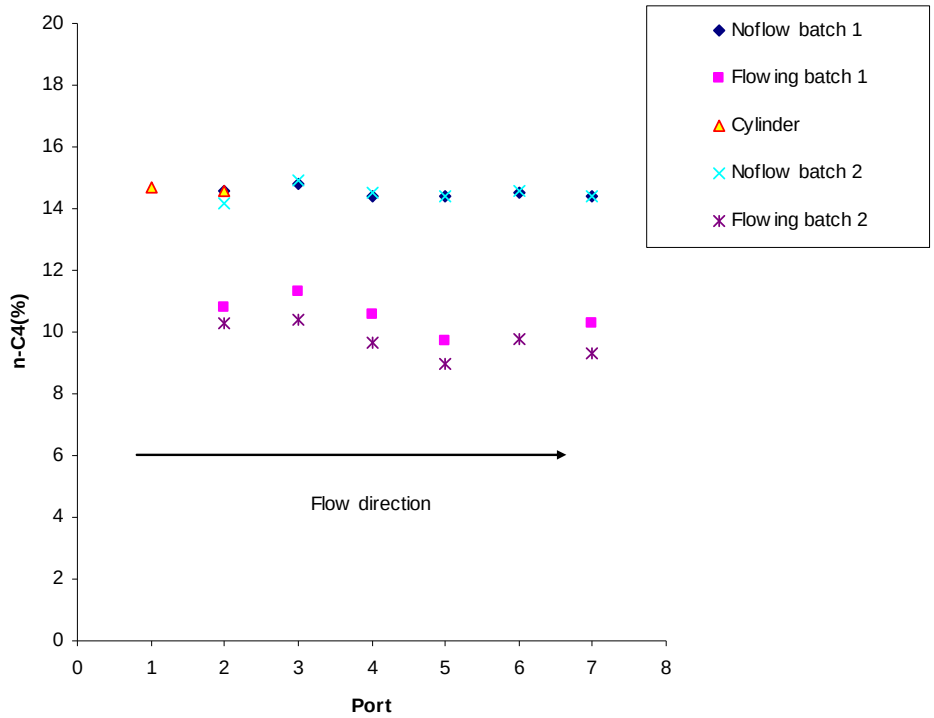

Figure 4-10: Gas-condensate capture experiment 2.

Figure 4-11 shows the result of another capture experiment. However in this case, after taking samples in the capture mode, we discharged all gas and condensate into a vacuumed empty cylinder. When the core and discharge cylinder reached pressure equilibrium (at low pressure), we disconnected the core from the cylinder and took samples from each of them. The nC_4 compositions in the discharge cylinder and core were very high, which confirmed that the liquid condensate that had deposited in the core was rich in nC_4.

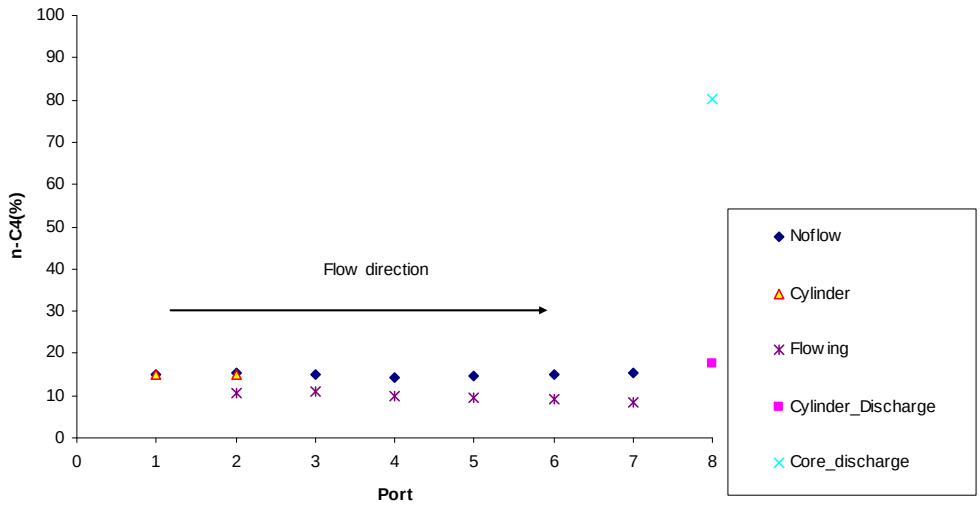

Figure 4-11: Gas-condensate capture experiment 3.

4.3.2. Gas-Condensate-immobile Water Core Flooding Experiments

Noncapture Experiments

Comparing Figures 4-2 to 4-8 (without water in the core) to Figures 4-12 and Figure 4-13 for the system with immobile water in the core, it is clear that in the presence of immobile water condensate still dropped out in the core. The higher the pressure drop, the more liquid dropped out in the core and accumulated in the rock. The flowing mixture became lighter (more C_1) and the concentration of nC_4 in the flowing phase decreased.

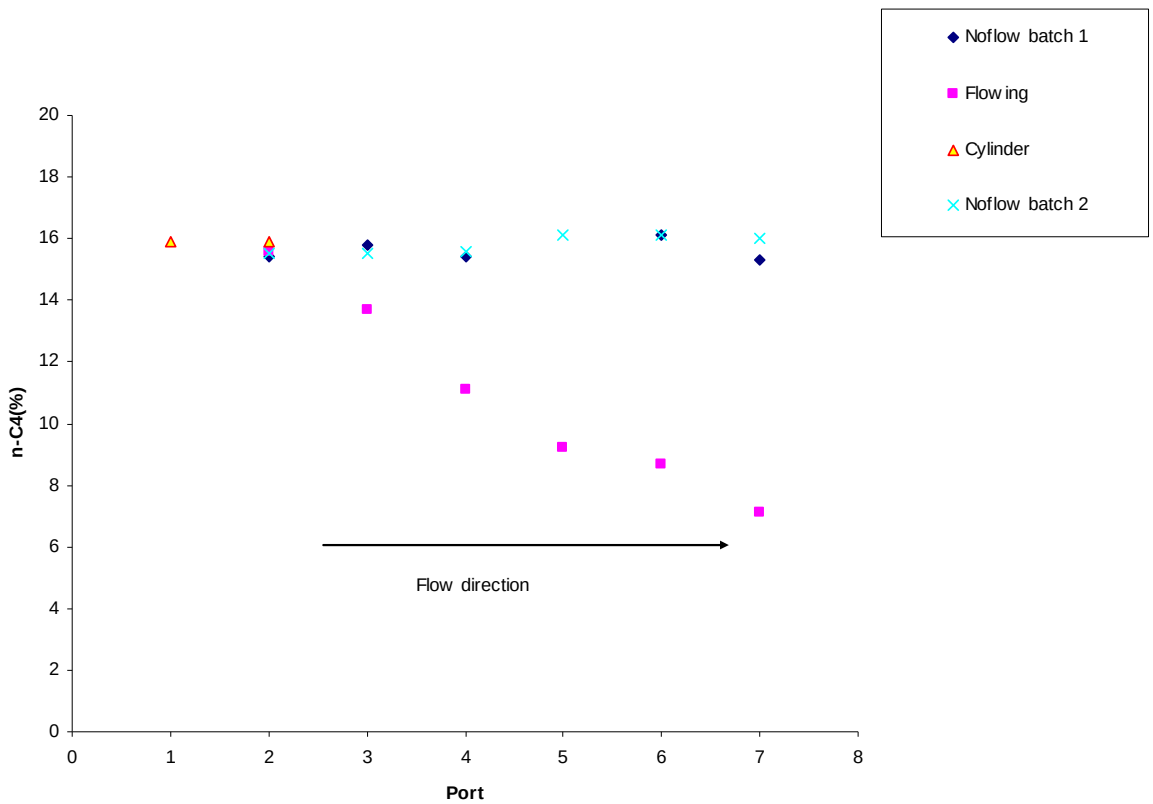

Figure 4-12: Gas-condensate-immobile water noncapture experiment 1: nC_4 in the flowing mixture.

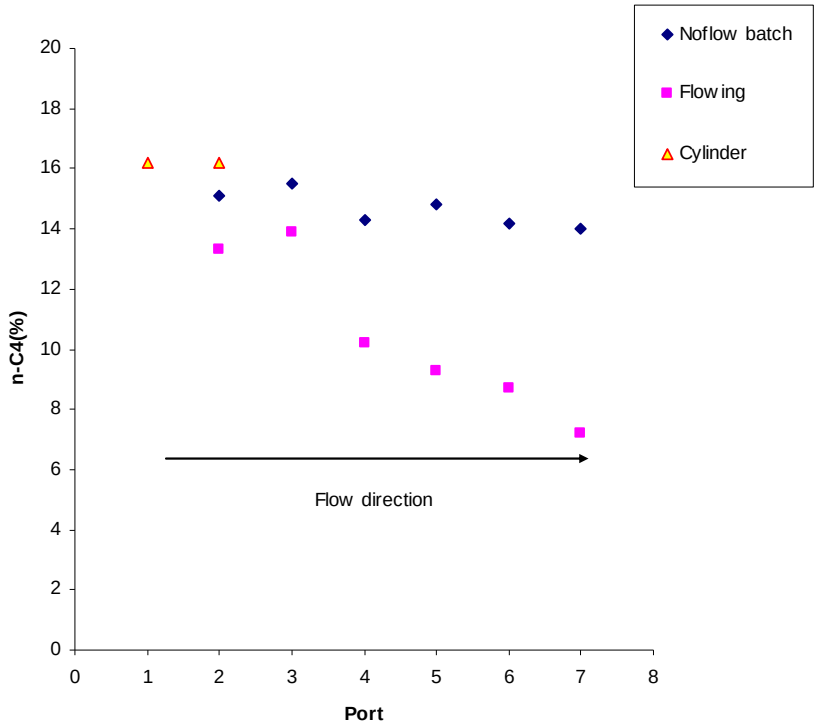

Figure 4-13: Gas-condensate-immobile water noncapture experiment 2: nC_4 in the flowing mixture.

Capture Experiments

Again, water did not have any significant effect on the compositional variation (Figure 4-14 and Figure 4-15). Condensate drop-outs were the same as in the two-phase system in Figures 4-9 to 4-11. The nC_4 compositions of the discharge cylinder sample and core samples also increased, which further confirmed the accumulation of nC_4 in the condensate that had dropped out in the core.

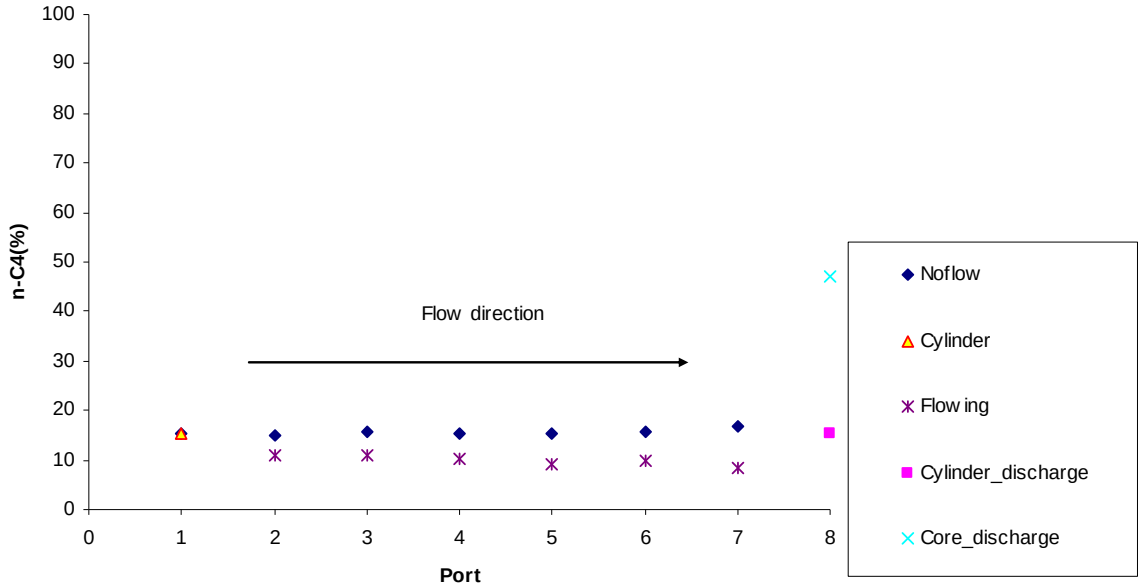

Figure 4-14: Gas-condensate-immobile water capture experiment 1.

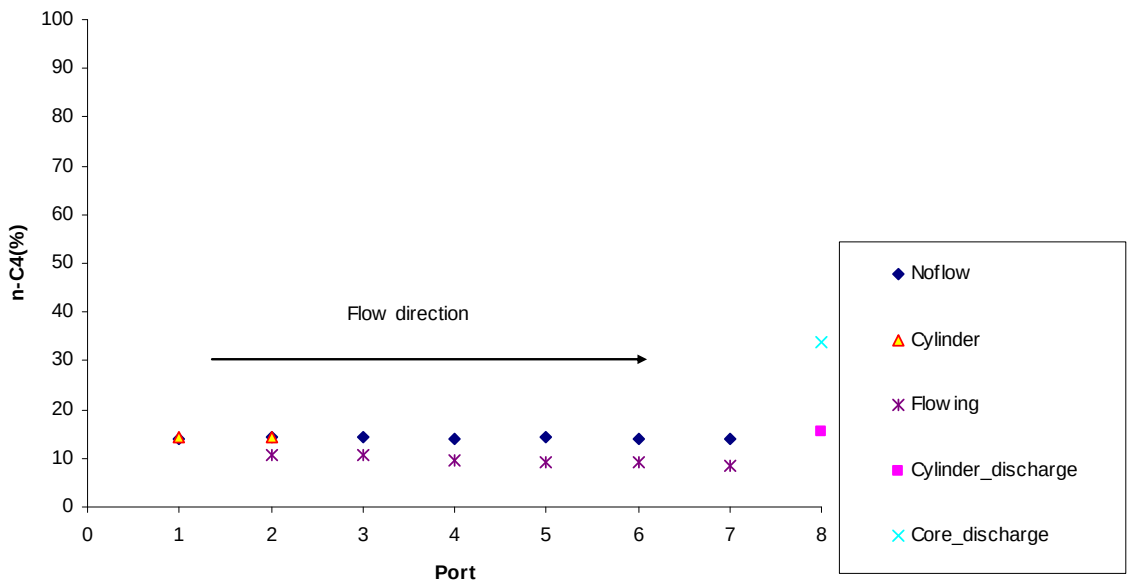

Figure 4-15: Gas-condensate-immobile water capture experiment 2.

4.4. Saturation

Figures 4-16 shows condensate saturation distribution calculated from *CT* scanning. Slice #1 is on the upstream of P_2, slice #2 is between P_1 and P_2, etc., and slices #7 and #8 are on the downstream of P_7. The condensate saturation profile is consistent with the nC_4 compositional profile, even though the saturation value estimated at slice #8 is suspect. It should be noted that due to the low porosity rock, there is only a small density difference between the liquid n-butane and methane, so the difference between *CT* numbers of C_1-nC_4 mixture saturated, C_1-saturated and nC_4-saturated rock is not large. This limits the accuracy of the saturation estimation. Besides that, the titanium core holder caused beam hardening which reduces the signal to noise ratio and increased the measurement error.

Figure 4-17 shows scanning of the titanium core holder with only air and water inside (no core). Due to the beam hardening, the *CT* values of air and water inside the titanium core holder were falsely measured as -625 H and 837 H respectively whereas the correct values are -1000 H and 0 H respectively. Figure 4-18 shows *CT* scanning of air and water inside an aluminum tube. The *CT* number of air and water inside the aluminum tube were -965 H and -1 HA respectively which are very close to the correct values. Hence a high pressure aluminum core holder would be better than titanium for *CT* scanning as the aluminum is more transparent to the X-rays.

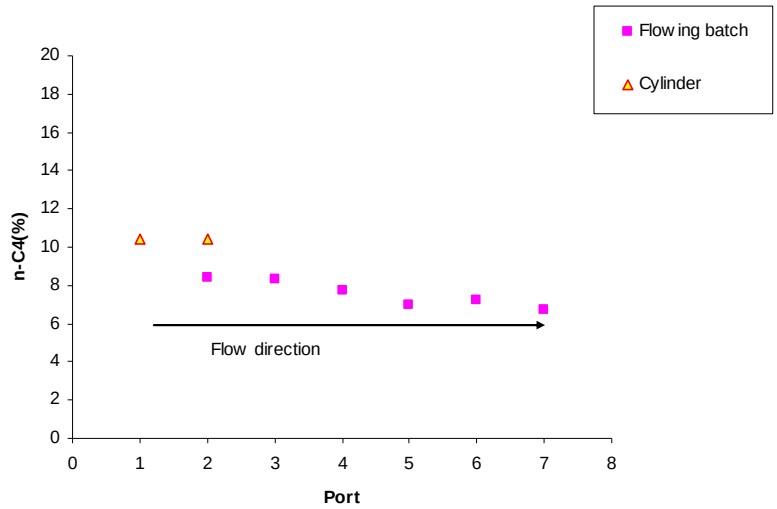

(a)

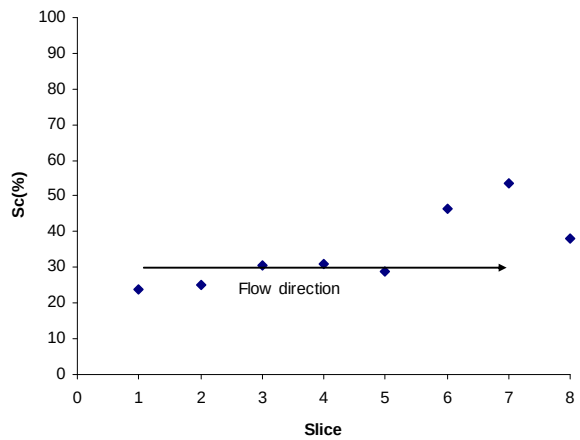

(b)

Figure 4-16: Gas-condensate noncapture experiment 3: (a) nC_4 in the flowing phases. (b) condensate saturation profile.

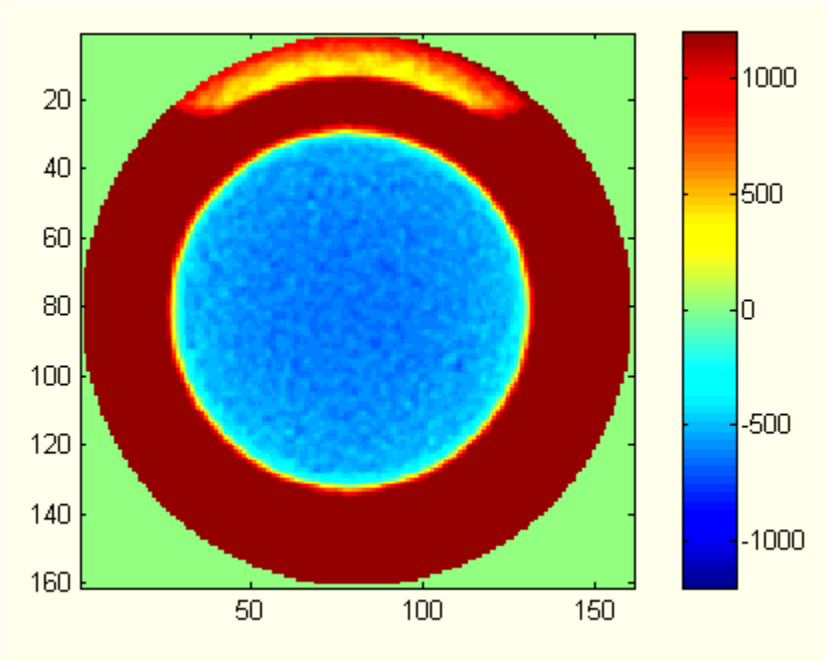

(a)

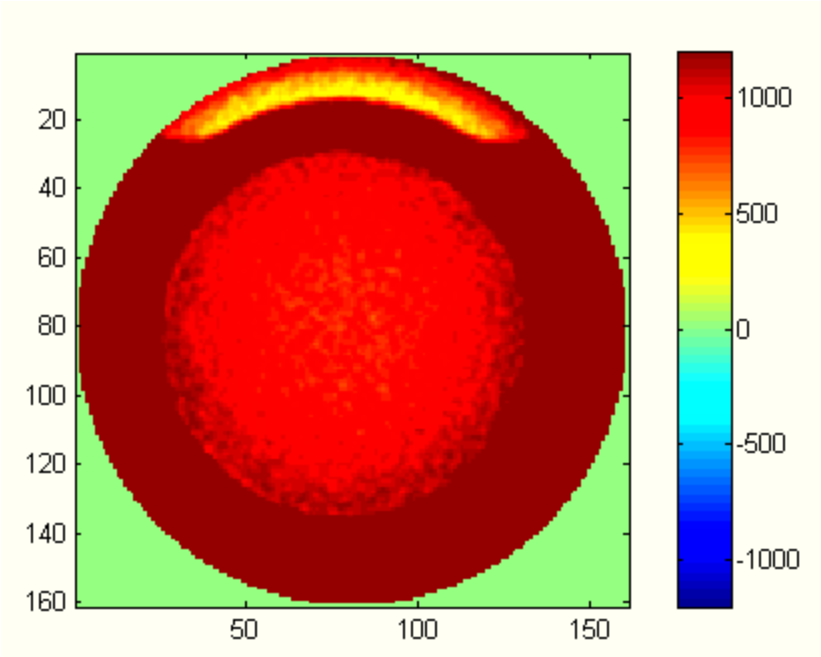

(b)

Figure 4-17: *CT* scanning of the empty titanium core holder: (a) with air inside. (n) with a water bottle inside.

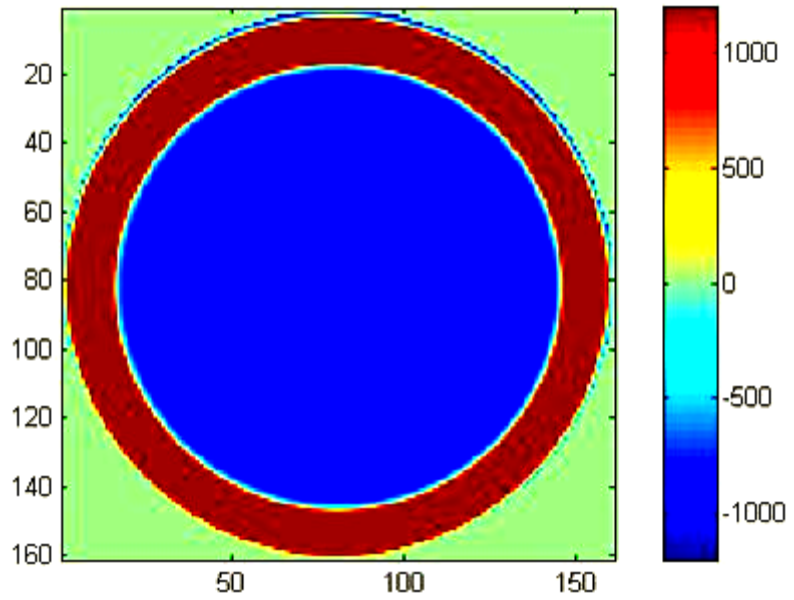

(a)

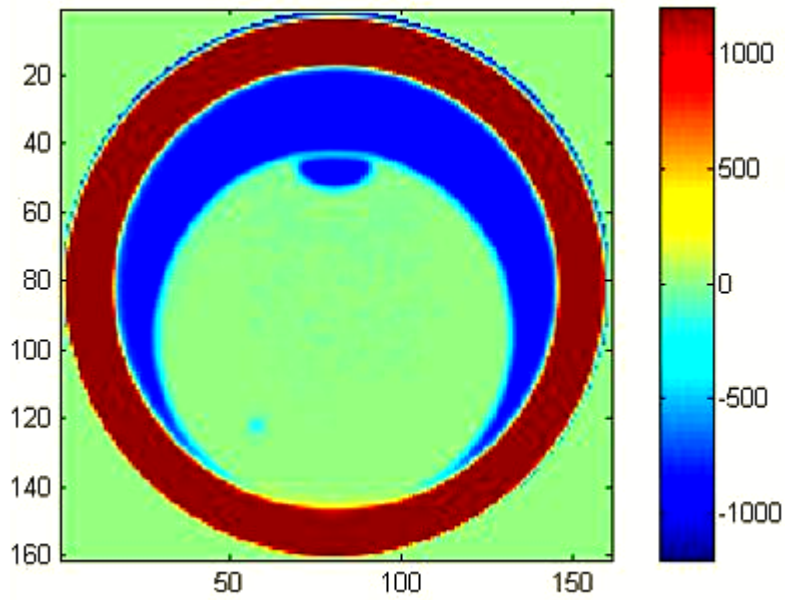

(b)

Figure 4-18: *CT* scanning of an aluminum tube: (a) with air inside. (b) with a water bottle inside.

Chapter 5

5. Theoretical Modeling of Compositional Variation

Compositional variation effect of the gas condensate system undergoing depletion has been seen from the simulation and experimental results in previous chapters. A theoretical knowledge of how the composition varies with time around a well is important to increase the conceptual understanding of the condensate banking dynamics. This chapter summarizes the theoretical model in the literature of how the condensate fluid mixture changes with time and presents some results using the theoretical model.

Neglecting dispersion, capillary pressure and gravity, the compositional conservation equation of component i^{th} in the region around the well with a volume V and surface area S can be defined as Equation (5-1):

$$\frac{\partial}{\partial t}\left(\phi \sum_{j=1,N_p} S_j \rho_j x_{i,j}\right) + \nabla \sum_{j=1,N_p} \rho_j x_{i,j}\left(-k\frac{k_{rj}}{\mu_j}\cdot\left(\nabla p_j\right)\right) = 0 \qquad \textbf{(5-1)}$$

where ϕ is the porosity; S_j, ρ_j, k_{rj}, ∇p_j are saturation, molar density, relative permeability, and pressure gradient of phase j respectively; $x_{i,j}$ is mole fraction of component i^{th} in phase j^{th}.

After a series of algebraic manipulations, we are able to have an equation that expresses the variation of the composition versus time in a cylindrical coordinate system as in Equation (5-2):

$$\frac{\partial z_i}{\partial t} = A_i \frac{\partial p}{\partial t} + B_i\left(\frac{\partial p}{\partial r}\right)^2 \qquad \textbf{(5-2)}$$

where:

$$A_i = \left(\frac{m_i}{m} - z_i\right)\frac{\partial \ln G}{\partial p} \qquad \textbf{(5-3)}$$

$$B_i = \frac{m_i}{\phi G}\frac{\partial}{\partial p}\left(\frac{m_i}{m}\right) \qquad \textbf{(5-4)}$$

$$m_i = \sum_{j=1,N_p} x_{i,j}\rho_j\left(k\frac{k_{rj}}{\mu_j}\right) \qquad \textbf{(5-5)}$$

$$m = \sum_{i=1,N_c} m_i \qquad \textbf{(5-6)}$$

$$G_i = \sum_{j=1,N_p} x_{i,j} \rho_j S_j \quad \textbf{(5-7)}$$

$$G = \sum_{i=1,N_c} G_i \quad \textbf{(5-8)}$$

A_i and B_i, coefficients of time derivative of pressure and pressure gradient respectively, are functions of relative permeability, viscosity, pressure, and PVT properties.

To explore the theoretical model, we used three different fluids consisting of methane and n-butane only. The mole fraction of the heavier component nC_4 varies from 0.15 to 0.25. The phase diagrams for the fluids are shown in Figure 5-1. Figure 5-2 shows *CCE* liquid dropout. At the reservoir temperature of 70°F, the fluid with 15% n-butane is a lean gas-condensate system; the fluid with 20% n-butane is rich gas-condensate system, while the fluid with 25% n-butane is light oil.

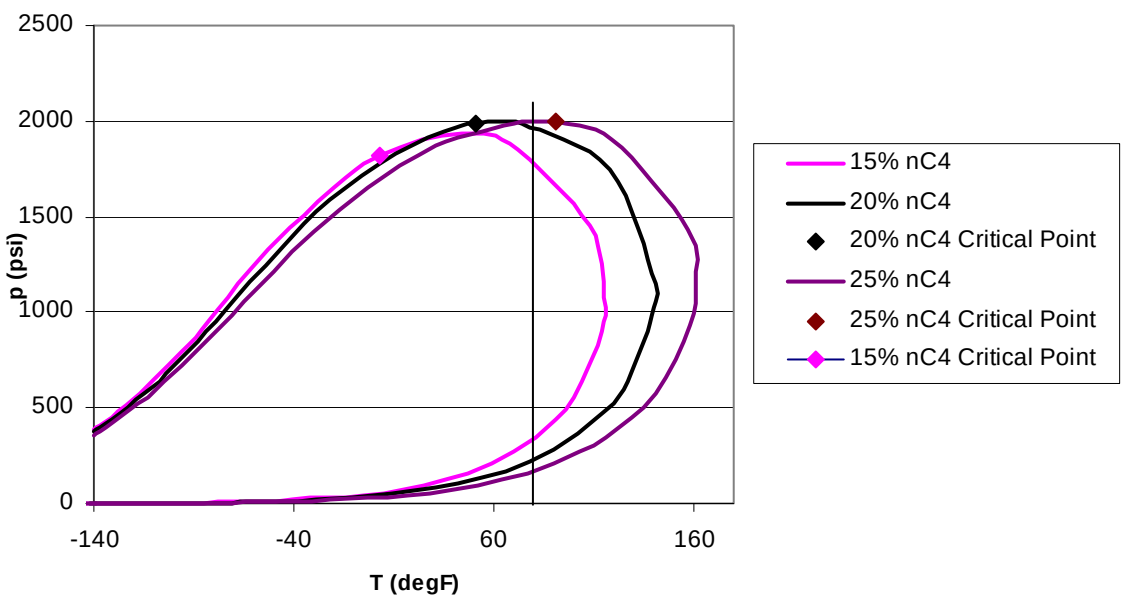

Figure 5-1: Phase diagram of the C_1- nC_4 systems.

The *PVT* properties and viscosity necessary for the theoretical modeling were calculated using a *PVT* simulator. The Peng-Robinson equation of state was used for the *PVT* properties calculation. The viscosity calculation was based on the Pederson correlation. Samples of *PVT* properties and viscosity are shown in Figure 5-3, Figure 5-4 and Figure 5-5.

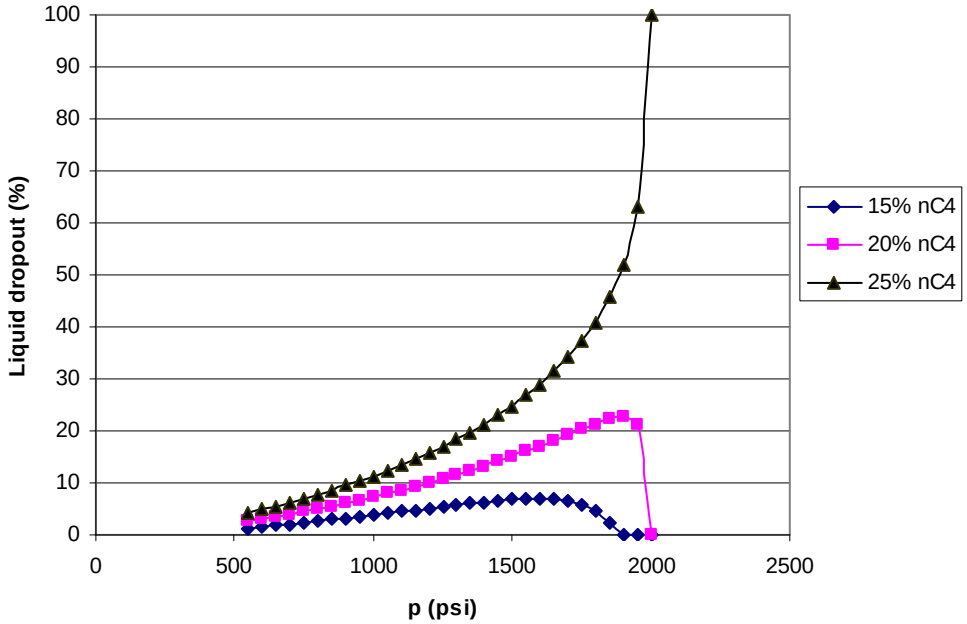

Figure 5-2: *CCE* liquid dropout of the C_1- nC_4 systems.

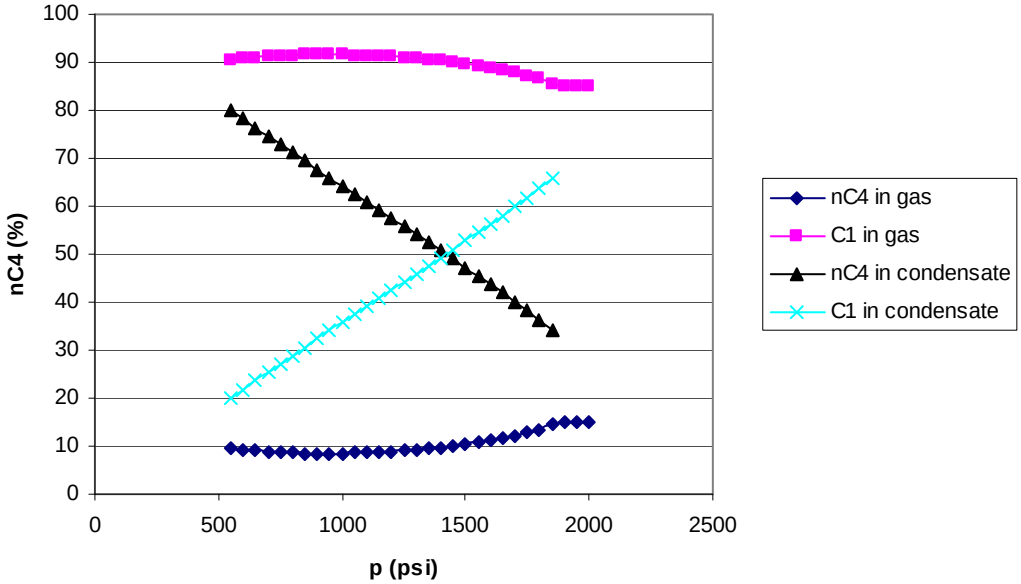

Figure 5-3: Component mole fractions of 85%-15% C_1- nC_4 mixture at 70°F.

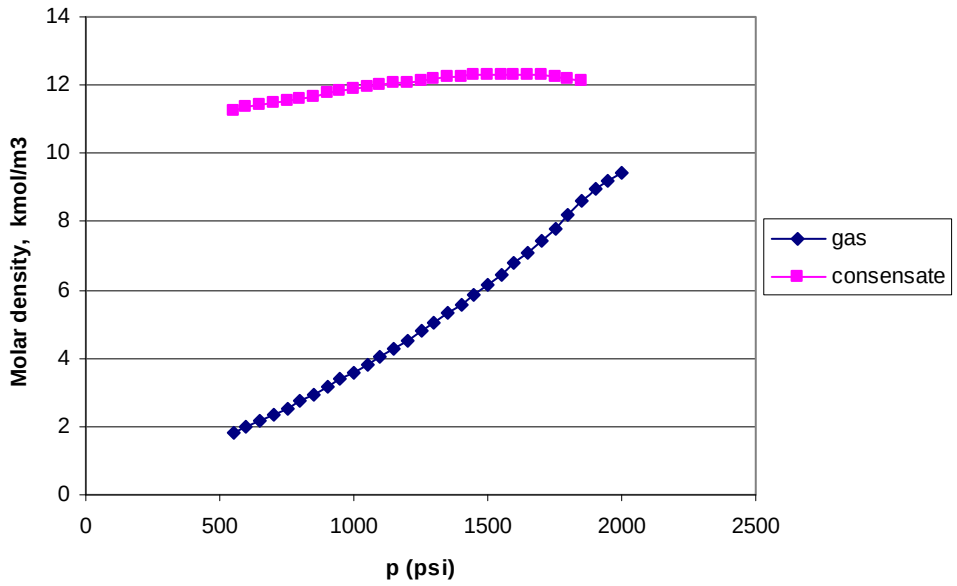

Figure 5-4: Phase molar density of 85%-15% C_1- nC_4 mixture at 70°F.

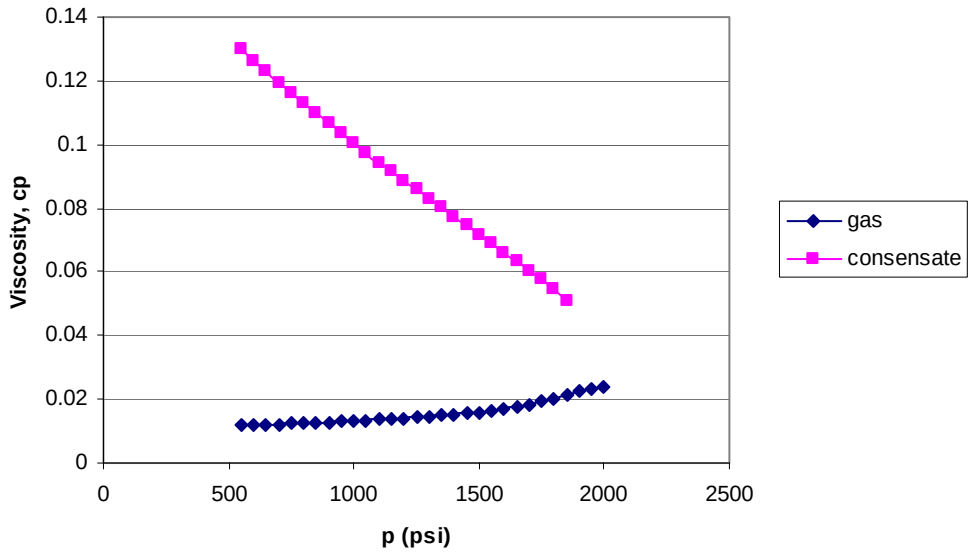

Figure 5-5: Phase viscosity of 85%-15% C_1- nC_4 mixture at 70°F.

The relative permeability model used in this study depends on the interfacial tension (*IFT*) to account for the influence of high interfacial tension between phases for the case that the gas condensate system is far away from the critical point. The *IFT* dependent relative permeability model was proposed initially by Coats (1980) then developed further by Bette et al. (1991) and Hartman and Cullick (1994). The relative permeability of condensate k_{rc} and permeability of gas k_{rg} at a specified saturation are related to the

completely immiscible and completely miscible relative permeabilities as in Equations (5-9) and (5-10):

$$k_{rc} = f(\sigma)k_{rci} + [1 - f(\sigma)]k_{rcm} \quad \textbf{(5-9)}$$

$$k_{rg} = f(\sigma)k_{rgi} + [1 - f(\sigma)]k_{rgm} \quad \textbf{(5-10)}$$

$$f(\sigma) = \left(\frac{\sigma}{\sigma^*}\right)^N \quad \textbf{(5-11)}$$

where σ is the *IFT*, σ^* is a reference *IFT*, *N* is an adjustable exponent.

The completely miscible k_{rcm} and k_{rgm} are X-shape curves and given by:

$$k_{rcm} = \frac{1 - S_{crg}(\sigma) - S_g}{1 - S_{crg}(\sigma)} \quad \textbf{(5-12)}$$

$$k_{rgm} = \frac{S_g}{1 - S_{gc}(\sigma)} \quad \textbf{(5-13)}$$

where:

$$S_{gc}(\sigma) = \left(\frac{\sigma}{\sigma^*}\right)S_{gc} \quad \textbf{(5-14)}$$

$$S_{crg}(\sigma) = \left(1 + 0.67\log\left(\frac{\sigma}{\sigma^*}\right)\right)S_{crgi} \quad \textbf{(5-15)}$$

The completely immiscible k_{rci} and k_{rgi} are condensate and gas relative permeabilities for the fluids at *IFT* values greater or equal to σ^*:

$$k_{rcm} = \left(\frac{1 - S_{crg}(\sigma^*) - S_g}{1 - S_{crg}(\sigma^*)}\right)^2 \quad \textbf{(5-16)}$$

$$k_{rgm} = \left(\frac{S_g}{1 - S_{gc}(\sigma^*)}\right)^2 \quad \textbf{(5-17)}$$

Figure 5-6 shows the calculated *IFT* versus pressure for the three binary fluids used in this study. *IFT* is almost independent of fluid type, and it decreases sharply with increasing pressure. Furthermore, the *IFT* is equal to zero at the dew point and above where only a single phase exists.

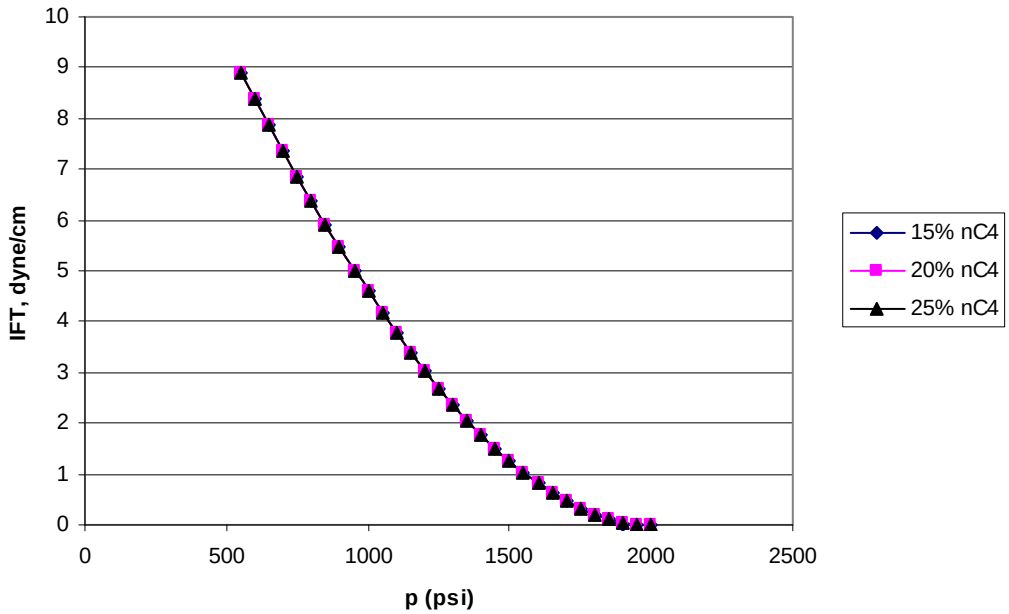

Figure 5-6: *IFT* versus pressure.

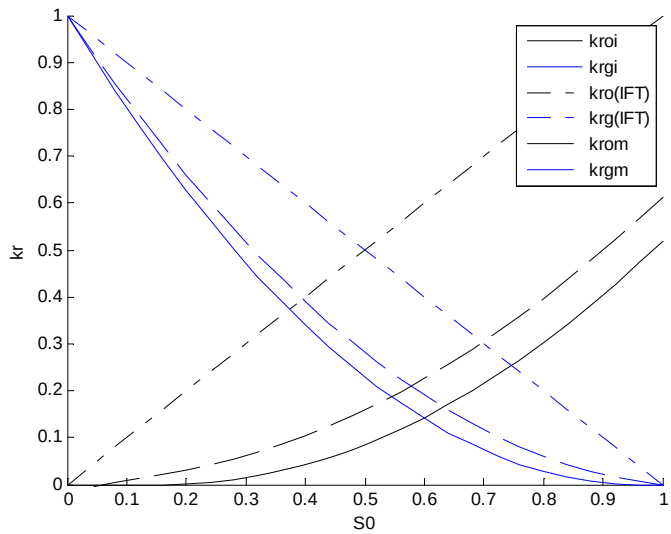

Figure 5-7: Different relative permeability models.

Figure 5-7 illustrates the *IFT* dependent relative permeability models. The completely miscible relative permeability model has an X-shape curve and it also has the lowest critical saturation thresholds. Consequently, for the case of complete miscibility, liquid and gas are easier to move than other cases. As the miscibility decreases in the fluid system, the distinction between phases is more so the phases need to overcome greater critical saturation to become mobile.

Figure 5-8, Figure 5-9 and Figure 5-10 show plots of mC_4/m versus pressure with different relative permeability models for different fluid types. In the lean gas-condensate case (zC_4= 0.15), mC_4/m values from different relative permeability curves show small difference. However, impact of relative permeability is higher in the case of the richer fluid (zC_4= 0.20 and zC_4= 0.25). The relative permeability from completely miscible treatment always has the highest mC_4/m value in all cases, and the completely immiscible treatment of relative permeability has the lowest mC_4/m value.

Plots of molar density G for different fluids are shown in Figure 5-11, Figure 5-12, and Figure 5-13.

Using G and mC_4/m as above, we were able to compute the A_{C4} and B_{C4} coefficients. Figures 5-14, 5-15, and 5-16 show plots of A_{C4}. First of all, we observe that A_{C4} is very small. Secondly, A_{C4} is negative. Thirdly, the impact of relative permeability is higher in the case of richer fluid. Finally, A_{C4} approaches zero as the pressure is at or above the dew-point pressure. Compared with term A_{C4}, term B_{C4} is about 1,000 times greater (Figure 5-17, Figure 5-18, and Figure 5-19). Again, the impact of relative permeability is higher in the case of richer fluid. Unlike A_{C4}, B_{C4} is positive when the pressure is above a certain threshold. Both A_{C4} and B_{C4} decrease as pressure decreases.

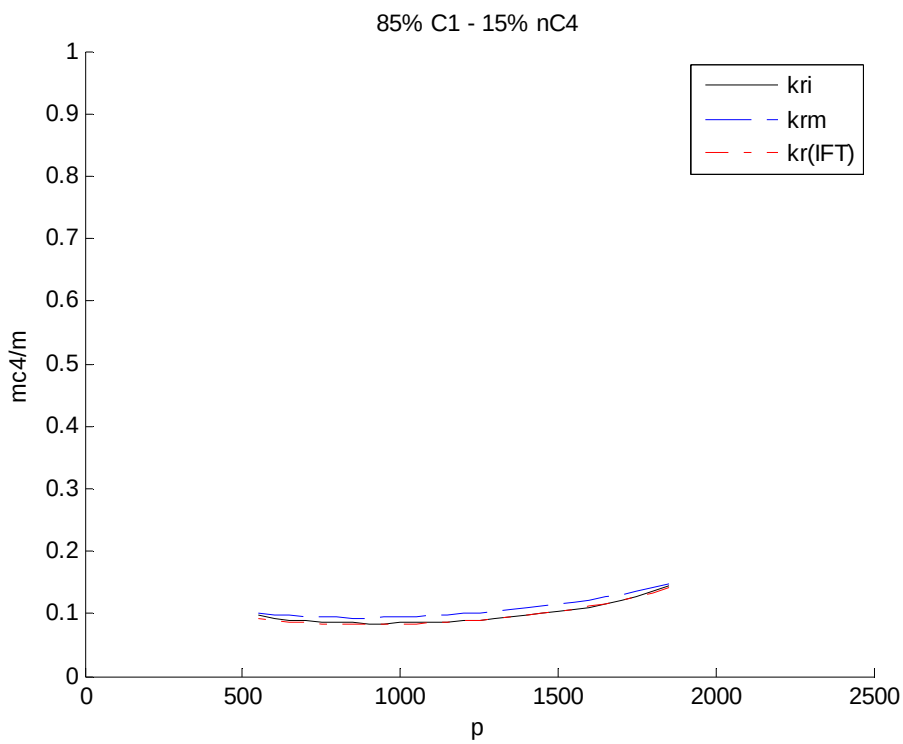

Figure 5-8: m_{c4}/m *vs.* p for z_{C4} = 0.15 with different relative permeability models.

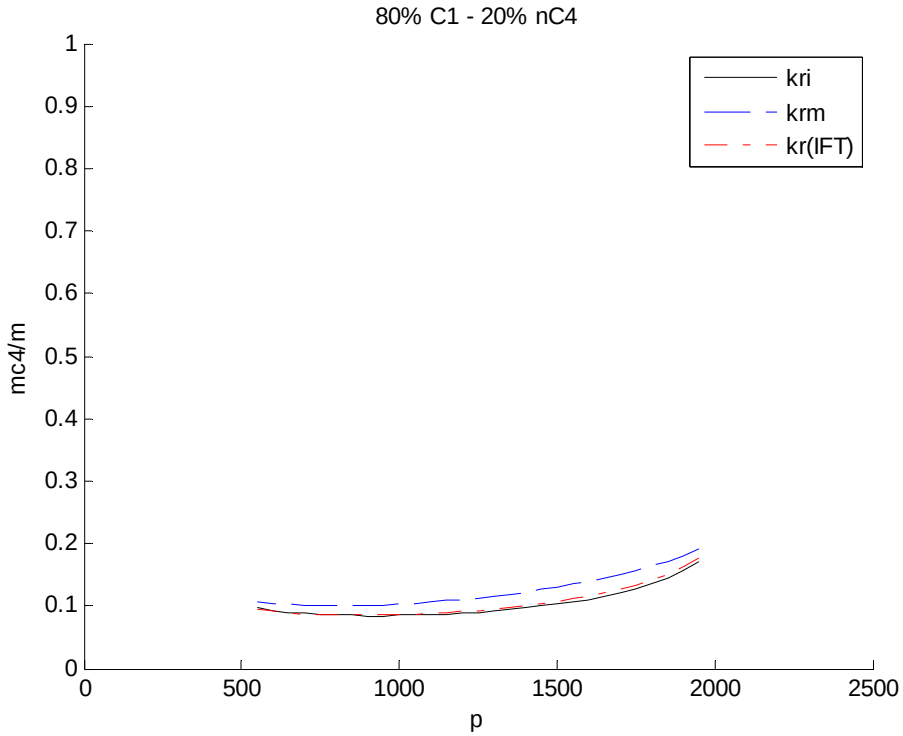

Figure 5-9: m_{c4}/m *vs.* p for $z_{C4} = 0.20$ with different relative permeability models.

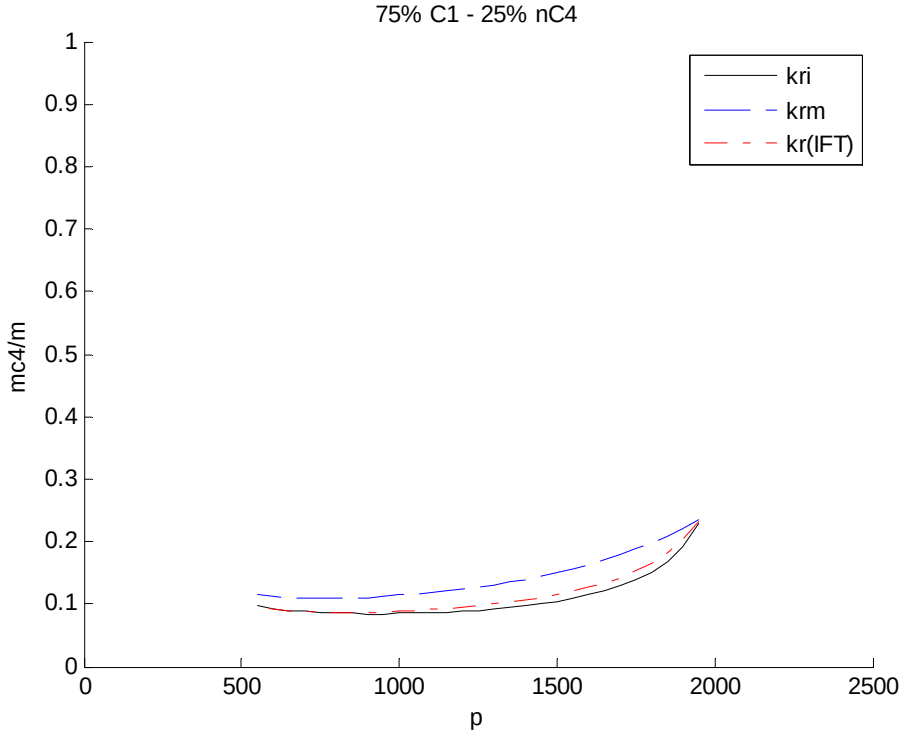

Figure 5-10: m_{c4}/m *vs.* p for $z_{C4} = 0.25$ with different relative permeability models.

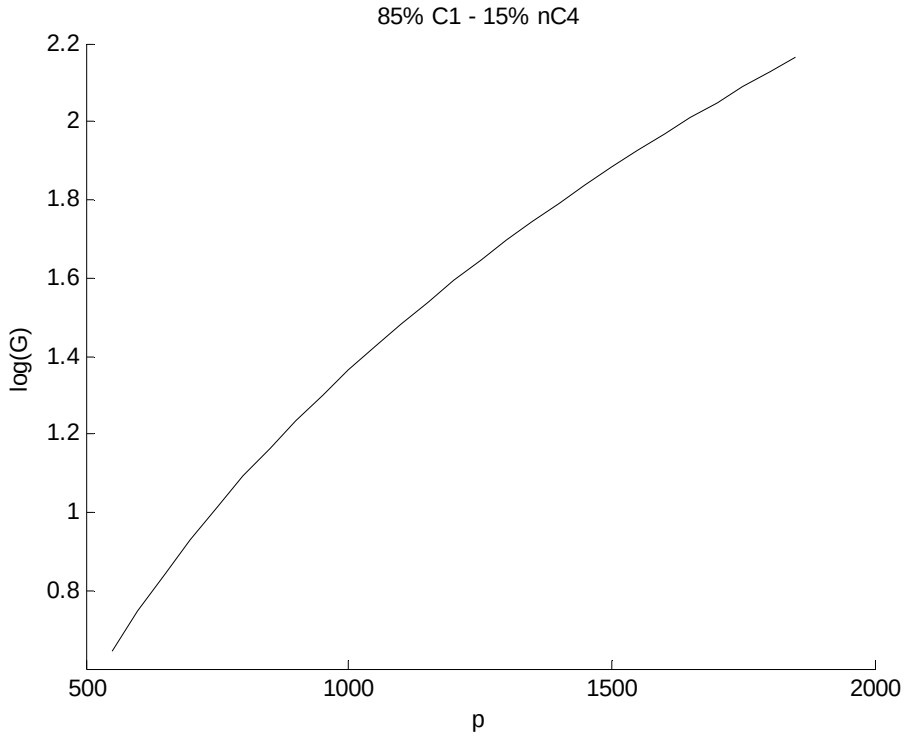

Figure 5-11: *G vs. p* for $z_{C4} = 0.15$.

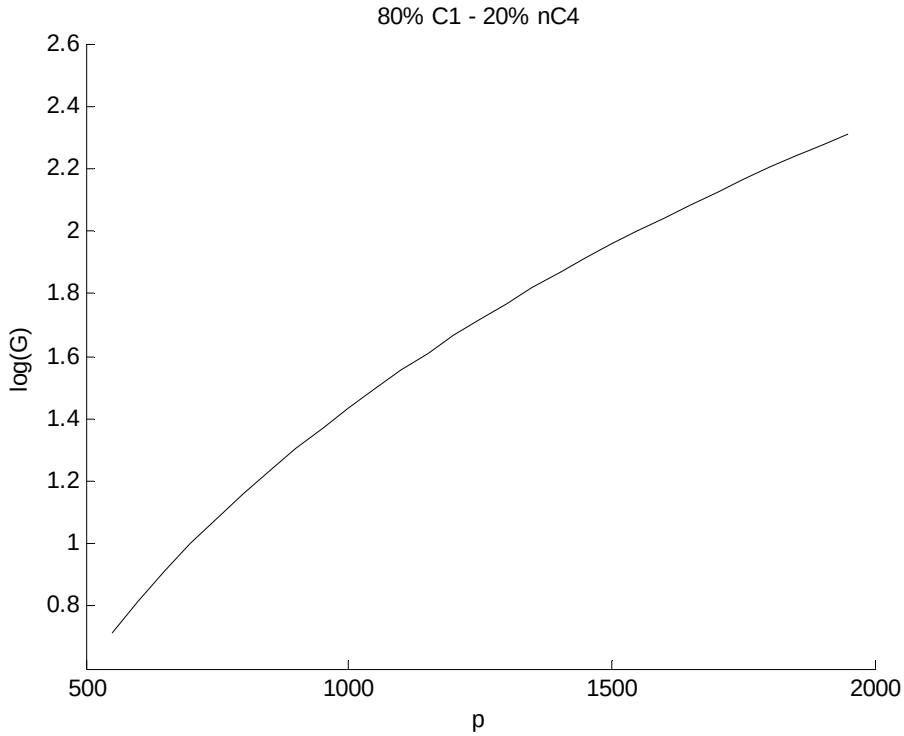

Figure 5-12: *G vs. p* for $z_{C4} = 0.20$.

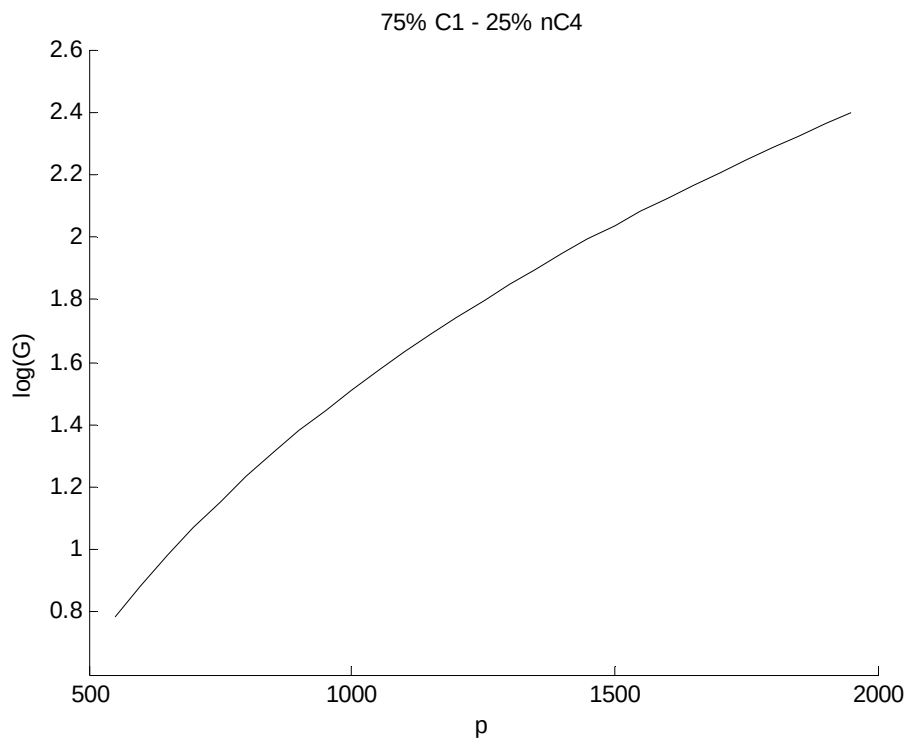

Figure 5-13: *G vs. p* for $z_{C4} = 0.25$.

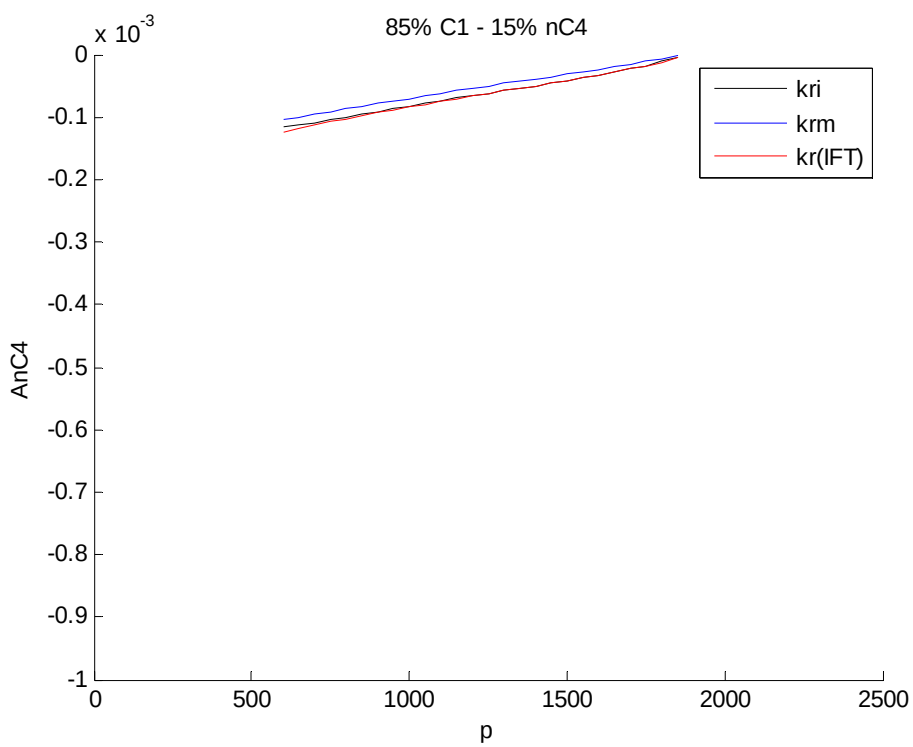

Figure 5-14: A_{C4} *vs. p* for $z_{C4} = 0.15$ with different relative permeability models.

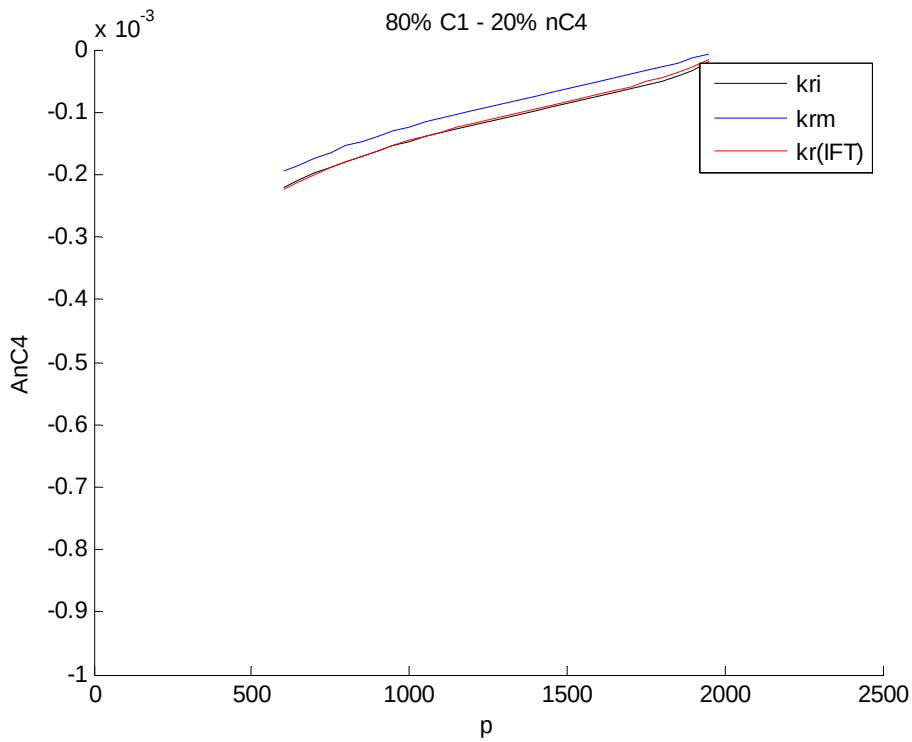

Figure 5-15: A_{C4} *vs.* p for z_{C4} = 0.20 with different relative permeability models.

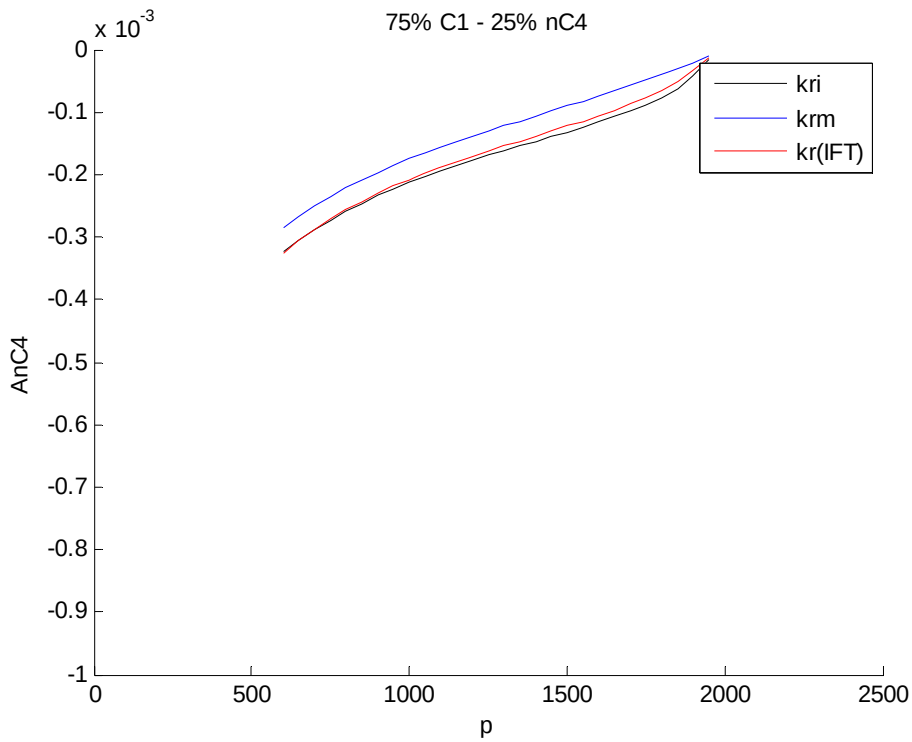

Figure 5-16: A_{C4} *vs.* p for z_{C4} = 0.25 with different relative permeability models.

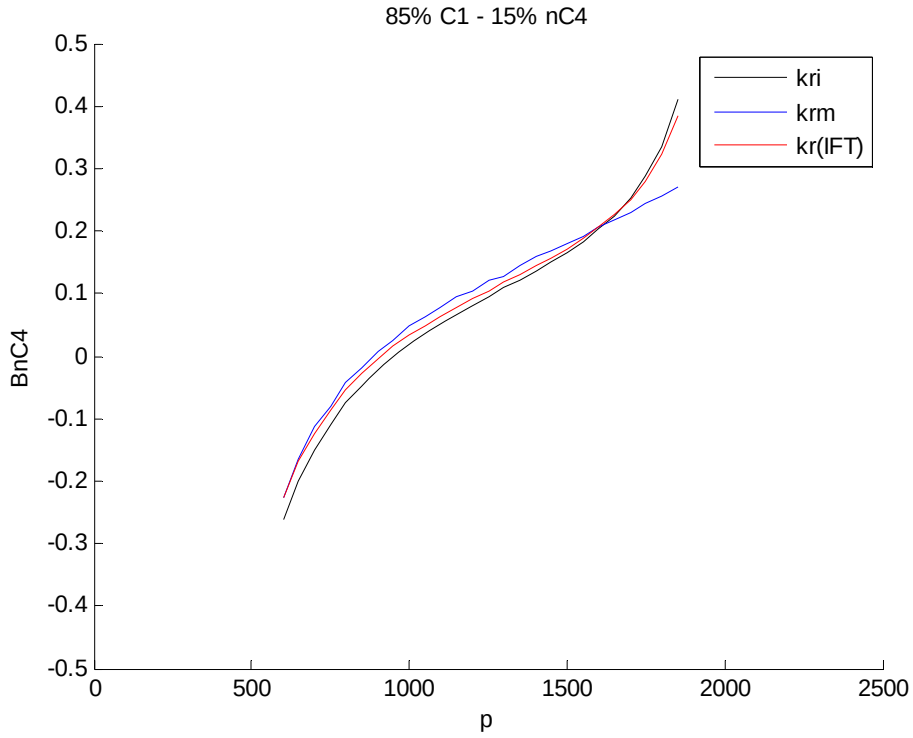

Figure 5-17: B_{C4} *vs.* p for $z_{C4} = 0.15$ with different relative permeability models.

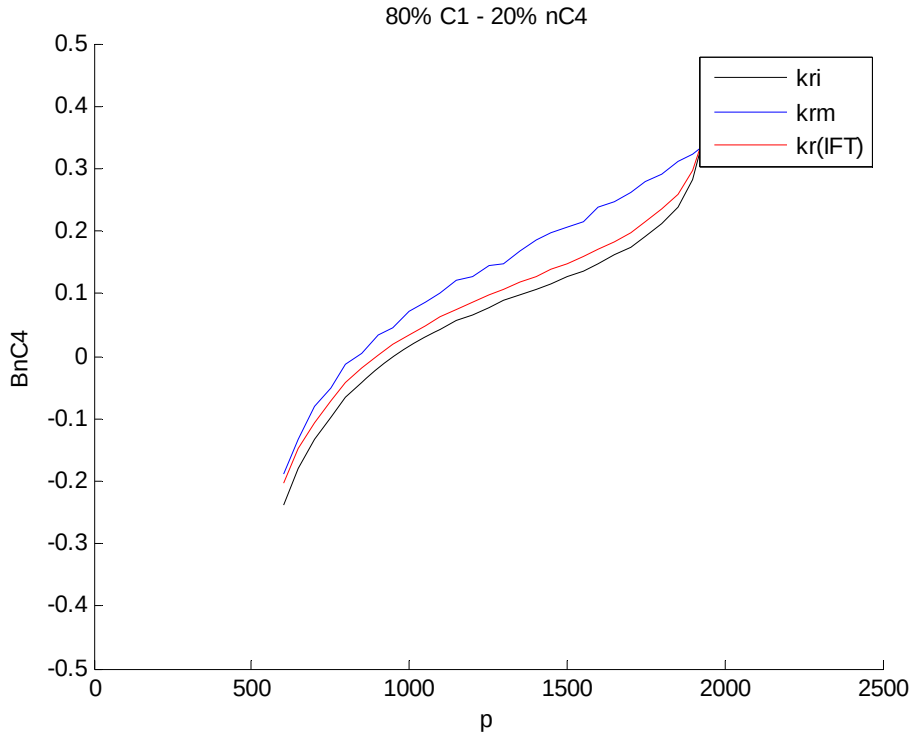

Figure 5-18: B_{C4} *vs.* p for $z_{C4} = 0.20$ with different relative permeability models.

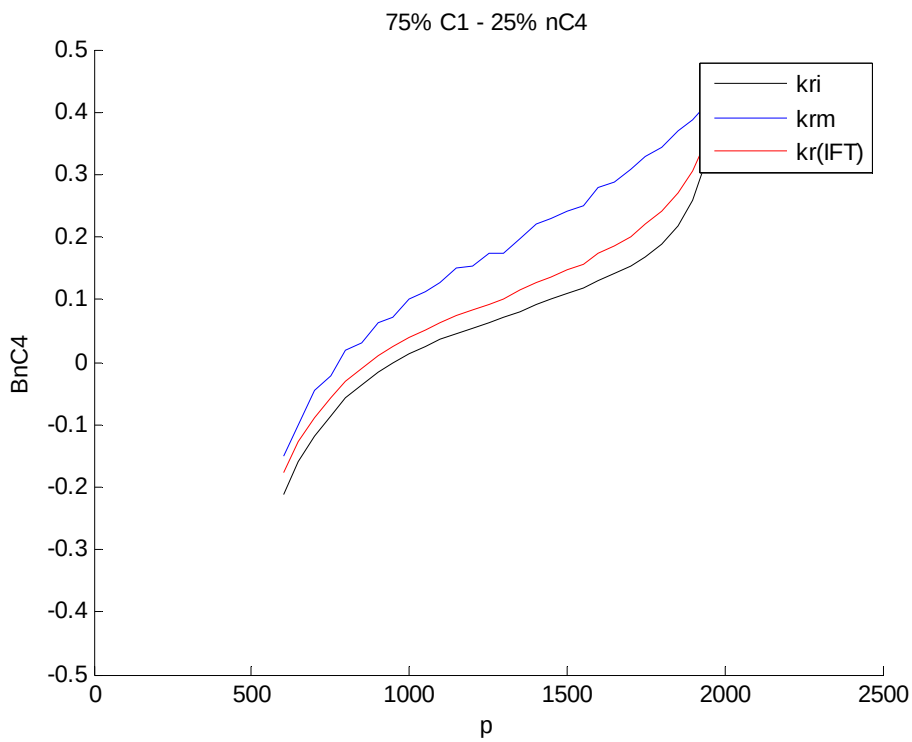

Figure 5-19: B_{C4} *vs.* p for $z_{C4} = 0.25$ with different relative permeability models.

In conclusion, pressure, relative permeability and fluid type, all have impact on terms A_{C4} and B_{C4}, hence $\partial z_{C4}/\partial t$.

Near to the well, assuming a constant bottom hole flowing pressure, $(\partial p/\partial t)$ is small and $(\partial p/\partial r)$ is large. Therefore, the term $B_{C4}(\partial p/\partial r)^2$ will dominate in the near wellbore region. The compositional variation rate of n-butane can be either positive or negative depending on the sign of B_{C4}. At pressure is high, $B_{C4} > 0$, the overall concentration of n-butane increases with time. At lower pressure, $B_{C4} < 0$, the overall concentration of n-butane decreases with time. On the other hand, further away from the well, $A_{C4}(\partial p/\partial t)$ term will dominate.

If we shut in the well after depletion, the direction of pressure change will be reversed and $(\partial p/\partial t)$ will be positive, then the term $A_{C4}(\partial p/\partial t)$ will become negative. This term would cause the composition of the heavy component to decrease. However, this term is very small compared to the positive term $B_{C4}(\partial p/\partial r)^2$ (pressure is above the threshold) which causes the composition of the heavy component to increase. So the net increase in the concentration of heavy components near the well will still continue. Hence, it would not be possible to remove the condensate bank fully, by simply shutting in the well to increase pressure in the near well region once this region of condensate is formed. This is consistent with the observations in the experiments (Figures 4-6 to 4-8 shown earlier).

Chapter 6

6. Optimization of Recovery in Gas-Condensate Reservoirs

6.1. Production Enhancement of Gas-Condensate Reservoir Using Production Strategies

6.1.1. Binary System

In this section, we looked at the possibility to enhance the performance of a gas condensate reservoir at the field scale by designing an appropriate production scheme. This was done using numerical simulation. We considered a cylindrical reservoir model with a single production well. The radius of the reservoir is 9,699 ft (the same case considered by Shi, 2009). The reservoir fluid used for simulation was the binary C_1-nC_4 mixture with overall mole fractions 0.85-0.15 respectively. This reservoir fluid mixture is the same as the fluid mixture that we used for experiments. The purpose was to simplify the problem and to configure a model that can reflect the physics that we saw in the experiments. The production well was controlled by a constant gas production rate and a minimum bottom-hole pressure setting. If the well pressure reaches the minimum bottom-pressure, the control mode will be switched from constant gas rate to the constant bottom-hole pressure. The investigation was performed by using the same gas production rate but with six different minimum well bottom-hole pressure settings (Figure 6-1). The simulation was carried out for a short period before extending to a longer period and a more complex model.

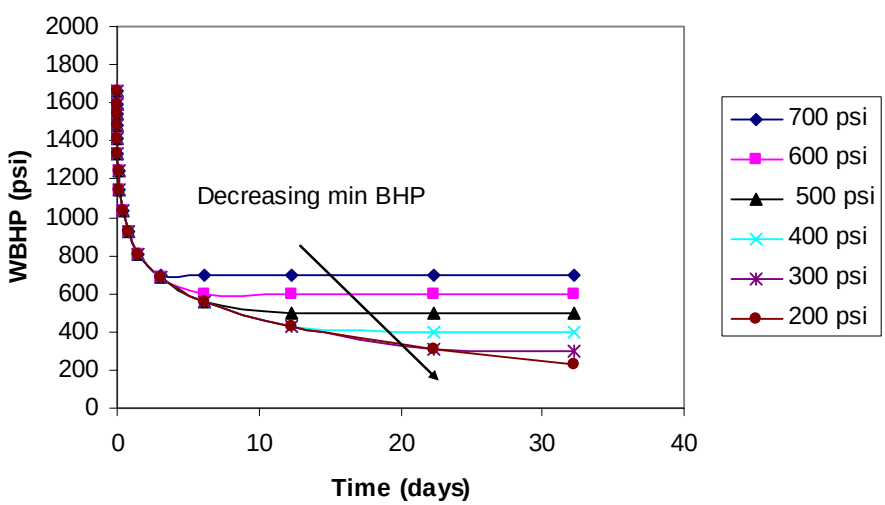

Figure 6-1: Well bottom-hole pressure history with different minimum bottom-hole pressure.

The simulation results are shown in Figure 6-2 and Figure 6-3. From these figures, we can see that as the minimum bottom-hole pressure decreases, the well shows a delay in its drop of production rate hence a higher total production is achieved.

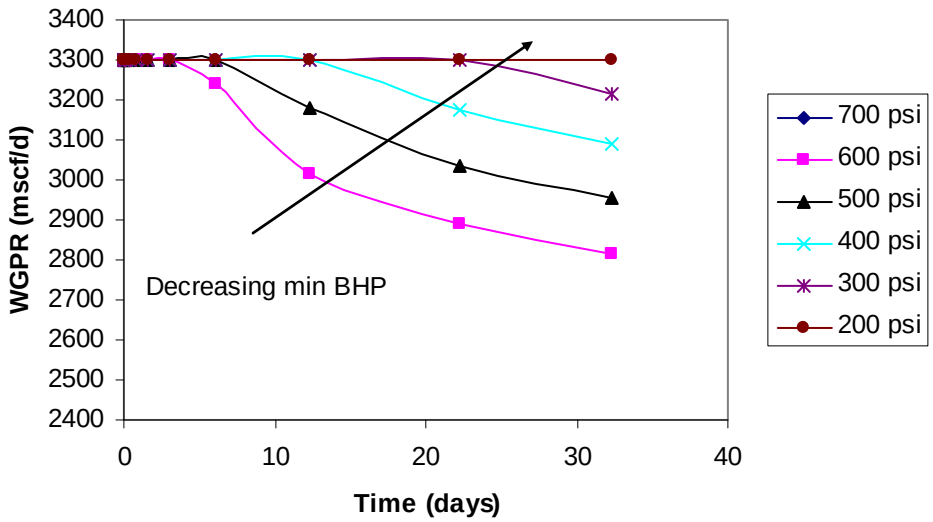

Figure 6-2: Gas production rate history.

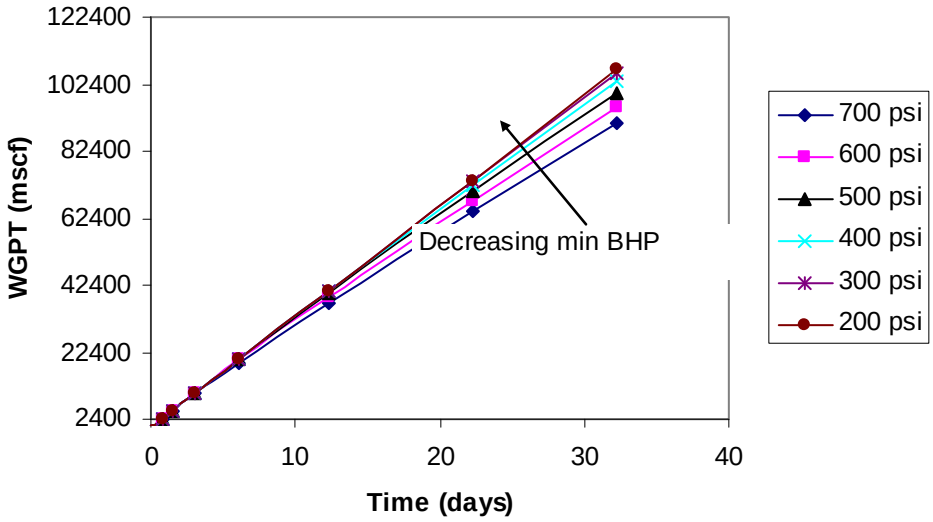

Figure 6-3: Cumulative gas production history.

Figure 6-4, moving from right to left, shows that when the well bottom-hole pressure falls below the dew-point pressure (1837 psia), the condensate drops out and accumulates in the reservoir and stays immobile because the condensate saturation is still below the critical condensate saturation. The producing gas becomes leaner. As the pressure decreases further, some of the condensate vaporizes and the nC_4 composition in the producing gas increases slightly. At some point (around 700 psia in this case) the critical

liquid saturation is reached and part of the condensate starts to flow, resulting in a sharp increase in production of the heavier component.

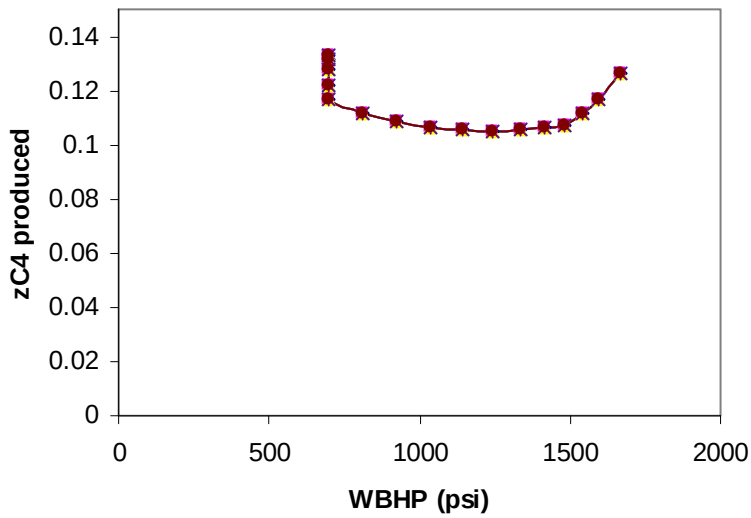

Figure 6-4: Overall nC_4 mole fraction produced versus well bottom-hole pressure.

The effect of well bottom-hole pressure on the production history is shown in Figure 6-5 and Figure 6-6. The lower the well bottom-hole pressure, the higher fraction of nC_4 in the liquid phase in the well block (where liquid has accumulated) and less heavier component is produced at the surface (because the lighter fluid is flowing). The producing fluid is leaner initially due to the loss of the heavier component into the accumulating liquid bank, but then it becomes richer as the pore space to hold liquid becomes filled and part of the condensate starts to flow.

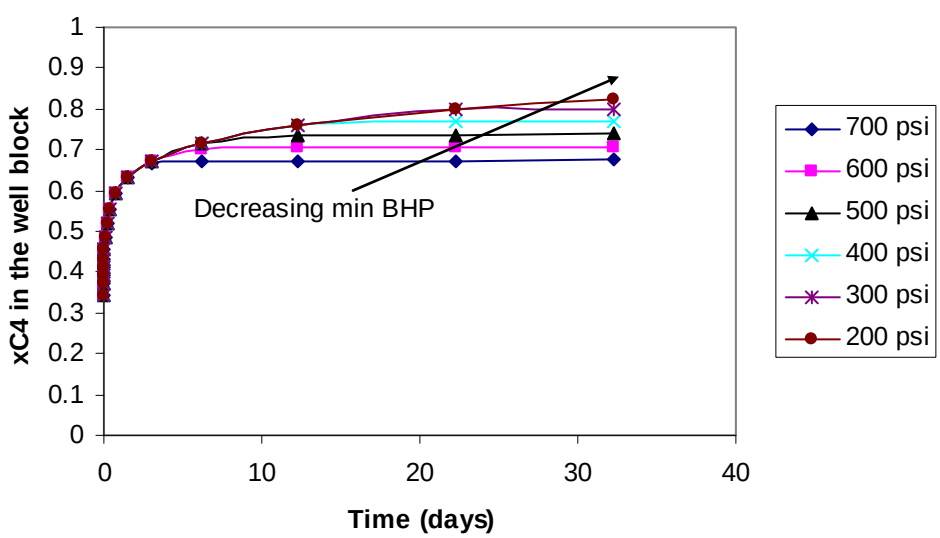

Figure 6-5: History of nC_4 mole fraction in the liquid phase in the well block

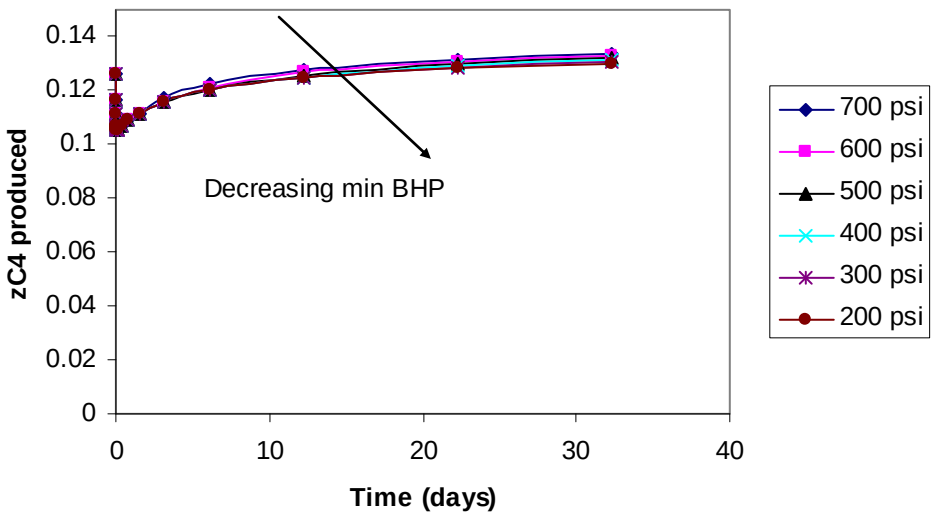

Figure 6-6: History of overall nC_4 mole fraction produced.

Next, we performed our study using a constant bottom-hole pressure production control mode and a much longer simulation period (3,600 days). Figure 6-7, Figure 6-8 show the well gas production rate and well gas production total corresponding to different bottom-hole pressure settings. As expected from productivity index (PI) considerations, the lowest bottom-hole pressure setting has the highest gas production rate and the highest gas production total. However, the composition of the produced gas is different at different bottomhole flowing pressure, as shown next.

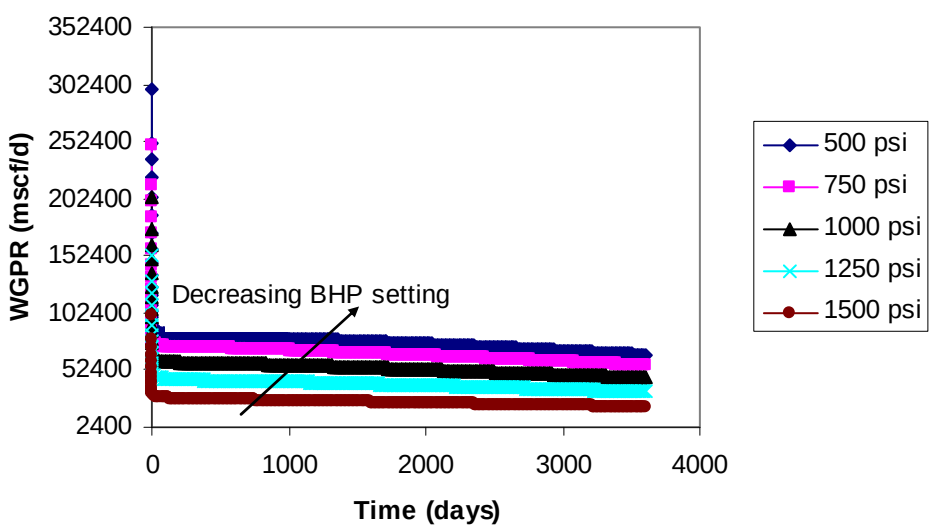

Figure 6-7: Gas production rate history.

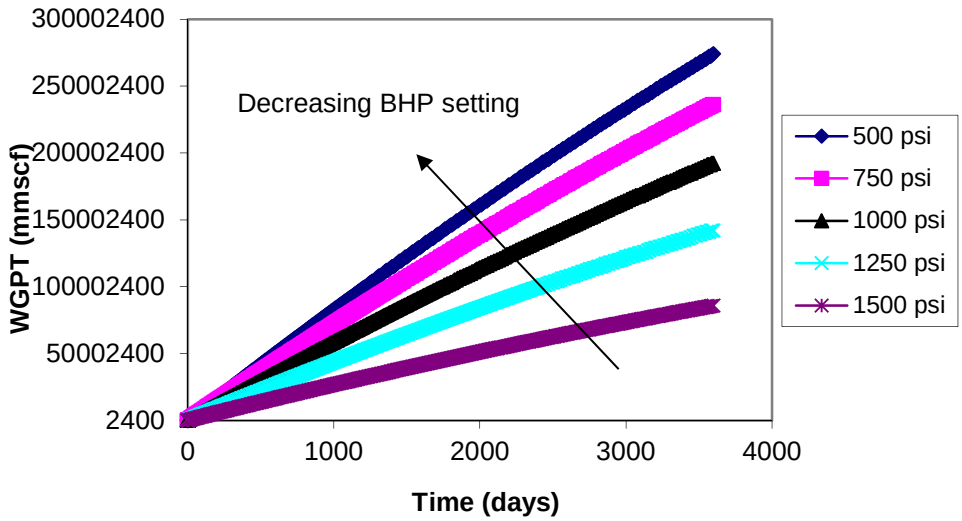

Figure 6-8: Accumulated gas production history.

The effect of well bottom-hole pressure on the composition is shown in Figure 6-9 and Figure 6-10. The lower the well bottom-hole pressure, the higher the fraction of nC_4 in the liquid phase in the well block and less heavy component is produced. The producing fluid is leaner initially, then it becomes richer as part of the condensate starts to vaporize into gas. After that, the overall composition of produced nC_4 decreased.

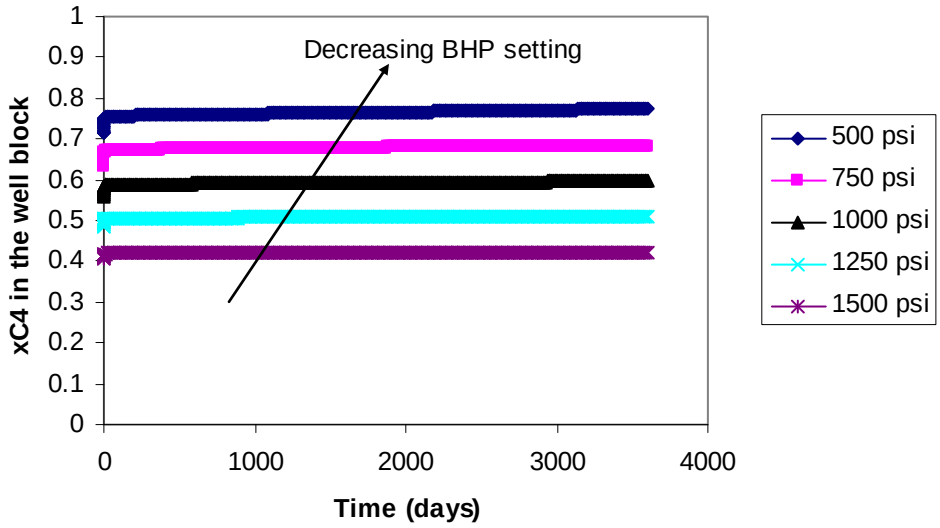

Figure 6-9: History of nC_4 mole fraction in the liquid phase in the well block with different bottom-hole pressure settings.

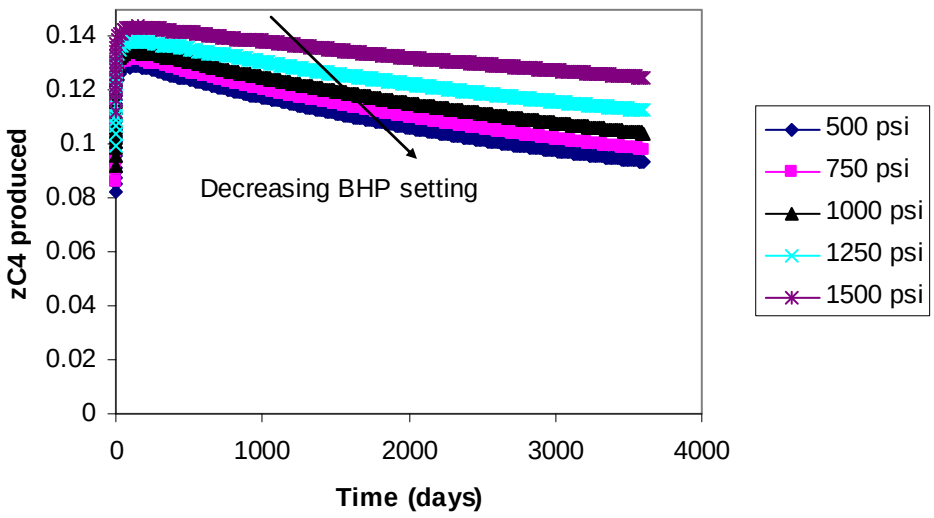

Figure 6-10: History of overall nC_4 mole fraction produced.

The results from a production strategy with constant bottom-hole pressure control are very similar to the results from the production strategy with constant gas production rate with different pressure setting. The lowest *BHP* produces the highest gas production rate and the gas production in total, as would be expected based on productivity index (PI) alone. However the composition of the produced fluid, and hence its commercial value, is not the same for different BHP values.

6.1.2. Multicomponent System

In a more complex case, we studied the possibility to enhance performance of a multicomponent gas condensate reservoir at field scale by selecting the production scheme. The first model we used is almost the same as the *SPE3* model (Kenyon and Behie, 1987) but without an injection well (Figure 6-11). The reservoir has 9×9×4 blocks in Cartesian coordinates. There are four layers and only one production well at the center of the reservoir which is perforated in layers 3 and 4. The reservoir fluid is gas-condensate with multiple components. Figure 6-12 shows the phase diagram of the reservoir fluid, which has the composition shown in Table 6-1. At the reservoir temperature of 200°*F*, there is a large condensate region between 3500 psia and 500 psia (reservoir pressure is 3500 psia). The initial conditions for the location of the gas/water contact and the capillary pressure data generate a water/gas transition zone extending into the pay layers. Using different bottom-hole pressures, we were able to simulate the condensate production rate and gas production rate using the constant bottom-hole pressure control mode as shown in Figure 6-13 and Figure 6-14. From these figures, we can see that at the lower bottom-hole pressure the gas and condensate production rates are higher.

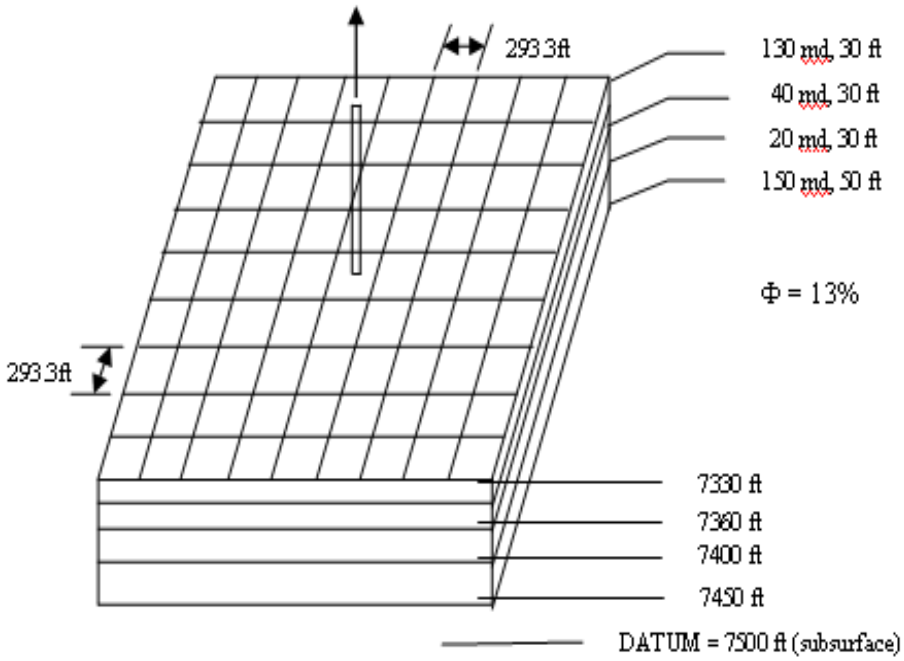

Figure 6-11: Reservoir model.

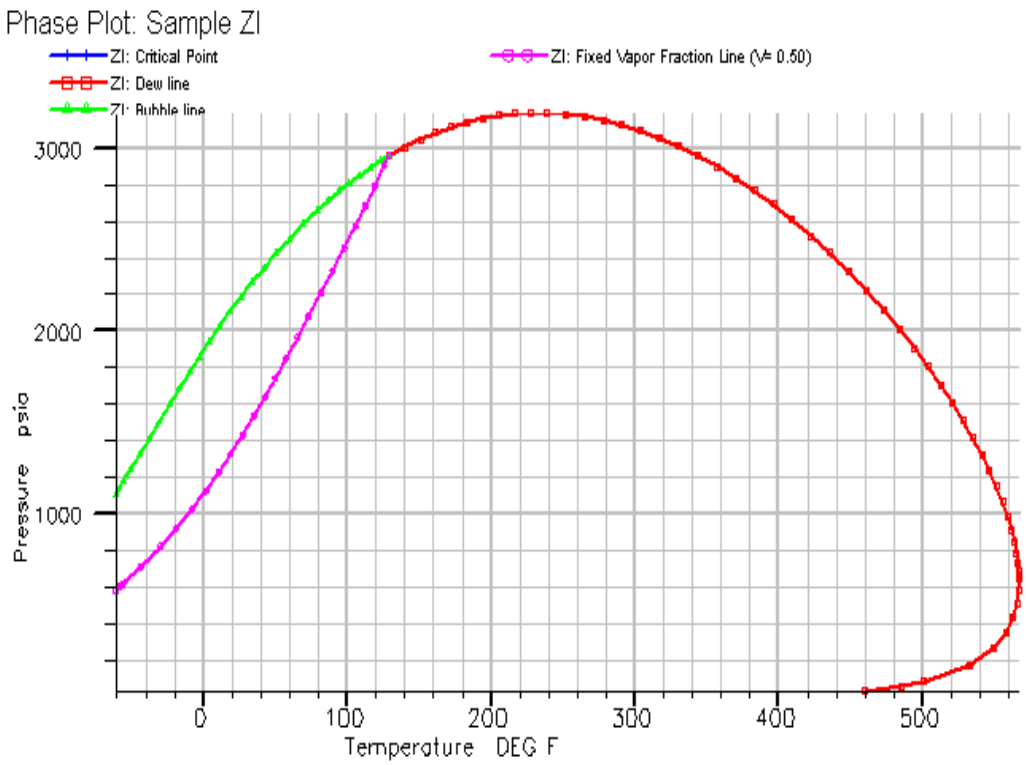

Figure 6-12: Phase diagram of the gas-condensate reservoir fluid.

Table 6-1: Composition of fluid in SPE3 reservoir model.

	z	MW
CO2	0.0121	44.01
N2	0.0194	28.01
C1	0.6599	16.04
C2	0.0869	30.07
C3	0.0591	44.10
C4-6	0.0967	66.87
C7+1	0.0475	107.78
C7+2	0.0152	198.56
C7+3	0.0033	335.20

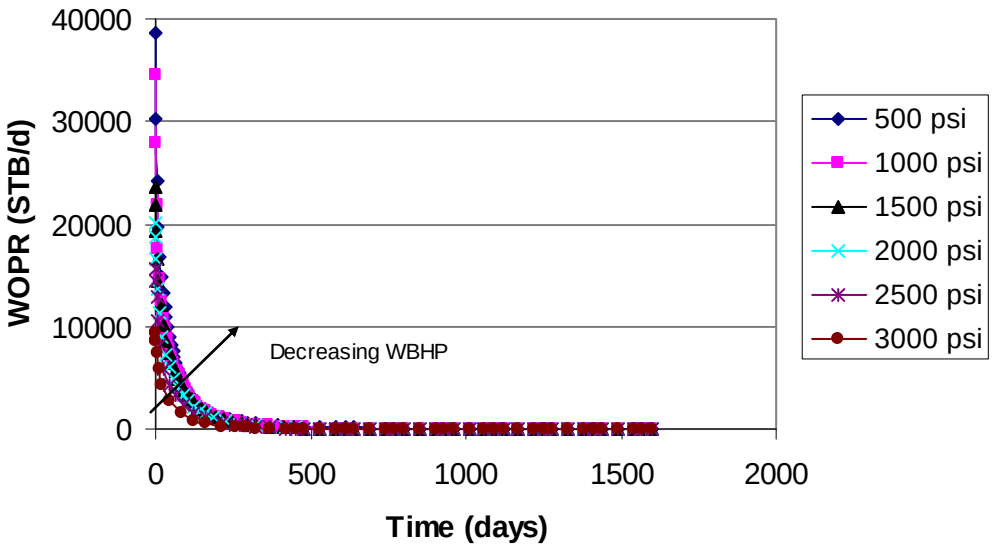

Figure 6-13: Condensate production rate (WOPR) with different bottom-hole pressures for the case with capillary pressure.

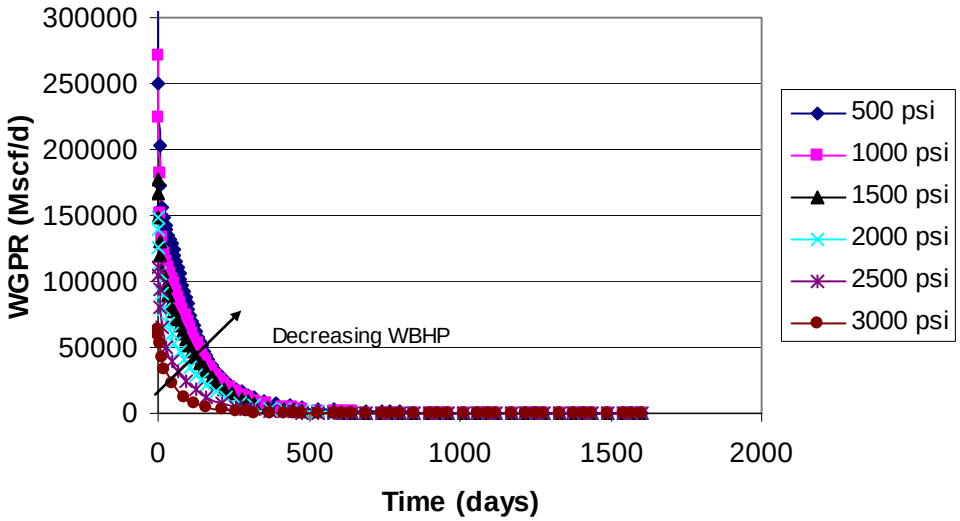

Figure 6-14: Gas production rate (WGPR) with different bottom-hole pressures for the case with capillary pressure.

After that, we set the reservoir to have immobile water instead of mobile water by setting the gas/water capillary pressure to zero. The reason is to simplify the fluid model to see if mobile water in the reservoir affects the gas and oil production. Figure 6-15 and Figure 6-16 show the results, which are in line with what we found for the binary gas-condensate mixture case as described in Section 6.1.1.

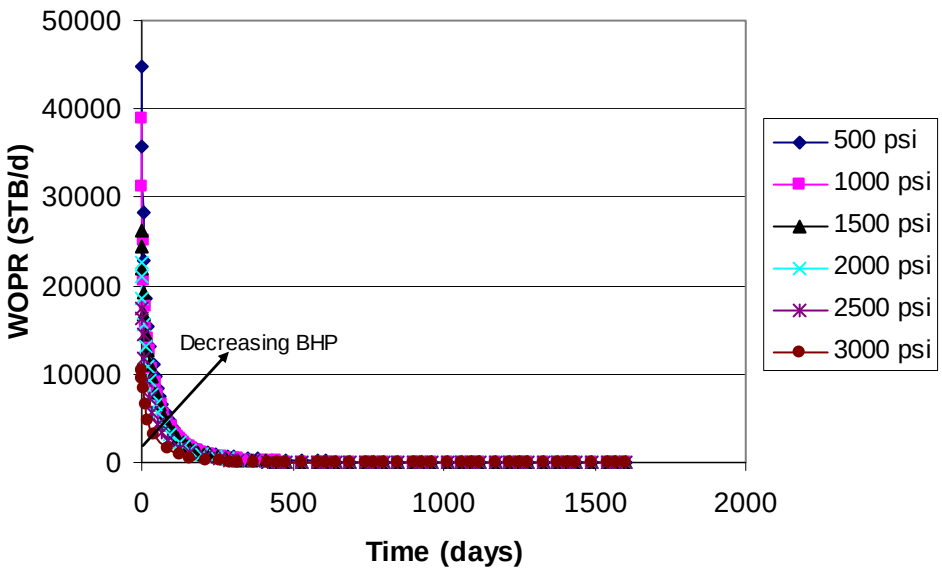

Figure 6-15: Condensate production rate (WOPR) with different bottom-hole pressures for the case without capillary pressure.

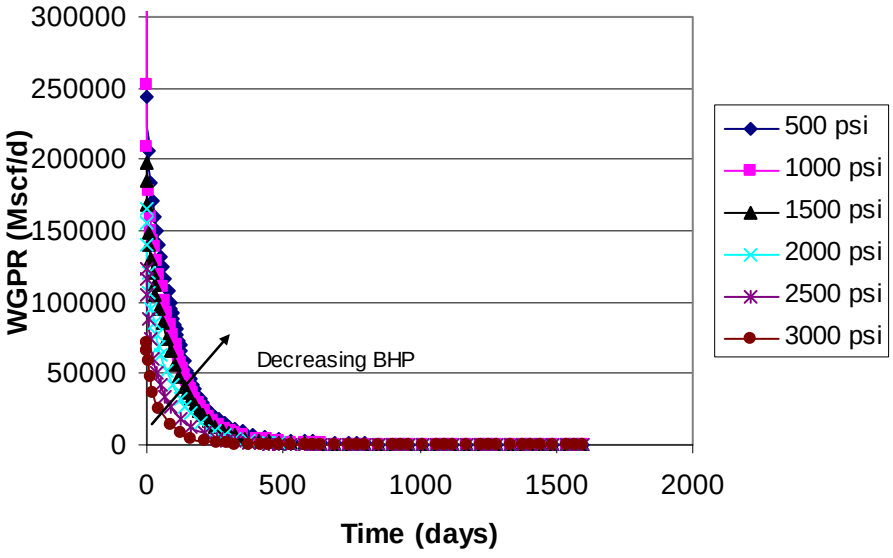

Figure 6-16: Gas production rate with different bottom-hole pressures for the case without capillary pressure.

In order to study the compositional behavior of the system, we simplified the simulation model. Now, we have only one layer and only immobile water in the reservoir. The motivation was to make the model as simple as possible to understand the compositional behavior in the absence and presence of water.

Figure 6-17 and Figure 6-18 show the condensate and gas production rates with different bottom-hole pressures for this model. As expected, the results show that at lower bottom-hole pressure, the gas and condensate production rates are higher in this case.

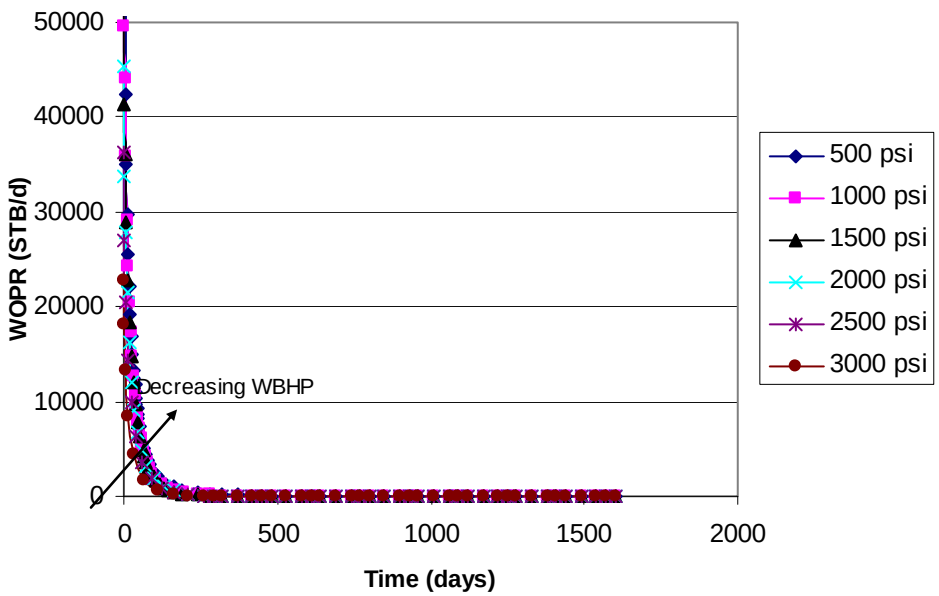

Figure 6-17: Condensate production rate with different bottom-hole pressures for one-layer model.

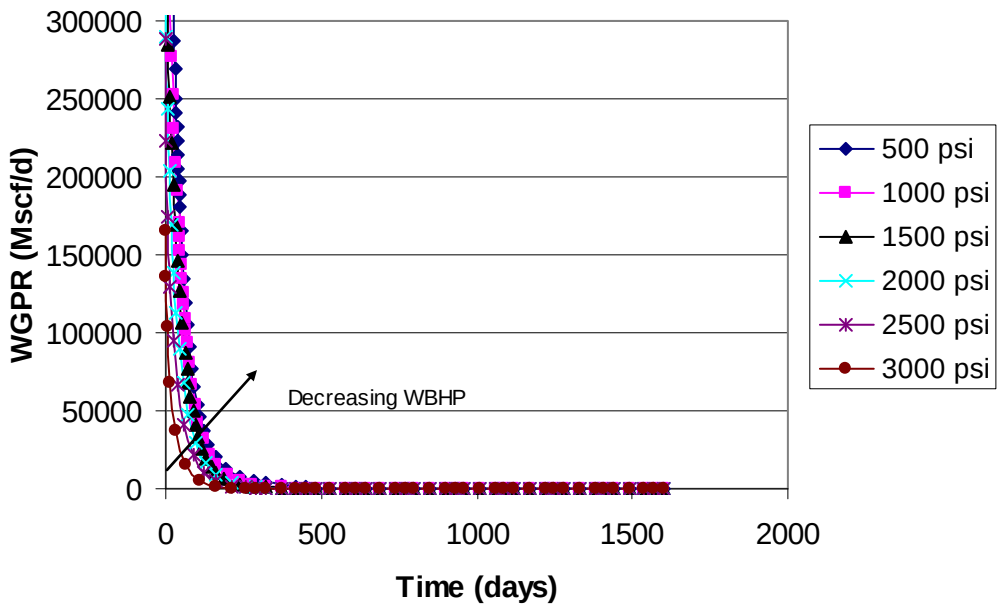

Figure 6-18: Gas production rate with different bottom-hole pressures for one-layer model.

Figure 6-19 shows saturation and C_{7+} mole fractions versus time at the well block with 500 psi bottom-hole pressure. As we can see from the figure, at very early time, only gas exists and its composition is constant. As soon as the bottom-hole pressure falls below the dew-point and the condensate drops out, the heavy component is more prevalent in the liquid phase even as the condensate saturation decreases. Finally, the composition of the liquid becomes constant again as a steady state is reached.

The spatial distributions of condensate saturation and C_{7+} mole fractions with 500 psi bottom-hole pressure are shown in Figure 6-20 and Figure 6-21. The well is located in block 5. There is a large condensate bank near the well which decreases the production of the gas. Over time, the C_{7+} mole fraction is lower in the well block compared to the blocks further away from the well.

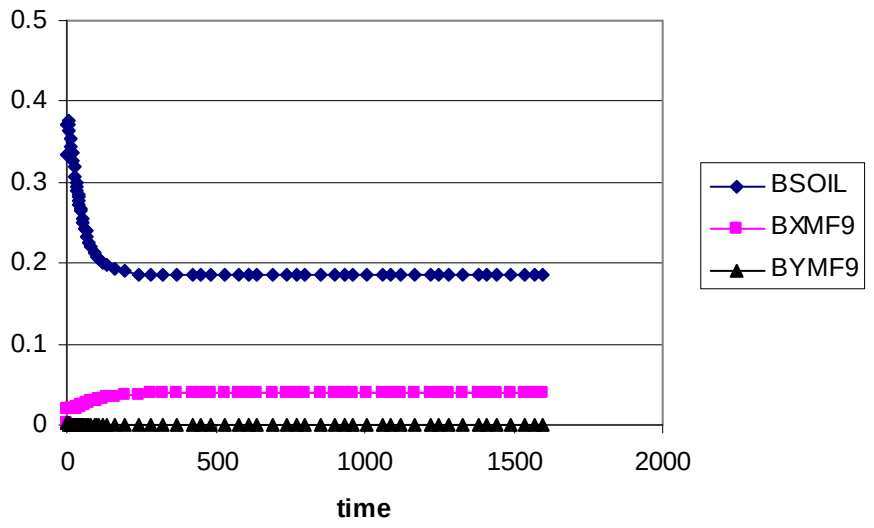

Figure 6-19: Condensate saturation (BSOIL) and C_{7+} mole fractions (liquid BXMF9, and gas BYMF9) versus time at the well block with 500 psi bottom-hole pressure.

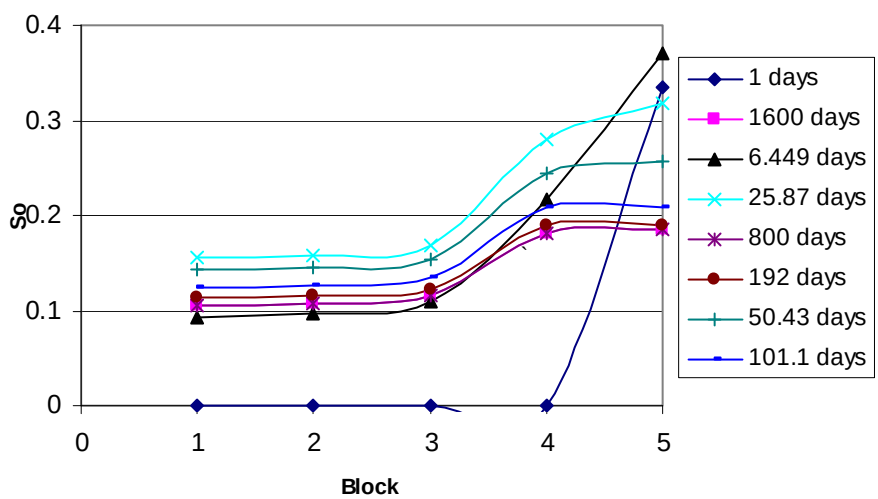

Figure 6-20: Spatial distribution of condensate saturation with 500 psi bottom-hole pressure.

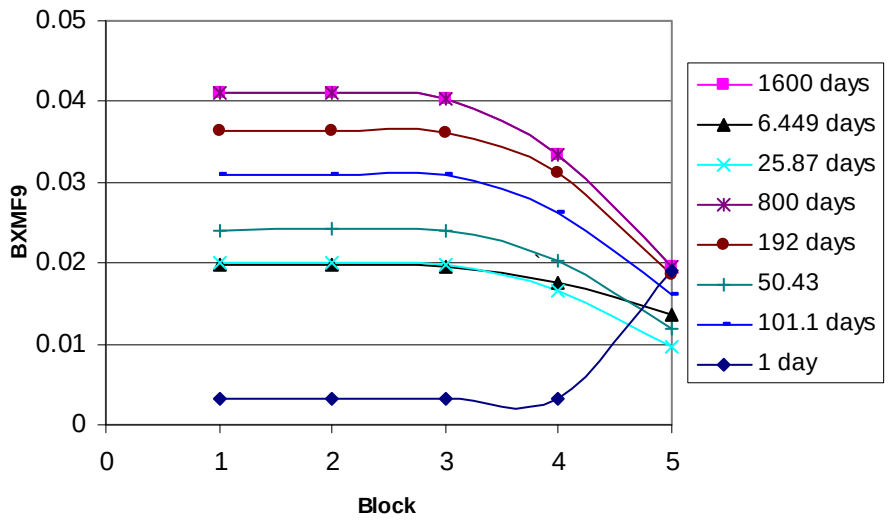

Figure 6-21: Spatial distribution of C_{7+} mole fraction in liquid with 500 psi bottom-hole pressure.

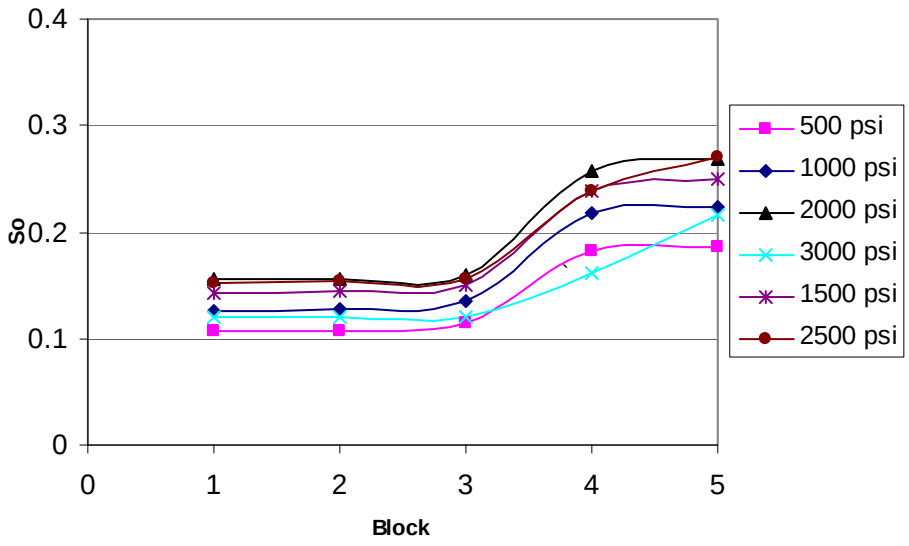

Figure 6-22: Condensate saturation with different bottom-hole pressures at 1600 days.

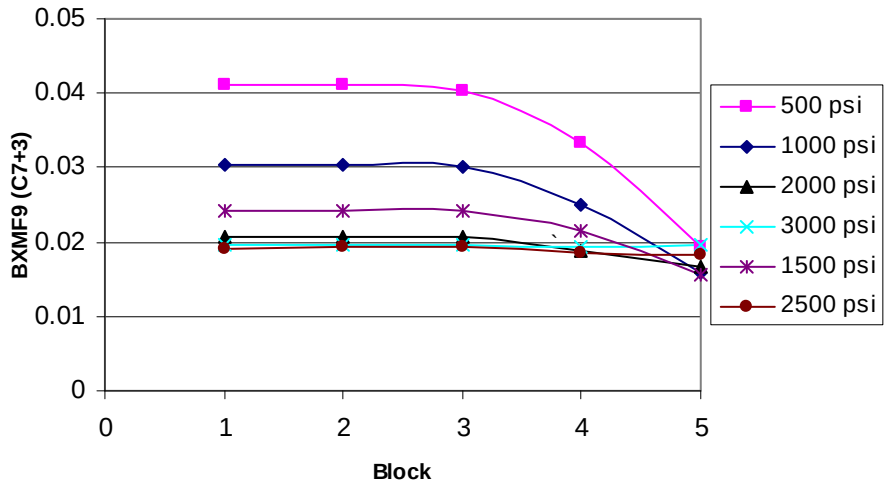

Figure 6-23: of C_{7+} mole fraction in liquid with different bottom-hole pressures at 1600 days.

Figure 6-22 and Figure 6-23 show spatial distributions of condensate saturation and C_{7+} mole fractions with different bottom-hole pressures. The lower the bottom-hole pressure, the lower the condensate saturation and higher mole fraction of C_{7+} in the liquid. The values for bottomhole pressure of 3000 psi are anomalous in the simulation, however the reason for this is unknown.

Next, we decreased the porosity of the reservoir from 13% to 7% and horizontal permeability from 100 md to 1 md. Figure 6-24 and Figure 6-25 show the condensate and gas production rates with different bottom-hole pressures.

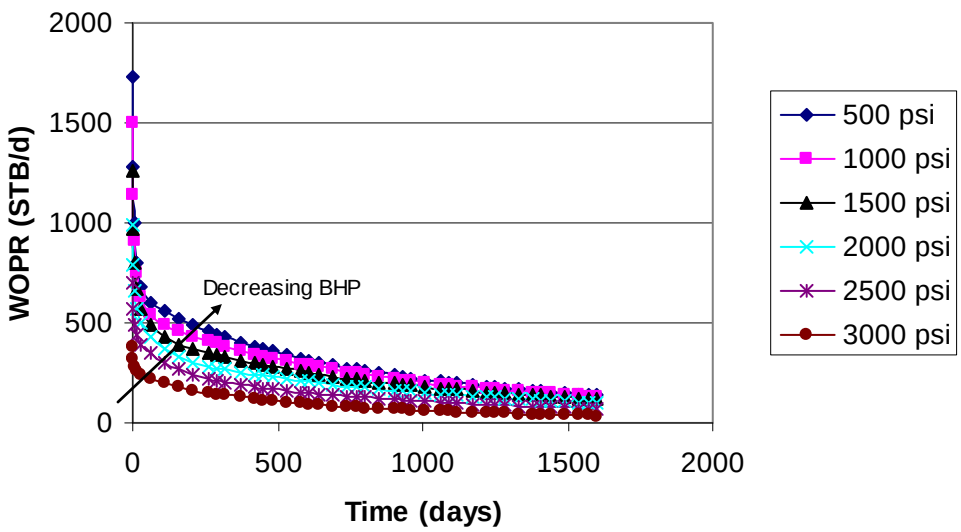

Figure 6-24: Condensate production rate WOPR with different bottom-hole pressures for a tight reservoir.

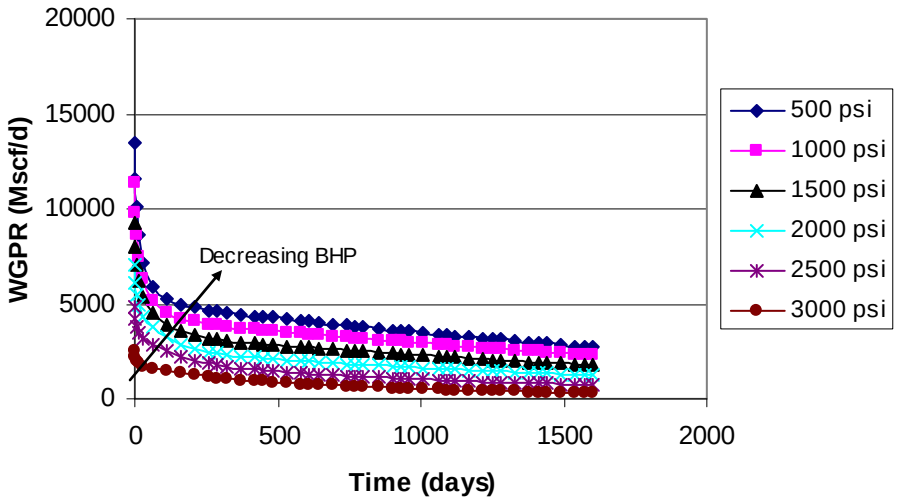

Figure 6-25: Gas production rate WGPR with different bottom-hole pressures for a tight reservoir.

Figure 6-26 shows Well Block Condensate Saturation (BSOIL), Mole Fraction of the Heaviest Component C_{7+} in liquid phase (BXMF9) and Mole Fraction of the Heaviest Component C_{7+} in vapor phase (BYMF9) versus time with 500 psi bottom-hole pressure. The saturation builds up to a maximum value after the pressure drop below the dew-point pressure then decreases gradually indicating the vaporization of the condensate bank.

Figure 6-27 and Figure 6-28 show spatial distributions of condensate saturation and C_{7+} mole fractions with 500 psi bottom-hole pressure.

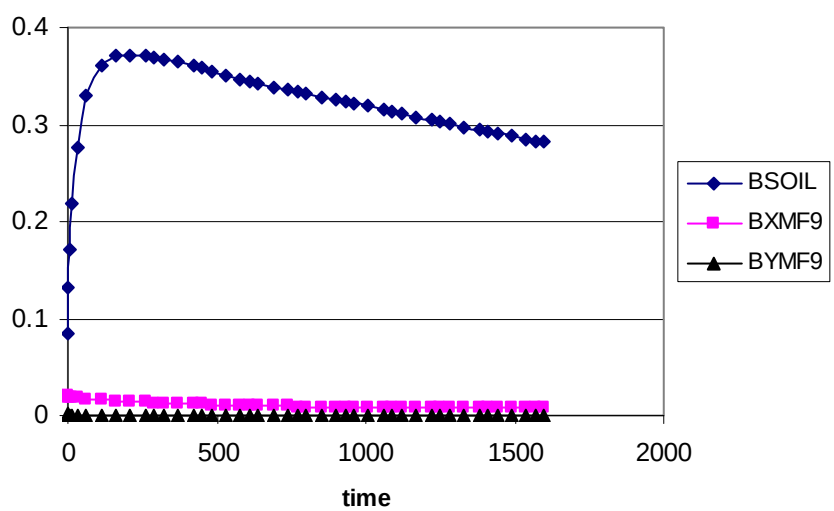

Figure 6-26: Saturation (BSOIL) and C_{7+} mole fractions (liquid BXMF9 and gas BYMF9) versus time at the well block with 500 psi bottom-hole pressure for a tight reservoir.

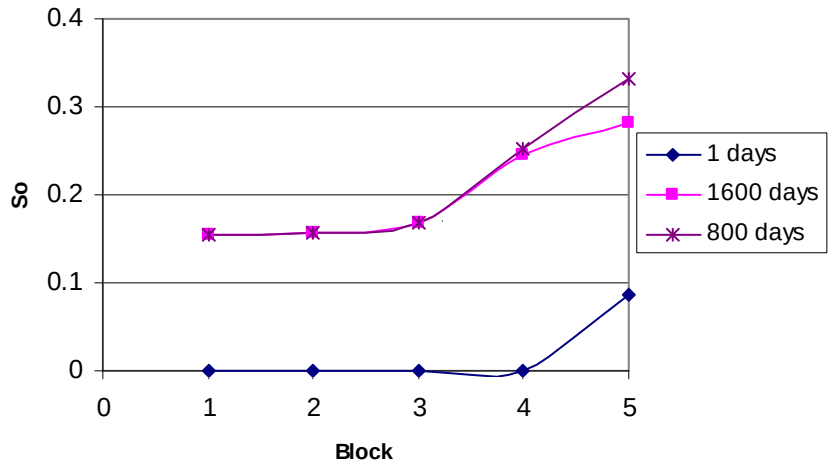

Figure 6-27: Spatial distribution of condensate saturation with 500 psi bottom-hole pressure for a tight reservoir.

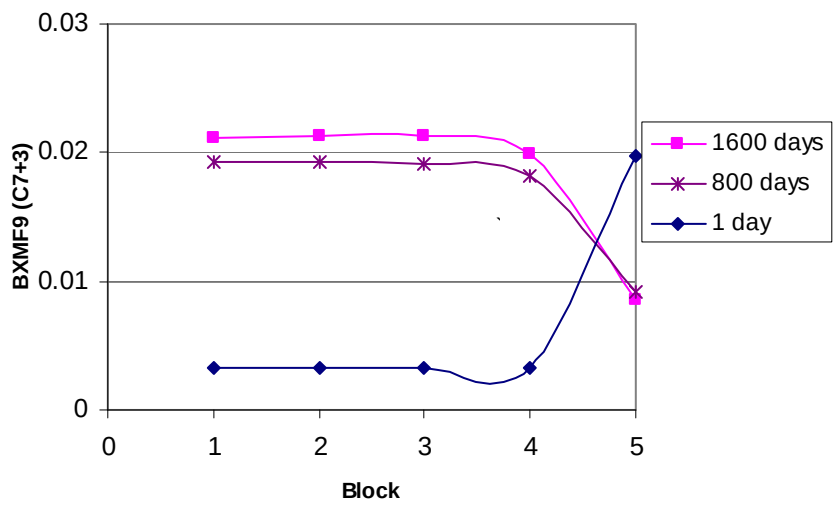

Figure 6-28: Spatial distribution of C_{7+} mole fraction (BXMF9) with 500 psi bottom-hole pressure for a tight reservoir.

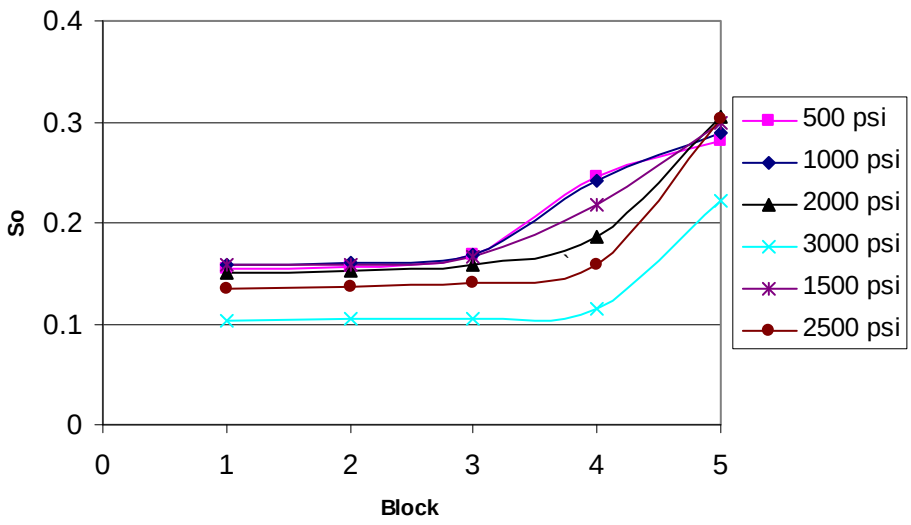

Figure 6-29: Condensate saturation with different bottom-hole pressures at 1600 days for a tight reservoir.

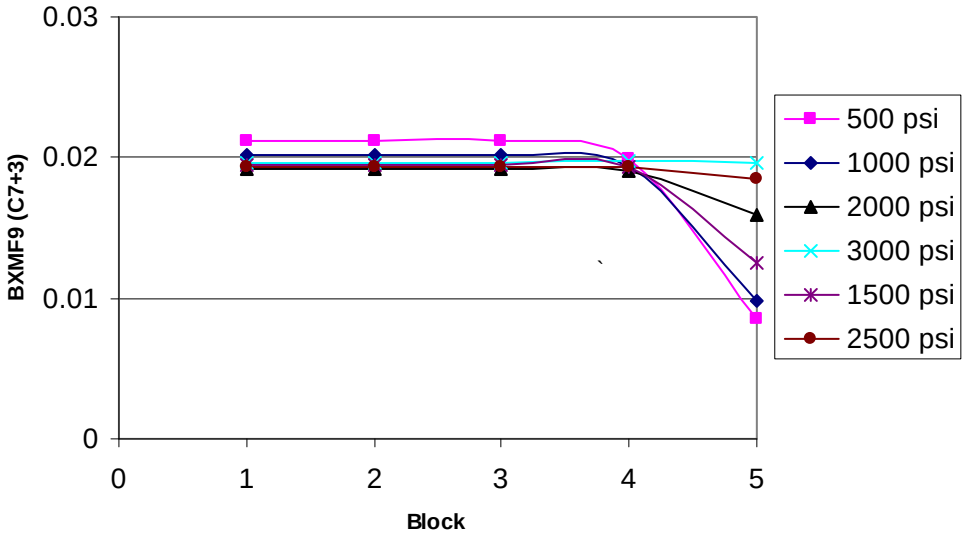

Figure 6-30: C_{7+} mole fraction (BXMF9) with different bottom-hole pressures at 1600 days for a tight reservoir.

Figure 6-29 and Figure 6-30 show spatial distributions of condensate saturation and C_{7+} mole fractions with different bottom-hole pressures.

At low bottom-hole pressures, the condensate bank in this tight reservoir is bigger than the case we considered before (compare Figure 6-19 in the previous case to Figure 6-26 in the tight reservoir case, and similarly Figure 6-20 compared to 6-27).

From these results, we can conclude that the loss of productivity in gas-condensate reservoirs due to condensate banking is more severe in the tight reservoir case.

6.2. Production Enhancement of Gas-Condensate Reservoir Using Hydraulic Fracturing and Gas Injection

6.2.1. Hydraulic Fracturing

As we have seen, due to the buildup of condensate bank around wells when the bottom-hole pressure drops below the dew-point pressure, the gas production rate drops rapidly and a significant part of valuable condensate is stuck in the well. Although we can increase the production rate a little bit by using a proper production strategy, the improvement is very small. There are many techniques to mitigate the productivity loss of gas-condensate reservoir. Hydraulic fracturing is a common one. The hydraulic fracture reduces the drawdown hence allow the wells produce a longer period before the condensate banking effect occurs.

Figure 6-31, Figure 6-32, and Figure 6-33 show effect of a hydraulic fracture on performance of a well in a gas-condensate reservoir. The hydraulic fracturing delays the time the bottom-hole pressure drops below the dew-pressure, decreases the magnitude con the condensate bank and results in higher production rates.

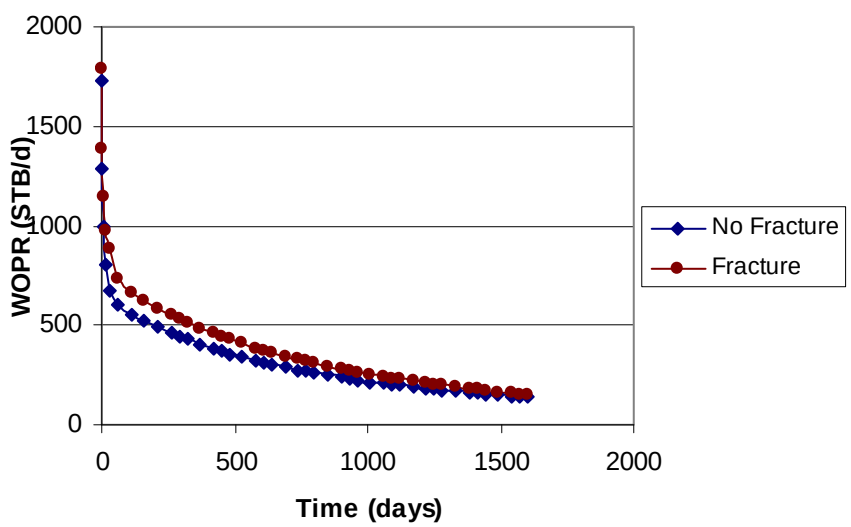

Figure 6-31: Effect of fracture on condensate production rate (WOPR).

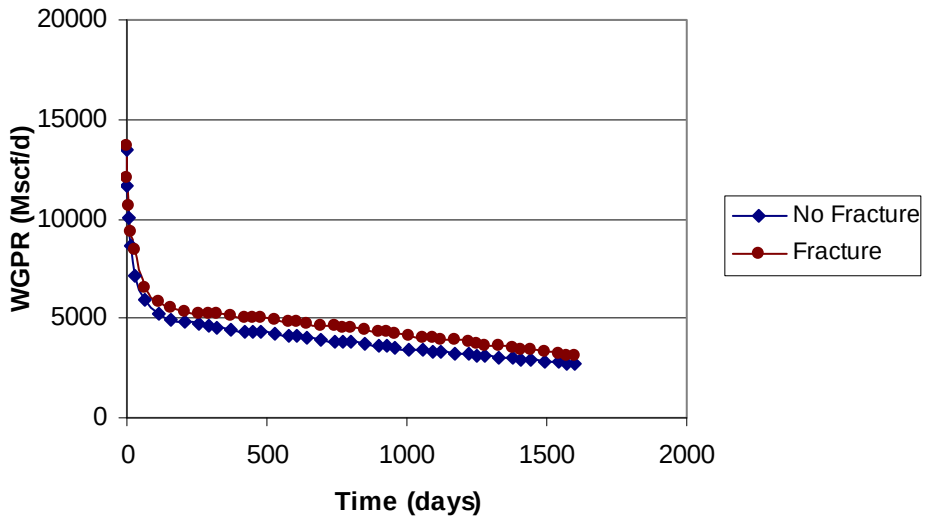

Figure 6-32: Effect of fracture on gas production rate (WGPR).

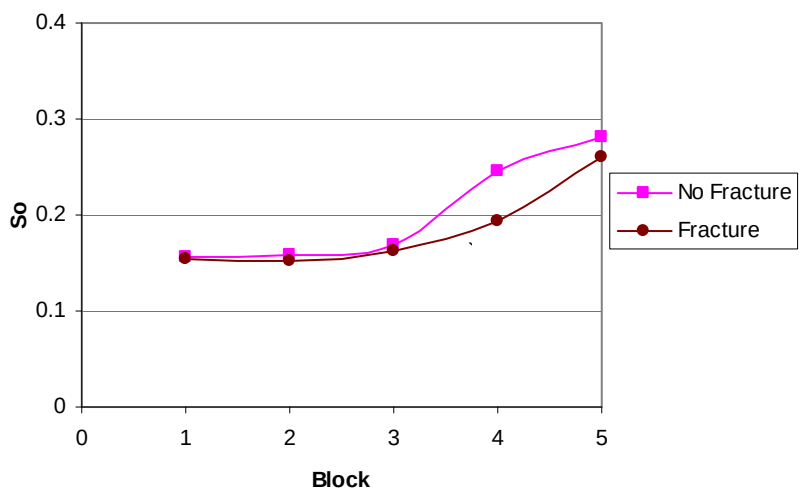

Figure 6-33: Effect of fracture on condensate saturation profile.

6.2.2. Gas Cycling

After that, we studied the effect of gas-cycling on the condensate production rate and condensate dropout in the reservoir. The model considered is similar to the simplified model SPE3 that we considered before. The reservoir has only one layer and contains only immobile water. A single injector is at the corner block 1x1 and a single producer is at the center of the reservoir. The producer is set at a target gas rate of 6200 MSCF/day with a minimum bottom-hole pressure of 500 psi. The gas injected is the lean gas from the producer. Figure 6-34, Figure 6-35 and Figure 6-36 show that the more gas injected

back in reservoir, the more condensate is produced and the smaller the amount of condensate in the producing well block.

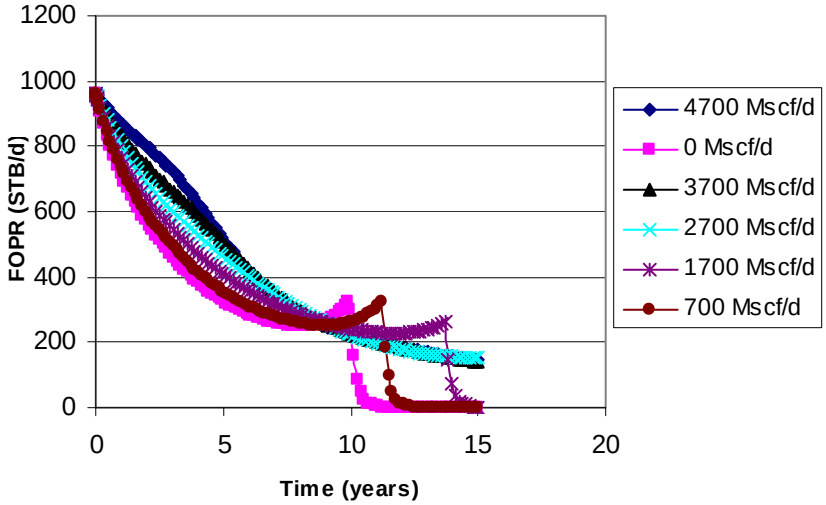

Figure 6-34: Condensate field production rate (FOPR) with different lean gas injection rates.

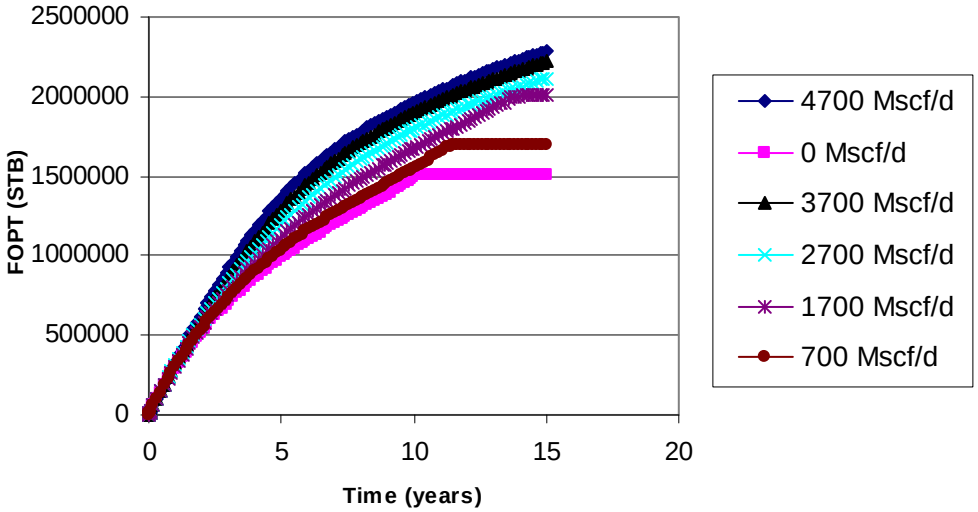

Figure 6-35: Condensate field production total (FOPT) with different lean gas injection rates.

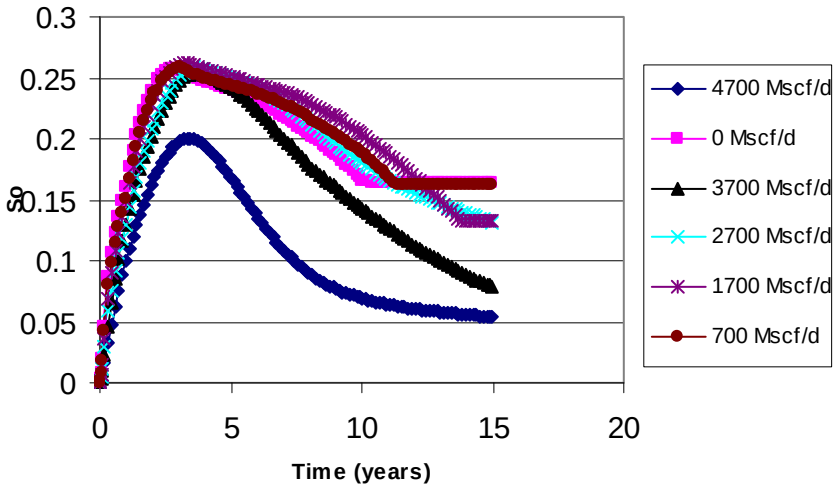

Figure 6-36: Condensate saturation in the production well block with different lean gas injection rates.

6.2.3. Different Injection Gases

The efficiency of different injection gases was also studied. Figure 6-37, Figure 6-38 and Figure 6-39 show that the condensate recovery and amount of condensate in the producing well block also depend on the type of gas used as the injection gas.

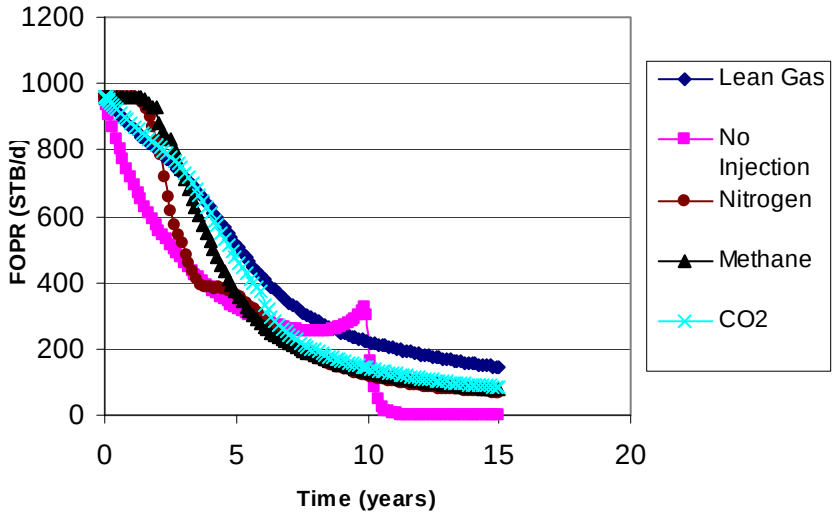

Figure 6-37: Condensate field production rate (FOPR) with different injection gases.

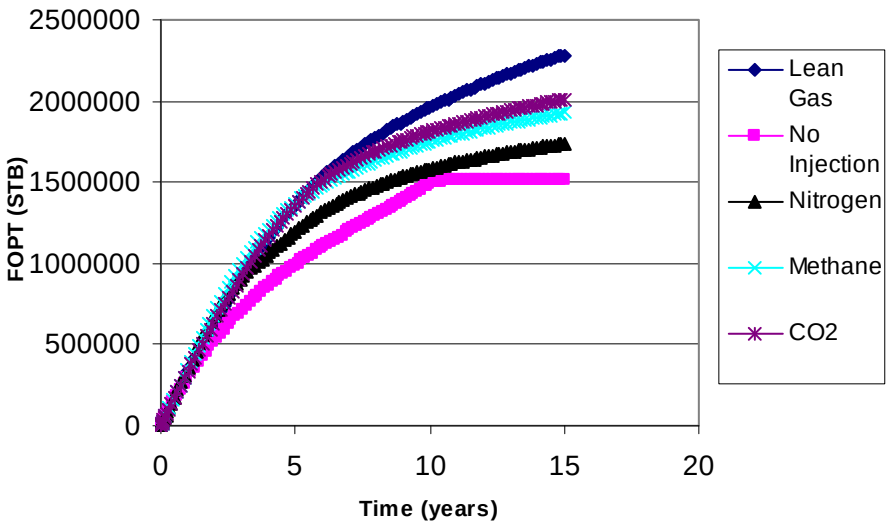

Figure 6-38: Condensate field production total (FOPT) with different injection gases.

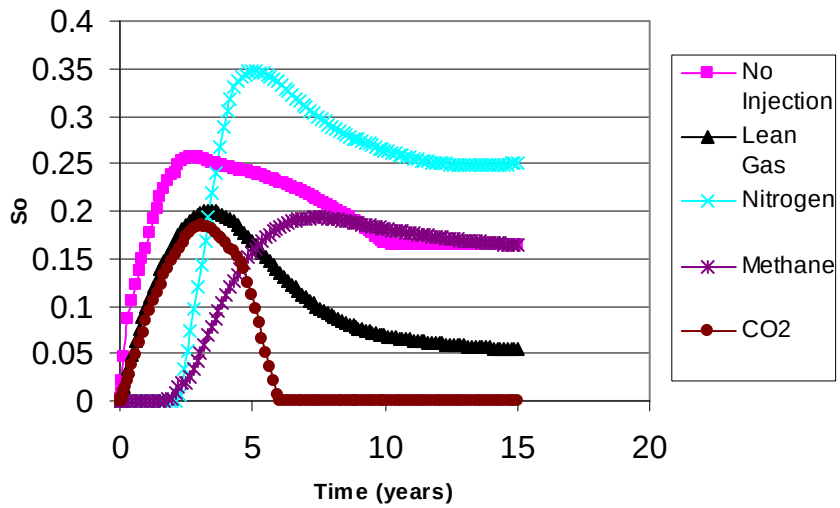

Figure 6-39: Condensate saturation in the production well block with different injection gases.

6.3. Optimization of Revenue from Gas-Condensate Reservoirs

This section deals with the optimization problem of a gas condensate reservoir using C_1 injection. The reservoir model for the optimization problem in this case consists of one injector and two producers. The two producers are set at a constant gas production rate of 4,500 Mscf/d. The gas injection rate is varied to achieve the maximum NPV. The objective function is:

$$NPV = FOPT \times 80 + FGPT \times 4 - FGIT \times 6. \quad (6.1)$$

FOPT: Field Oil Production Total (STB)

FGPT: Field Gas Production Total (Mscf)

FGIT: Field Gas Injection Total (Mscf).

In this calculation, the discount factor was taken to be zero. 80 is the oil price ($/STB), 4 is the produced gas price ($/Mscf), and 6 is the cost for injecting gas ($/Mscf).

There are two categories of optimization algorithms being used: stochastic and gradient based. Stochastic algorithms like Genetic Algorithm (GA), or Particle Swarm Optimization (PSO), in theory are capable of finding a global optimum. However, these algorithms require many function evaluation runs (flow simulations) and do not guarantee minimization/maximization of the objective function. On the other hand, gradient-based algorithms only assure local optimal points but require fewer function evaluation runs. For the compositional problem of gas-condensate in a large and complex reservoir, gradient-based algorithms are preferred because of the computational cost of the simulation runs (function evaluations). The difficulty with a gradient-based algorithm is to calculate gradients of the objective function with respect to the control parameters. This requires either access to the source code or a simulator that has the gradient based optimization capabilities built-in. ECLIPSE 300 is such a simulator. Figures 6-40 to 6-45 show results. In this case the optimal result is not the one with maximum injection rate. It is evident that injecting C_1 changes the thermodynamic properties of the fluid system.

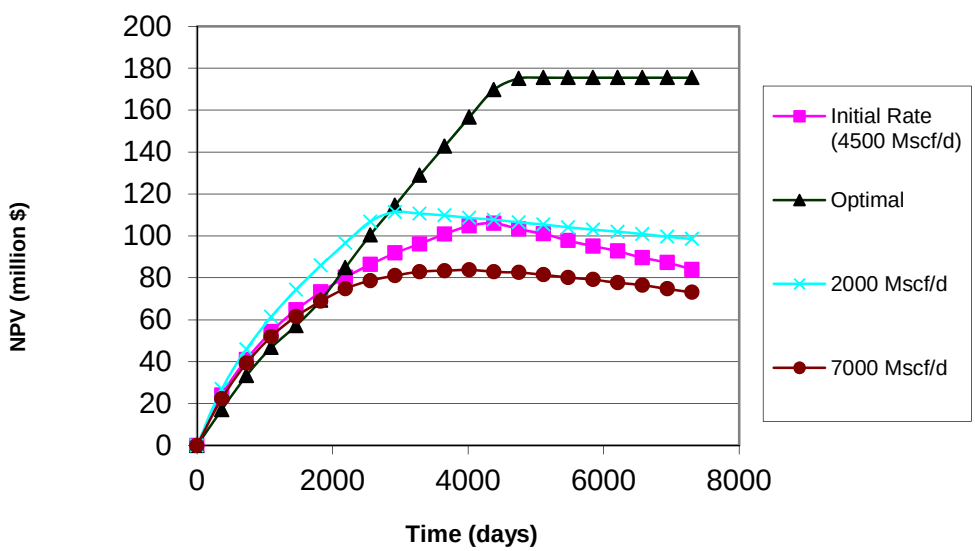

Figure 6-40: Revenue of a gas-condensate reservoir under different injection rate scenarios.

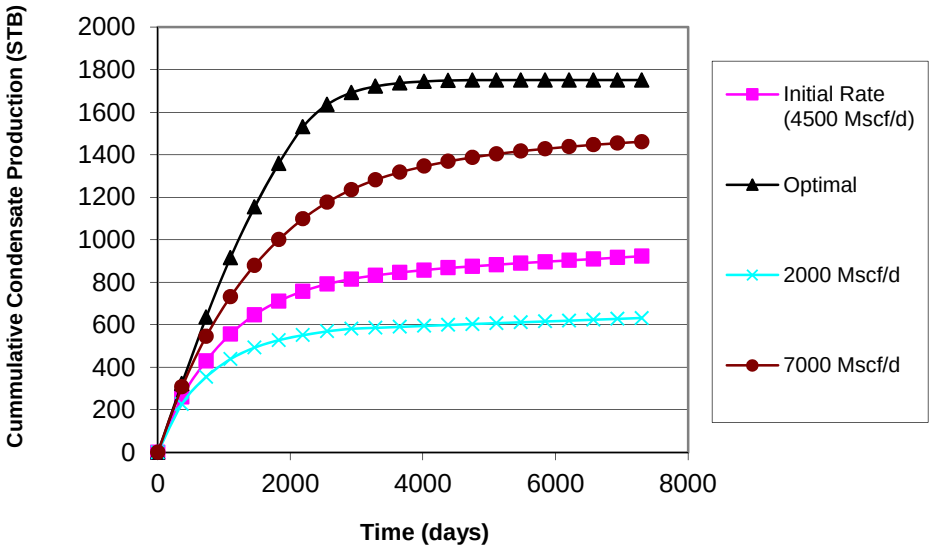

Figure 6-41: Cumulative condensate production of the optimization problem.

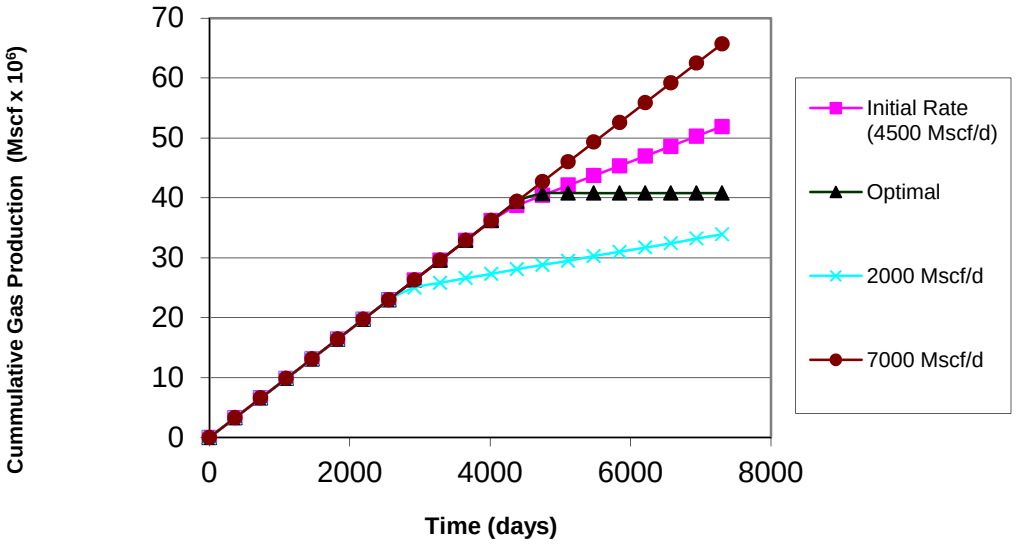

Figure 6-42: Cumulative gas production of the optimization problem.

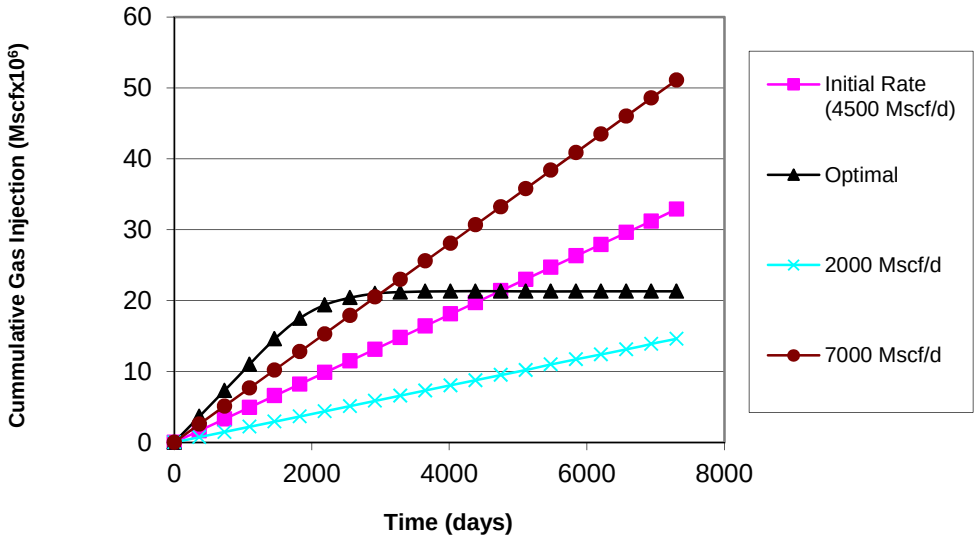

Figure 6-43: Cumulative gas injection of the optimization problem.

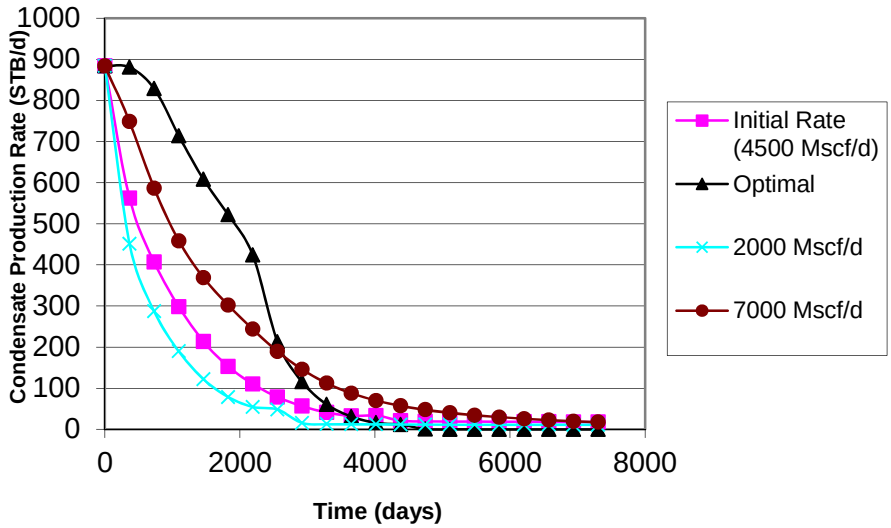

Figure 6-44: Condensate production rate of the optimization problem.

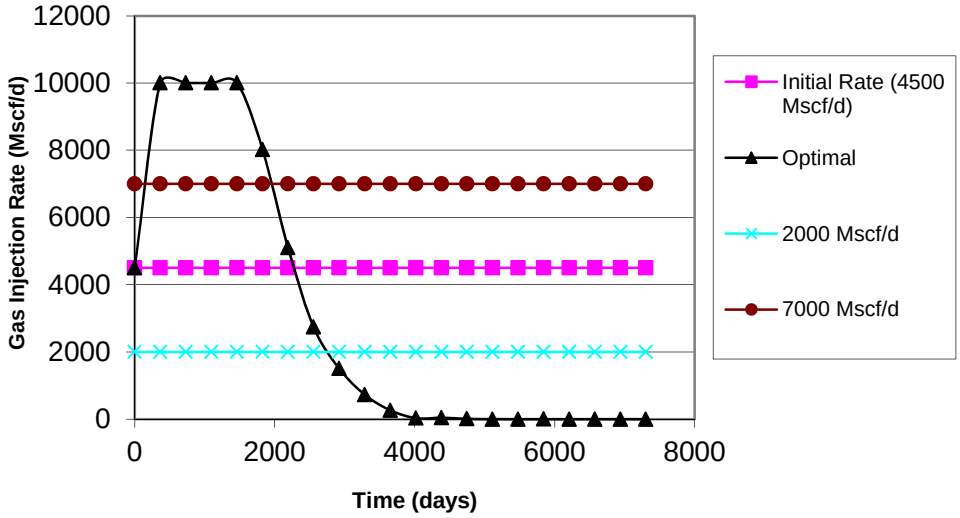

Figure 6-45: Gas injection rate of the optimization problem.

Chapter 7

7. Conclusion

7.1. General Conclusions

The main conclusions of this study are:

- Repeatability of the capture and noncapture experiments was achieved, demonstrating the validity of the results.

- Due to the relative permeability and the consequent difference in mobilities of gas and condensate phase, the local composition will change hence the phase envelope of the mixture will shift from a gas-condensate to a volatile oil. This shift was evident in both the experiments and the simulation results, as the thermodynamic behavior followed a different phase envelope during production than that of the original fluid.

- Condensate banking still occurs in the presence of immobile water. Water did not have any measurable effect on the compositional variation of the gas condensate in the experiments done here.

- Shutting a well to remove the condensate banking is not a good strategy as the condensate will not be able to revaporize due to the shift of the phase envelope.

- Condensate banking can be reduced by minimizing the pressure drop below the dew point, either by producing the well slowly or by applying partial pressure maintenance using gas injection.

- The performance of gas condensate well can be improved by using a proper production strategy.

- Hydraulic fracturing and gas injection are the most common and efficient enhancement techniques for gas-condensate reservoirs.

7.2. Suggestions for Future Work

First, as we can see from saturation results in Section 4.4, the titanium core holder attenuated the X-rays during CT scanner. Future experiments should calibrate the scans to determine whether the range of CT value between all liquid and all gas is linear. Alternatively, an aluminum core holder may be more suitable.

Second, the Joule-Thompson effect, which can make the pressure depletion nonisothermal should be considered.

Thirdly, the sensitivity study of fracture length, fracture conductivity to the recovery of gas and condensate in a gas condensate reservoir should be carried out.

Finally, the study of reservoir optimization using gas injection should be extended.

Nomenclature

BHP	= well flowing bottom-hole pressure.
p_d	= dew-point pressure.
C_1	= methane.
C_4	= butane.
nC_4	= n-butane (normal butane).
N_2	= nitrogen.
CO_2	= carbon dioxide.
C_{7+}	= heptanes plus.
CCE	= Constant Composition Expansion.
CVD	= Constant Volume Depletion.
PVT	= Pressure Temperature Volume.
T_c	= critical temperature.
p_c	= critical pressure.
C_5	= pentane.
S_{wi}	= immobile water saturation.
CT	= Computerized Tomography.
CT_A	= CT number of the object “A”.
μ_A	= linear attenuation coefficient of object “A".
S_c	= condensate saturation.
CT_{gr}	= CT number of gas saturated rock.
CT_{cr}	= CT number of condensate saturated rock.
CT_{exp}	= CT number of rock during experiments with C1-nC4 mixture.
P_2	= port #2.
GC	= Gas Chromatography.
TCD	= thermal conductivity detector.
$PLOT$	= Porous Layer Open Tubular.
DI	= Deionized.
k_g	= gas permeability.
k_{rcm}	= completely miscible condensate relative permeability.
k_{rgm}	= completely miscible gas relative permeability.
k_{rci}	= completely immiscible condensate relative permeability.

k_{rgi} = completely immiscible gas relative permeability.

p_{in} = inlet pressure.

p_{out} = outlet pressure.

q_{out} = volumetric flowrate measured at the outlet.

L = length of a core.

A = cross-sectional area of a core.

ϕ = porosity.

S_j = saturation of phase j^{th}.

ρ_j = molar density of phase j^{th}.

k_{rj} = relative permeability of phase j^{th}.

∇p_j = pressure gradient of phase j^{th}.

$x_{i,j}$ = mole fraction of component i^{th} in phase j^{th}.

σ = interfacial tension (IFT)

References

Afidick, D., Kaczorowski, N.J., and Bette, S., 1994, "*Production Performance of a Retrograde Gas Reservoir: A Case Study of the Arun Field*", Presentation at SPE Asia Pacific Oil and Gas Conference, Melbourne, Australia, SPE 28749.

Agilent Technologies, 2008, "*Agilent 3000 Micro Gas Chromatograph*", User Information, Third Edition.

Agilent Technologies, "*Agilent Cerity Tutorial*".

Akin, S. and Kovscek, A.R., 2003, "*Computed Tomography in Petroleum Engineering Research*". Geological Society special publications, pp 22–38.

Al-Hasim, H.S., Hashim, S.S., 2000 "Long-Term Performance of *Hydraulically Fractured Layered Rich Gas Condensate Reservoir*", Presentation at SPE International Oil and Gas Conference and Exhibition, SPE 64774.

Ali, J.K., McGauley, P.J., and Wilson, C.J., 1997, "*Experimental Studies and Modeling of Gas Condensate Flow near the Wellbore*", Presentation at Fifth Latin America and Caribbean Petroleum Engineering Conference and Exhibition, Brazil, SPE 39053.

Allen F.H. and Roe R. P., 1950, "*Performance Characteristics of a Volumetric Condensate Reservoir*", Petroleum Transaction, AIME, Vol. 189.

Aziz, K., Durlofsky, L., and Tchelepi, H., Winter 2010, "*Notes for ENERGY 223: Reservoir Simulation*", Stanford University.

Aziz, R.M., 1985, "*Deliverability Projection Model for Overpressure Gas-Condensate Reservoirs*", SPE Middle East Oil Technical Conference and Exhibition, Bahrain, SPE 13706.

Barnum, R.S., Brinkman, F.P., Richardson, T.W., and Spillette, A.G., 1995, "*Gas Condensate Reservoir Behavior: Productivity and Recovery Reduction Due to Condensation*", Presentation at SPE Annual Technical Conference and Exhibition, Dallas, USA, SPE 30767.

Bengherbia, M. and Tiab, D., 2002, "*Gas-Condensate Well Performance Using Compositional Simulator: A Case Study*", Presentation at SPE Gas Technology Symposium, SPE 75531.

Coats, K. H. and Thomas, L.K., 1998, "*Compositional and Black Oil Reservoir Simulation*", SPE Reservoir Evaluation & Engineering, August 1998.

Coats, K. H., 1980, "*An Equation of State Compositional Model*", SPEJ, Oct 1980.

Coats, K. H., 1985, "*Simulation of Gas Condensate Reservoir Performance*", JPT.

Danesh, A., 1998, "*PVT and Phase Behaviour of Petroleum Reservoir Fluids*", Elsevier Science B.V.

Economides, M.J., Dehghani, K., Ogbe, D.O., and Ostermann, R.D., 1987, "*Hysteresis Effects of Gas Condensate Wells Undergoing Buildup Tests below the Dew-point Pressure*", Presentation at SPE Annual Technical Conference and Exhibition, Dallas, USA, SPE 16748.

Eilerts, C.K., Sumner E.F and Potts N.L., 1965, "*Integration of Partial Differential Equation for Transient Radial Flow of Gas-Condensate Fluids in Porous Structures*", SPEJ 141.

El-Banbi, A.H., ain W.D., and Semmelbeck, M.E., "*Investigation of Well Productivity in Gas-Condensate Reservoirs*", Presentation at SPE/CERI Gas Technology Symposium, Calgary, Canada, SPE 59773.

Fevang, Φ, 1995, "*Gas Condensate Flow Behavior and Sampling*", Ph. D. Dissertation, University of Trondheim.

Fevang, Φ and Whitson, C.H., 1996, "*Modeling Gas-Condensate Well Deliverability*", SPE Reservoir Engineering, pp 221-230.

Fussel, D.D., 1973, "*Single-Well Performance Predictions for Gas Condensate Reservoirs*", JPT 258, Trans. , AIME, 255.

GE Medical System, 2000, "*HiSpeed CT/i Technical Reference Manual*", Rev 8.

GE Medical System, "*HiSpeed CT/i TiP Tutorial*", Rev. 4, A Training in Partnership Program.

Gerritsen, M., 2008, "*Fundamental of Petroleum Engineering*", E120 lectures.

Hagoort, J., 1988, "*Fundamentals of Gas Reservoir Engineering*", Elsevier Science B.V.

Ikoku, C.U., 1984, "*Natural Gas Reservoir Engineering*", John Wiley & Sons Inc.

Jones, J.R. and Raghavan, R., 1985, "*Interpretation of Flowing Well Responses in Gas – Condensate Wells*", Presentation at SPE Annual Technical Conference and Exhibition, Las Vegas , Nevada, SPE 14204.

Jones, J.R., Vo, D.T., and Raghavan, R., 1986, "*Interpretation of Pressure Buildup Responses in Gas – Condensate Wells*", Presentation at SPE Annual Technical Conference and Exhibition, New Orleans, SPE 15535.

Kay, W. B., 1940, "*Pressure-Volume-Temperature Relations for n-Butane*", Ind. Eng. Chem., 32 (3), pp 358–360.

Kenyon, D. E., Behie, G. A., 1987: "Third SPE Comparative Solution Project: Gas Cycling of Retrograde Condensate Reservoirs". *Journal of Petroleum Technology*, August 1987.

Kniazeff, V.J. and Naville, S.A., 1965, "*Two-Phase Flow of Volatile Hydrocarbons*", SPEJ 37, Trans., AIME, 234.

Kovscek, A. R., Autumn 2010, "*Petroleum Hydrocarbon Thermodynamics: An Equation of State Approach*", Stanford University.

Lal, R.R., 2003, "*Well Testing in Gas-Condensate Reservoirs*", M.S. Thesis, Stanford University.

McCain, W.D., Jr., 1990, "*The Properties of Petroleum Fluids*", Second edition, PennWell Books.

McCain, W.D., Jr., Bridges, B., 1994, "*Heavy Components Control Reservoir Fluid Behavior*", JPT, Sep. 1994.

McCain, W.D., Jr., 1994, "*Volatile Oils and Retrograde Gases – What's the difference*?", Petroleum Engineering International 35.

Muscat, M., 1949, "*Physical Principles of Oil Production"*, McGraw-Hill Book Company, Inc.

Nikravesh, M. and Soroush, M., 1996, "*Theoretical Methodology for Prediction of Gas-Condensate Flow Behavior*", Presentation at SPE Annual Technical Conference and Exhibition, Denver, USA, SPE 36704.

Novosad, Z., 1996, "*Compositional and Phase Changes in Testing and Producing Retrograde Gas Wells*", SPE Reservoir Engineering, November 1996.

O'Dell, H.G. and Miller, R.N., 1967, "*Successfully Cycling a Low Permeability, High-Yield Gas-Condensate Reservoir*", JPT 41, Trans., AIME, 240.

Pedersen, K.S., Fredenslund, A., and Thomassen, P., 1989, "*Properties of Oils and Natural Gases*", Gulf Publishing Company.

Perry, A.J, 1981, "*Introduction to Analytical Gas Chromatography*", Marcel Dekker, Inc.

Ravari, R.R., Wattenbarger, R.A., Ibrahim, M., 2005, "*Gas Condensate Damage in Hydraulically Fractured Wells*", Presentation at 2005 Asia Pacific Oil & Gas Conference and Exhibition, SPE 93248.

Roebuck, I.F., Henderson, G.E., Doughlas, J., Ford, W.T., 1968, "*The Compositional Reservoir Simulator: Case I –The Linear Model*", SPEJ March, 1969 115-130.

Roebuck, I.F., Ford, W.T., Henderson, G.E., Doughlas, J., 1968, "*The Compositional Reservoir Simulator; Case IV – The Two Dimensional Model*", SPE Annual Meeting, Houston, Texas, SPE 2235.

Roussennac, B., 2001, "*Gas Condensate Well Testing Analysis*", M.S. Thesis, Stanford University, California.

Saeidi, A. and Handy, L.L., 1974, "*Flow and Phase Behavior of Gas Condensate and Volatile Oils in Porous Media*", SPE Annual California Regional Meeting, SPE 4891.

Salam, E.A., Mucharam, L., Abdassah, D., Parhusip, B., and Panjaitan, P.R., 1996, "*Modification of the CVD Test Approach and Its Application for Predicting Gas Deliverability from Gas-Condensate Reservoir of Talang Akar Formation in Indonesia*", Presentation at SPE Gas Technology Conference, Calgary, Canada, SPE 35648.

Scott, R. P.W., 1998, "*Introduction to Analytical Gas Chromatography*", Chromatographic Sciences Series, Volumes 76.

Seminar papers from two conferences held, "*North Sea Gas Condensate Reservoir & Their Development 1982*", May & October 1982, published by Oyez Scientific & Technical Services Ltd.

Shen, P., Luo, K., Zheng, X., Li, S., Dai, Z., and Liu, H., 2001, "*Experimental Study of Near-Critical Behavior of Gas Condensate Systems*", Presentation at SPE Production and Operation Symposium, Oklahoma, USA, SPE 67285.

Shi, Chunmei, 2009, "*Flow Behaviors of Gas Condensate Wells*", Ph.D. Dissertation, Stanford University, California.

Sigmund P.M., Dranchuk, P.M., Morrow, N.R., and Purvis, R.A., 1971, "*Retrograde Condensation in Porous Media*'', Presentation at SPE Annual Fall Meeting, New Orleans, SPE 3476.

Standing, M.B., 1952, "*Volumetric and Phase Behavior of Oilfield Hydrocarbon Systems*", Reinhold Publishing Corporation.

Vinegar, H. and Wellington, S., 1987, "*Tomographic imaging of three-phase flow experiments*". Rev. Sci. Instrum. 58 January 1987.

Vinegar, H. and Wellington, S., 1987, "*X-Ray Computerized Tomography*", Journal of Petroleum Technology, August 1987.

Whitson, C. H. and Brulé, M. R., 2000, "*Phase Behavior*", SPE monograph, volume 20.

Zhang, H.R. and Wheaton, R.J., 2000, "*Condensate Banking Dynamics in Gas Condensate Fields: Compositional Changes and Condensate Accumulation around Production Wells*", Presentation at SPE Annual Technical Conference and Exhibition, SPE 62930.

Appendix A

A. Gas-condensate Simulation Input File for Experiments

```
--                    ECLIPSE INPUT FILE
--   Production PERFORMANCE OF A L= 30 cm, D=5.06 cm Cylindrical core.
--   Gas-condensate draw down test
--        Permeability = 9 mD, Porosity = 16.0%
--        Modified 05/14/10 Add smooth krw functions
--        Simulator: Eclipse 300, 2001 v
--        The purpose is to design the Gas-condensate:
--        determine the composition and liquid saturation
--        distribution in the core.

RUNSPEC  ============================================================

OIL
GAS


FULLIMP

WELLDIMS
 10 50 3 3 5 10 5 4 3 0 /

DIMENS
51 1 1 /

NSTACK
50/

-- condensate

ISGAS

-- Units:

LAB

-- Number of components: implies compositional run
COMPS
 2 /

MISCIBLE
/
```

```
FMTOUT
UNIFOUT

GRID    ============================================================

-- PV = 0.3*5000 m^2

INIT

DX
  51*0.51837  /
DY
  51*4.48  /

DZ
  51*4.48  /

--OLDTRAN

-- Porosity and permeability

--- (Rock)
BOX
---   IX1-IX2   JY1-JY2   KZ1-KZ2
      1   51    1   1     1   1    /
INCLUDE
'Perm.txt'/

---   TOP Specification
--BOX
---   IX1-IX2   JY1-JY2  KZ1-KZ1
--          1  1     1   1    1  1 /
TOPS
    51*0.0 /

ENDBOX

---   TOP Specification
--BOX
---   IX1-IX2   JY1-JY2  KZ1-KZ1
--          1  1     1   1    1  1 /
TOPS
    51*1 /

ENDBOX


PROPS   ============================================================

-- Properties section: PVT data from INCLUDE file

EOS
PR  /

-- Names of Components
```

```
CNAMES
C1
nC4
/

-- Miscibility exponent
MISCEXP
0.000000001 /

-- Component Critical Temperatures  (K)
TCRIT
190.5611111
425.2
/

-- Component Critical Pressures   (atm)
PCRIT
45.44
37.46953
/
-- Component Critical Volumes  (m3/kg-mole)
--  set by user
VCRIT
0.098
0.255
/

-- Component acentric factor
ACF
0.013
0.201
/


-- Components Parachors  (dyn/cm)
--        (for IFT - Fanchi 1990)
--PARACHOR
--77
--189.9
/

-- Peneleux Correction (Shift parameters DM-less)
SSHIFT
0.
0.
/

-- Component Molecular Weight  g/mol
MW
16.04
58.12
/

-- Binary interaction parameters
BIC
```

```
0.0
/

STCOND
15.0 1.0 /

-- Reservoir temperature: Deg C / K
RTEMP
--20  / 293.15K
20  / 293.15K

-- Rock and fluid properties

ROCK
132.7  0.00000000001  /

--Gas saturation functions
INCLUDE
KrgoGC2.dat
/

MISCSTR
-- miscibility surface tension reference
12.3048 /
/

STVP
-- Surface tension with respect to pressure
300  12.3048
400  11.1124
500  9.9551
600  8.837
700  7.7623
800  6.7356
900  5.7616
1000 4.8454
1100 3.9918
1200 3.2063
1300 2.4941
1400 1.8605
1500 1.311
1600 0.8507
1700 0.4848
1800 0.2181
1850 0.1234
1900 0.0552
1925 0.0311
1950 0.0139
1975 0.0035 /
/
FVST
--Specify miscibility variation with surface tension
0.0035  0.441977
0.0139  0.507334
0.0311  0.549881
```

```
0.0552  0.582353
0.1234  0.631138
0.2181  0.668126
0.4848  0.723684
0.8507  0.765544
1.311   0.799379
1.8605  0.827857
2.4941  0.852479
3.2063  0.874164
3.9918  0.893531
4.8454  0.911015
5.7616  0.92693
6.7356  0.941521
7.7623  0.954974
8.837   0.967438
9.9551  0.979032
11.1124 0.989859
12.3048 1.0 /
/

SOLUTION ==============================================================

PRESSURE

--          Pressure (atm)
51*149.7      /

SGAS
1.0 50*1.0  /

-- XMF
-- 51*0.85 51*0.15  /

XMF
51*0.00 51*0.00 /

YMF
51*0.85 51*0.15 /

--  Calculate initial oil and gas in place at surface conditions

FIELDSEP
1 15.0 1.0 /
/

SUMMARY  ==============================================================

RUNSUM
RPTONLY
--Field Gas Production Rate
WGPR
PROD1 /
/
WGPT
PROD1 /
```

```
/
WPIG
PROD1 /
/
WOPR
PROD1 /
/
WOPT
PROD1 /
/
WGOR
PROD1 /
/
WBHP
PROD1 /
/
WYMF
PROD1 1 /
/
WYMF
PROD1 2 /
/
WZMF
PROD1 1 /
/
WZMF
PROD1 2/
/
--Producer block data

BVOIL
50 1 1 /
/

--saturation and composition history for layer 4
INCLUDE
'BPRES.txt'/

INCLUDE
'BSOIL.txt'/

INCLUDE
'BXMF1.txt'/

INCLUDE
'BXMF2.txt'/

INCLUDE
'BYMF1.txt'/

INCLUDE
'BYMF2.txt'/

INCLUDE
'BBOIL.txt'/
```

```
INCLUDE
'BBGAS.txt'/

INCLUDE
'BMLSC2.txt'/

INCLUDE
'BMLST.txt'/

INCLUDE
'BVMF.txt'/
/

SCHEDULE ==============================================================

/

WELLSPEC
INJ1  G1  1 1 3* /
PROD1 G2  51 1 3*   /
/

WELLCOMP
INJ1     1  1  1  1 1* 0.15875 5* /
PROD1    51  1  1  1  1* 0.15875 5*  /
/

-- Specify compositions of injection gas stream
WELLSTRE
LEANGAS   0.85 0.15                                        /
/

WCONINJE
--INJ1 GAS AUTO BHP 125. /
INJ1 GAS AUTO BHP 2* 149.7/
/

WINJGAS
INJ1 STREAM LEANGAS/
/

WCONPROD
PROD1 OPEN BHP 5* 68.72642 /
--PROD1 OPEN BHP 2* 75./
/


--RPTSCHED
--PRESSURE  SOIL KRG KRO /
--PRESSURE  SOIL XMF YMF ZMF VMF DENO DENG VOIL VGAS BOIL BGAS KRG KRO /

--TSCRIT
--0.00001 0.0000001 10
--/
```

```
TUNING
  .000277 0.05  0.0000277 /
  /
   /


TSTEP
60*0.00166667 60*0.5 /

END
```

Appendix B

B. Gas-condensate with Immobile Water Simulation Input File for Experiments

```
--                    ECLIPSE INPUT FILE
--    Production PERFORMANCE OF A Cylindrical core with dimesnsion L= 27.4 cm, D=5.06 cm .
--    Gas-condensate draw down test
--          Permeability = 2.1 mD, Porosity = 15.0%
--          Modified from Shi's input file on 02/02/10 by adding water phase
--          Simulator: Eclipse 300, 2001 v
--          The purpose is to design the Gas-condensate experiment with the presence of immobile water:
--          determine the length, permeability to get a suitable liquid saturation
--          distribution in the core.

RUNSPEC  ==============================================================

OIL
GAS

WATER


FULLIMP

WELLDIMS
 10 50 3 3 5 10 5 4 3 0 /

DIMENS
51 1 1 /

NSTACK
50/

-- condensate

ISGAS

-- Units:

LAB

-- Number of components: implies compositional run
COMPS
 2 /

MISCIBLE
```

```
/
FMTOUT
UNIFOUT

GRID    ============================================================

-- PV = 0.3*5000 m^2

INIT

DX
  51*0.51837  /
DY
  51*4.48  /

DZ
  51*4.48  /

--OLDTRAN

-- Porosity and permeability

--- (Rock)
BOX
---   IX1-IX2   JY1-JY2   KZ1-KZ2
      1   51    1   1     1   1    /
INCLUDE
'Physicalprop.txt'/

---   TOP Specification
--BOX
---   IX1-IX2   JY1-JY2  KZ1-KZ1
--          1  1     1   1    1  1 /
TOPS
    51*0.0 /

ENDBOX

---   TOP Specification
--BOX
---   IX1-IX2   JY1-JY2  KZ1-KZ1
--          1  1     1   1    1  1 /
TOPS
    51*1 /

ENDBOX


PROPS   ============================================================

-- Properties section: PVT data from INCLUDE file

EOS
PR  /
```

```
-- Names of Components
CNAMES
C1
nC4
/

-- Miscibility exponent
MISCEXP
0.000000001 /

-- Component Critical Temperatures  (K)
TCRIT
190.5611111
425.2
/

-- Component Critical Pressures   (atm)
PCRIT
45.44
37.46953
/
-- Component Critical Volumes  (m3/kg-mole)
--  set by user
VCRIT
0.098
0.255
/

-- Component acentric factor
ACF
0.013
0.201
/


-- Components Parachors  (dyn/cm)
--        (for IFT - Fanchi 1990)
--PARACHOR
--77
--189.9
/

-- Peneleux Correction (Shift parameters DM-less)
SSHIFT
0.
0.
/

-- Component Molecular Weight  g/mol
MW
16.04
58.12
/

-- Binary interaction parameters
```

```
BIC
0.0
/

STCOND
15.0 1.0 /

-- Reservoir temperature: Deg C / K
RTEMP
--20  / 293.15K
20  / 293.15K

-- Rock and fluid properties

ROCK
132.7  0.00000000001  /

--Gas saturation functions
INCLUDE
kr3phase.txt
/

MISCSTR
-- miscibility surface tension reference
12.3048 /
/

STVP
-- Surface tension with respect to pressure
300  12.3048
400  11.1124
500  9.9551
600  8.837
700  7.7623
800  6.7356
900  5.7616
1000 4.8454
1100 3.9918
1200 3.2063
1300 2.4941
1400 1.8605
1500 1.311
1600 0.8507
1700 0.4848
1800 0.2181
1850 0.1234
1900 0.0552
1925 0.0311
1950 0.0139
1975 0.0035 /
/
FVST
--Specify miscibility variation with surface tension
0.0035  0.441977
0.0139  0.507334
```

```
0.0311  0.549881
0.0552  0.582353
0.1234  0.631138
0.2181  0.668126
0.4848  0.723684
0.8507  0.765544
1.311   0.799379
1.8605  0.827857
2.4941  0.852479
3.2063  0.874164
3.9918  0.893531
4.8454  0.911015
5.7616  0.92693
6.7356  0.941521
7.7623  0.954974
8.837   0.967438
9.9551  0.979032
11.1124 0.989859
12.3048 1.0 /
/

SOLUTION ==============================================================

PRESSURE

--          Pressure (atm)
51*149.7      /

SWAT
0.16 50*0.16  /
SGAS
0.84 50*0.84  /

XMF
--51*0.85 51*0.15  /
51*0.00 51*0.00  /

YMF
51*0.85 51*0.15 /

--  Calculate initial oil and gas in place at surface conditions

FIELDSEP
1 15.0 1.0 /
/

SUMMARY  ==============================================================

RUNSUM
RPTONLY
--Field Gas Production Rate
WGPR
PROD1 /
/
WGPT
```

```
PROD1 /
/
WPIG
PROD1 /
/
WOPR
PROD1 /
/
WOPT
PROD1 /
/
WGOR
PROD1 /
/
WBHP
PROD1 /
/
WYMF
PROD1 1 /
/
WYMF
PROD1 2 /
/
WZMF
PROD1 1 /
/
WZMF
PROD1 2/
/
--Producer block data

BVOIL
50 1 1 /
/

--saturation and composition history
INCLUDE
'BPRES.txt'/

INCLUDE
'BSOIL.txt'/

INCLUDE
'BSWAT.txt'/

INCLUDE
'BSGAS.txt'/

INCLUDE
'BXMF1.txt'/

INCLUDE
'BXMF2.txt'/

INCLUDE
```

```
'BYMF1.txt'/

INCLUDE
'BYMF2.txt'/

INCLUDE
'BBOIL.txt'/

INCLUDE
'BBGAS.txt'/

INCLUDE
'BMLSC2.txt'/

INCLUDE
'BMLST.txt'/

INCLUDE
'BVMF.txt'/
/

SCHEDULE ============================================================

/

WELLSPEC
INJ1  G1  1 1 3* /
PROD1 G2  50 1 3*   /
/

WELLCOMP
INJ1     1  1  1  1 1* 0.15875 5* /
PROD1    51  1  1  1  1* 0.15875 5*  /
/

-- Specify compositions of injection gas stream
WELLSTRE
LEANGAS   0.85 0.15                                        /
/

WCONINJE
--INJ1 GAS AUTO BHP 125. /
INJ1 GAS AUTO BHP 2* 149.7 /
/

WINJGAS
INJ1 STREAM LEANGAS/
/

WCONPROD
PROD1 OPEN BHP 5* 68.72642 /
--PROD1 OPEN BHP 2* 75./
/
```

```
--RPTSCHED
--PRESSURE  SOIL KRG KRO /
--PRESSURE  SOIL XMF YMF ZMF VMF DENO DENG VOIL VGAS BOIL BGAS KRG KRO /

--TSCRIT
--0.00001 0.0000001 10
--/

TUNING
  .000277 0.05  0.0000277 /
  /
    /


TSTEP
60*0.00166667 60*0.5 /

END
```

Appendix C

C. Simulation Input File for Binary Gas-Condensate System at Field Scale

```
--                    ECLIPSE INPUT FILE
--
-----------------------------------------------------------------------
-->Binary Gas-condensate problem
-- 2 components
-- Peng-Robinson EoS with correction
-- Grid dimensions 36x1x4, RADIAL
-- Fully implicit solution method
-- FIELD units
-- 3-stage separator
-----------------------------------------------------------------------

--RUNSPEC section-----------------------------------------------

RUNSPEC

RADIAL

--Request the FIELD unit set
FIELD

--Water is present
WATER

--FULLIMP solution method

FULLIMP
--Nine components in study ( plus water )

COMPS
2 /

--Peng-Robinson equation of state to be used
EOS
PR /

DIMENS
36 1 4 /

TABDIMS
1 1 40 40 /
```

```
--Is a gas condensate study
ISGAS

MULTSAVE
0 /
--DEBUG3
--4*0 1 1 0 1 /
/
--Grid section-------------------------------------------------------

GRID
--Basic grid block sizes
INRAD
0.3/
/
DR
0.630957 0.794328 1.000000 1.258925 1.584893 1.995262 2.511886 3.162278 3.981072
5.011872 6.309572 7.943282 10.00000 12.58925 15.84893 19.95262 25.11886 31.62278
39.81072 50.11872 63.09573 79.43282 100.0000 125.8925 158.4893 199.5262 251.1886
316.2278 398.1072 501.1872 630.9573 794.3282 1000.000 1258.925 1584.893 1995.262
0.630957 0.794328 1.000000 1.258925 1.584893 1.995262 2.511886 3.162278 3.981072
5.011872 6.309572 7.943282 10.00000 12.58925 15.84893 19.95262 25.11886 31.62278
39.81072 50.11872 63.09573 79.43282 100.0000 125.8925 158.4893 199.5262 251.1886
316.2278 398.1072 501.1872 630.9573 794.3282 1000.000 1258.925 1584.893 1995.262
0.630957 0.794328 1.000000 1.258925 1.584893 1.995262 2.511886 3.162278 3.981072
5.011872 6.309572 7.943282 10.00000 12.58925 15.84893 19.95262 25.11886 31.62278
39.81072 50.11872 63.09573 79.43282 100.0000 125.8925 158.4893 199.5262 251.1886
316.2278 398.1072 501.1872 630.9573 794.3282 1000.000 1258.925 1584.893 1995.262
0.630957 0.794328 1.000000 1.258925 1.584893 1.995262 2.511886 3.162278 3.981072
5.011872 6.309572 7.943282 10.00000 12.58925 15.84893 19.95262 25.11886 31.62278
39.81072 50.11872 63.09573 79.43282 100.0000 125.8925 158.4893 199.5262 251.1886
316.2278 398.1072 501.1872 630.9573 794.3282 1000.000 1258.925 1584.893 1995.262 /
/
PORO
144*0.13 /

PERMX
36*20 36*4 36*2 36*1.5 /

PERMY
36*20 36*4 36*2 36*1.5 /

PERMZ
36*20 36*4 36*2 36*1.5 /

EQUALS
 DTHETA     360  /
 DZ     30   1 36 1 1 1 2 /
 DZ     50   1 36 1 1 3 4 /
 TOPS   7340 1 36 1 1 1 1 /
 TOPS   7370 1 36 1 1 2 2 /
 TOPS   7400 1 36 1 1 3 3 /
 TOPS   7450 1 36 1 1 4 4 /
/
--Properties section---------------------------------------------
```

```
PROPS

NCOMPS
2 /

EOS
PR /

-- Peng-Robinson correction

PRCORR

-- Standard temperature and pressure in Deg F and PSIA

STCOND
60.0 14.7 /

-- Component names

CNAMES
C1  C4 /

-- Critical temperatures Deg R

TCRIT
343.08000    755.1    /

-- Critical pressures PSIA

PCRIT
667.78170    543.45/

-- Critical Z-factors

ZCRIT
 .28473      0.27717/

-- Acentric factors

ACF
 .01300      0.1956/

-- Molecular Weights

MW
 16.04300     58.124/

-- Omega_A values

OMEGAA
 .4572355   .4572355 /

-- Omega_B values
```

```
OMEGAB
 .0777961     .0777961  /

-- Default fluid sample composition
-- composition not varying with depth
ZMFVD
      1.00000       0.8500       0.1500
  10000.00000       0.8500       0.1500 /

-- Boiling point temperatures Deg R

TBOIL
             200.88 484.02 /

-- Reference temperatures Deg R

TREF
   201.06  527.4 /

-- Reference densities LB/FT3

DREF
    26.53189    35.69/

-- Parachors (Dynes/cm)

PARACHOR
    77.00000    187.2 /

-- Binary Interaction Coefficients

BIC
.000000
 /

-- Reservoir temperature in Deg F

RTEMP
60.0 /

--Water saturation functions

SWFN
   0.16  0      50
   0.20  0.002  32
   0.24  0.010  21
   0.28  0.020  15.5
   0.32  0.033  12.0
   0.36  0.049  9.2
   0.40  0.066  7.0
   0.44  0.090  5.3
   0.48  0.119  4.2
   0.52  0.150  3.4
   0.56  0.186  2.7
   0.60  0.227  2.1
```

```
   0.64  0.277  1.7
   0.68  0.330  1.3
   0.72  0.390  1.0
   0.76  0.462  0.7
   0.8   0.540  0.5
   0.84  0.620  0.4
   0.88  0.710  0.3
   0.92  0.800  0.2
   0.96  0.900  0.1
   1.00  1.000  0.0 /

--Gas saturation functions

SGFN
   0.00  0.000  0.0
   0.04  0.005  0.0
   0.08  0.013  0.0
   0.12  0.026  0.0
   0.16  0.040  0.0
   0.20  0.058  0.0
   0.24  0.078  0.0
   0.28  0.100  0.0
   0.32  0.126  0.0
   0.36  0.156  0.0
   0.40  0.187  0.0
   0.44  0.222  0.0
   0.48  0.260  0.0
   0.52  0.300  0.0
   0.56  0.349  0.0
   0.60  0.400  0.0
   0.64  0.450  0.0
   0.68  0.505  0.0
   0.72  0.562  0.0
   0.76  0.620  0.0
   0.80  0.680  0.0
   0.84  0.740  0.0
/

--Oil saturation functions

SOF3
   0.00  0.000  0.000
   0.04  0.000  0.000
   0.08  0.000  0.000
   0.12  0.000  0.000
   0.16  0.000  0.000
   0.20  0.000  0.000
   0.24  0.000  0.000
   0.28  0.005  0.005
   0.32  0.012  0.012
   0.36  0.024  0.024
   0.40  0.040  0.040
   0.44  0.060  0.060
   0.48  0.082  0.082
   0.52  0.112  0.112
```

```
   0.56  0.150  0.150
   0.60  0.196  0.196
   0.68  0.315  0.315
   0.72  0.400  0.400
   0.76  0.513  0.513
   0.80  0.650  0.650
   0.84  0.800  0.800 /

--Rock and water pressure data

ROCK
3550 0.000004 /

PVTW
3550 1.0 0.000003 0.31 0.0 /

--Surface density of water

DENSITY
1* 63.0 1* /

--Solution section-----------------------------------------------------

SOLUTION

--Equilibration data - initial pressure 1850 psi at 7500, which is
--the oil-water and the oil-gas contact depth

EQUIL
7500 1850 7500 0 7500 0 1 1 0  /

--RPTRST
--PRESSURE SOIL YMF VOIL /

--RPTSOL
--PRESSURE SOIL /

FIELDSEP
 1   80 815 /
 2   80  65 /
 3   60 14.7 /
/

SUMMARY   ==============================================================

--ALL

RUNSUM

--Field oil production rate and total, GOR and field pressure
WGPR
P /
/
WGPT
/
```

```
WBHP
P /
/
BPRES
1 1 4/
/
WZMF
P 2/
/
WOPR
P /
/
WOPT
P /
/
WGOR
P /
/
BVMF
1 1 4/
/
BXMF
1 1 4 2/
/
BYMF
1 1 4 2/
/
--Schedule section-----------------------------------------------------

SCHEDULE

--Define separator ; third stage represents stock tank

SEPCOND
SEP FIELD 1   80 815  /
SEP FIELD 2   80  65  /
SEP FIELD 3   60 14.7 /
/

--Define injection and production wells

--2000a WELLSPEC is used for back-compatibility, prefered keyword is WELSPECS
--WELLSPEC
--I FIELD 1 1 7330 /
--P FIELD 7 7 7400 SEP /
--/
WELSPECS
--I FIELD 1 1 7330 GAS/
P FIELD 1 1 7400 GAS/
/

--2000a uses WELSEPC to associate separator with wells
WSEPCOND
P SEP /
/
```

```
--2000a WELLCOMP is for back-compatibility, prefered keyword is COMPDAT
--WELLCOMP
--I 1 1 1 2 1 /
--P 7 7 3 4 1 /
--/
COMPDAT
--I 1 1 1 2 1* 1 /
P 1 1 3 4 1* 1 /
/

--Well P set to target gas rate of 6200, with min bhp of 500 psi

--2000a WELLPROD is for back-compatibility, prefered keyword is WCONPROD
--WELLPROD
--P GA 1* 1* 6200 1* 500 /

TSCRIT
0.001 0.00002 10 /

INCLUDE
WCONTROL_WGPR.DATA
END
```

Appendix D

D. Simulation Input File for Multicomponent Gas-Condensate System at Field Scale

```
--                    ECLIPSE INPUT FILE
--
-----------------------------------------------------------------------
-->SPE third comparative problem
-- 9 components
-- Peng-Robinson EoS with correction
-- Grid dimensions 9x9x4
-- AIM solution method
-- FIELD units
-- 3-stage separator
-- GRUPSALE and gas reinjection of remaining gas
--
-- Modified version of CASE1 for asphaltene prediction:
--    Heaviest hydrocarbon has been identified as an aromatic
--    BICs have not been changed
--    Solid saturation is used to flag asphaltene presence
--
-- Last modified May 2003
--
-----------------------------------------------------------------------

--RUNSPEC section-----------------------------------------------

RUNSPEC

--Request the FIELD unit set

FIELD

--Water is present

WATER

--AIM solution method

AIM

--Nine components in study ( plus water )

COMPS
9 /
```

```
--Peng-Robinson equation of state to be used

EOS
PR /

DIMENS
9 9 1 /

TABDIMS
1 1 40 40 /

ISGAS

MULTSAVE
0 /

MULTIPHASE

--Grid section-------------------------------------------------------

GRID

DX
81*293.3 /

DY
81*293.3 /

DZ
81*160 /

TOPS
81*7315 /

EQUALS
PORO 0.07 /
PERMX 1/
PERMY 1/
PERMZ 1/
/

--Properties section---------------------------------------------

PROPS

NCOMPS
9 /

EOS
PR /

-- Peng-Robinson correction

PRCORR
```

```
-- Standard temperature and pressure in Deg F      and PSIA

STCOND
60.0 14.7 /

-- Component names

CNAMES
CO2 N2 C1 C2 C3 C4-6 C7+1 C7+2 C7+3 /

HYDRO
 N N H H H H H H A /

-- Critical temperatures Deg R

TCRIT
548.46000    227.16000    343.08000    549.77400    665.64000
806.54054    838.11282   1058.03863   1291.89071              /

-- Critical pressures PSIA

PCRIT
1071.33111    492.31265    667.78170    708.34238    618.69739
514.92549    410.74956    247.56341    160.41589              /

-- Critical Z-factors

ZCRIT
 .27408       .29115       .28473       .28463       .27748
 .27640       .26120       .22706       .20137              /

-- Acentric factors

ACF
 .22500       .04000       .01300       .09860       .15240
 .21575       .31230       .55670       .91692              /

-- Molecular Weights

MW
 44.01000     28.01300     16.04300     30.07000     44.09700
 66.86942    107.77943    198.56203    335.19790              /

-- Omega_A values

OMEGAA
 .4572355     .4572355     .5340210     .4572355     .4572355
 .4572355     .6373344     .6373344     .6373344              /

-- Omega_B values

OMEGAB
 .0777961     .0777961     .0777961     .0777961     .0777961
 .0777961     .0872878     .0872878     .0872878              /
```

```
-- Default fluid sample composition

ZMFVD
     1.00000      .01210      .01940      .65990      .08690
      .05910      .09670      .04745      .01515      .00330
  10000.00000      .01210      .01940      .65990      .08690
      .05910      .09670      .04745      .01515      .00330 /

-- Boiling point temperatures Deg R

TBOIL
   350.46000   139.32000   201.06000   332.10000   415.98000
   523.33222   689.67140   958.31604  1270.40061           /

-- Reference temperatures Deg R

TREF
   527.40000   140.58000   201.06000   329.40000   415.80000
   526.05233   519.67000   519.67000   519.67000           /

-- Reference densities LB/FT3

DREF
    48.50653    50.19209    26.53189    34.21053    36.33308
    37.87047    45.60035    50.88507    55.89861           /

-- Parachors (Dynes/cm)

PARACHOR
    78.00000    41.00000    77.00000   108.00000   150.30000
   213.52089   331.78241   516.45301   853.48860           /

-- Binary Interaction Coefficients

BIC
-.0200
 .1000  .0360
 .1300  .0500  .000000
 .1350  .0800  .000000  .000
 .1277  .1002  .092810  .000 .000
 .1000  .1000  .130663  .006 .006 .0
 .1000  .1000  .130663  .006 .006 .0 .0
 .1000  .1000  .130663  .006 .006 .0 .0 .0 /

-- Reservoir temperature in Deg F

RTEMP
200.0 /

--Water saturation functions

SWFN
0.16     0        0
0.18     0        0
0.2      0.002    0
```

```
0.24      0.01      0
0.28      0.02      0
0.32      0.033     0
0.36      0.049     0
0.4       0.066     0
0.44      0.09      0
0.48      0.119     0
0.52      0.15      0
0.56      0.186     0
0.6       0.227     0
0.64      0.277     0
0.68      0.33      0
0.72      0.39      0
0.76      0.462     0
0.8       0.54      0
0.84      0.62      0
0.88      0.71      0
0.92      0.8       0
0.96      0.9       0
1         1         0/

--Gas saturation functions

SGFN
0         0         0
0.04      0.005     0
0.08      0.013     0
0.12      0.026     0
0.16      0.04      0
0.2       0.058     0
0.24      0.078     0
0.28      0.1       0
0.32      0.126     0
0.36      0.156     0
0.4       0.187     0
0.44      0.222     0
0.48      0.26      0
0.52      0.3       0
0.56      0.349     0
0.6       0.4       0
0.64      0.45      0
0.68      0.505     0
0.72      0.562     0
0.76      0.62      0
0.8       0.68      0
0.84      0.74      0/

--Oil saturation functions

SOF3
   0.00  0.000  0.000
   0.04  0.000  0.000
   0.08  0.000  0.000
   0.12  0.000  0.000
   0.16  0.000  0.000
```

```
   0.20  0.000  0.000
   0.24  0.000  0.000
   0.28  0.005  0.005
   0.32  0.012  0.012
   0.36  0.024  0.024
   0.40  0.040  0.040
   0.44  0.060  0.060
   0.48  0.082  0.082
   0.52  0.112  0.112
   0.56  0.150  0.150
   0.60  0.196  0.196
   0.68  0.315  0.315
   0.72  0.400  0.400
   0.76  0.513  0.513
   0.80  0.650  0.650
   0.84  0.800  0.800 /

--Rock and water pressure data

ROCK
3550 0.000004 /

PVTW
3550 1.0 0.000003 0.31 0.0 /

--Surface density of water

DENSITY
1* 63.0 1* /

--SOLUTION section-----------------------------------------------
SOLUTION

--Equilibration data - initial pressure 3500 psi at 7500, which is
--the oil-water and the oil-gas contact depth

EQUIL
7500 3550 7500 0 7500 0 1 1 0  /

OUTSOL
PRESSURE SOIL VOIL ZMF/

RPTSOL
PRESSURE SOIL PCO PCG XMF /

FIELDSEP
 1   80 815 /
 2   80  65 /
 3   60 14.7 /
/

--SUMMARY section-----------------------------------------------
SUMMARY

ALL
```

```
RUNSUM

--Field oil production rate and total, GOR and field pressure

FOPR
FOPT
FGOR
FPR
--WXMF
--P 1 /
--/
--WXMF
--P 2 /
--/
--WXMF
--P 3 /
--/
--WXMF
--P 4 /
--/


--Producer block data

--BVOIL
--7 7 1 /
--/
--BSOIL
--5 5 1 /
--/
--BSWAT
--7 7 1 /
--/
--BSGAS
--7 7 1 /
--/
--BPRES
--5 5 1 /
--/
--BXMF
--5 5 1  9 /
--/
--BYMF
--5 5 1  9 /
--/

--BSSOLID
--7 7 1 /
--/
--BPRES
--7 7 1 /
--/

--saturation and composition history
```

```
INCLUDE
'BSOIL.txt'/

INCLUDE
'BSWAT.txt'/

INCLUDE
'BSGAS.txt'/

INCLUDE
'BXMF1.txt'/

INCLUDE
'BXMF9.txt'/

INCLUDE
'BYMF1.txt'/

INCLUDE
'BYMF9.txt'/

INCLUDE
'BVMF.txt'/

--SCHEDULE section-----------------------------------------------
SCHEDULE


RPTSCHED
PRESSURE SOIL PCO PCG  BSOL DENS SSOLID /

RPTRST
 PRESSURE SOIL SGAS SSOLID  /

--Define separator ; third stage represents stock tank

SEPCOND
SEP FIELD 1   80 815  /
SEP FIELD 2   80  65  /
SEP FIELD 3   60 14.7 /
/

--Define injection and production wells

--2000a WELLSPEC is used for back-compatibility, prefered keyword is WELSPECS
--WELLSPEC
--I FIELD 1 1 7330 /
--P FIELD 7 7 7400 SEP /
--/
WELSPECS
--I FIELD 1 1 7330 GAS/
P FIELD 5 5 7395 GAS/
/

--2000a uses WELSEPC to associate separator with wells
```

```
WSEPCOND
P SEP /
/

--2000a WELLCOMP is for back-compatibility, prefered keyword is COMPDAT
--WELLCOMP
--I 1 1 1 2 1 /
--P 7 7 3 4 1 /
--/
COMPDAT
--I 1 1 1 2 1* 1 /
P 5 5 1 1 'OPEN' 1 /
/

--Well P set to target gas rate of 6200, with min bhp of 500 psi

--2000a WELLPROD is for back-compatibility, prefered keyword is WCONPROD
--WELLPROD
--P GA 1* 1* 6200 1* 500 /
--WCONPROD
--P OPEN GRAT 1* 1* 6200 1* /
--/
--WELTARG
--P BHP 1500 /
--/
WCONPROD
P    OPEN    BHP    1*  1*  1* 2* 3000/
/

--Sales gas rate of 1500 MSCF/Day specified

--GRUPSALE
--Field 1500 /
--/

--Well I injects all unsold vapour

--2000a WELLINJE is for back-compatibility, prefered keyword is WCONINJE
--for reinjection, use GCONINJE
--WELLINJE
--I GV Field REINJE 3* 4000 3* 1 /

--GCONINJE
--Field GAS REIN 2* 1 /
--/
--GINJGAS
--Field GV Field /
--/

--WCONINJE
--I GAS OPEN GRUP 2* 4000 /
--/

--Set 15 day initial time step
```

```
--Time steps to 1600 days
TSTEP
10*160 /

SAVE

--Change separator conditions

--SEPCOND
--SEP FIELD 1 80 315 /
--/

--Time steps to 10 years : ten day step after separator modification

--TSTEP
--10*36.5 /

--2000a WELLSHUT is for back-compatibility, prefered keyword is WELOPEN
--WELLSHUT
--I /
--WELOPEN
--I SHUT/
--P SHUT /

--WELTARG
--P GRAT 0.0001 /
--/

--TUNING
--.000277 0.05  0.0000277 /

--TSTEP
--30*0.05 1000*1 /

END
```

Appendix E

E. Simulation Input File for Multicomponent Hydraulically Fractured Gas-Condensate Reservoir

```
--                    ECLIPSE INPUT FILE
--
-----------------------------------------------------------------------
-->SPE third comparative problem
-- 9 components
-- Peng-Robinson EoS with correction
-- Grid dimensions 9x9x4
-- AIM solution method
-- FIELD units
-- 3-stage separator
-- GRUPSALE and gas reinjection of remaining gas
--
-- Modified version of CASE1 for asphaltene prediction:
--    Heaviest hydrocarbon has been identified as an aromatic
--    BICs have not been changed
--    Solid saturation is used to flag asphaltene presence
--
-- Last modified May 2003
--
-----------------------------------------------------------------------

--RUNSPEC section-----------------------------------------------

RUNSPEC

--Request the FIELD unit set

FIELD

--Water is present

WATER

--AIM solution method

AIM

--Nine components in study ( plus water )

COMPS
9 /
```

```
--Peng-Robinson equation of state to be used

EOS
PR /

DIMENS
9 9 1 /

TABDIMS
2 1 40 40 /

ISGAS

MULTSAVE
0 /

MULTIPHASE

--ICP
SCFDIMS
 4 /

--Grid section-------------------------------------------------------

GRID

DX
81*293.3 /

DY
81*293.3 /

DZ
81*160 /

TOPS
81*7315 /

EQUALS
PORO 0.07 /
PERMX 1/
PERMY 1/
PERMZ 1/
/
CONDFRAC
 'SCF3' 2 10.0 500.0 /
 6 6 4 5 1 1 'X'  /
 6 7 5 5 1 1 'Y'  /
 7 7 5 6 1 1 'X'  /
 7 8 6 6 1 1 'Y'  /
 8 8 6 8 1 1 'X'  /
 8 9 8 8 1 1 'Y'  /
 9 9 8 9 1 1 'X'  / <-- Intersects P1
/
```

```
--ICP
CONDFRAC
 'SCF1' 2 10.0 500.0 /
 4 7 2 2 1 1 'Y'  /
/

CONDFRAC
 'SCF2' 2 10.0 500.0 /
 2 2 2 5 1 1 'X'  /
/
--Properties section---------------------------------------------

PROPS

NCOMPS
9 /

EOS
PR /

-- Peng-Robinson correction

PRCORR

-- Standard temperature and pressure in Deg F      and PSIA

STCOND
60.0 14.7 /

-- Component names

CNAMES
CO2 N2 C1 C2 C3 C4-6 C7+1 C7+2 C7+3 /

HYDRO
 N N H H H H H H A /

-- Critical temperatures Deg R

TCRIT
548.46000    227.16000    343.08000    549.77400    665.64000
806.54054    838.11282   1058.03863   1291.89071              /

-- Critical pressures PSIA

PCRIT
1071.33111    492.31265    667.78170    708.34238    618.69739
514.92549    410.74956    247.56341    160.41589              /

-- Critical Z-factors

ZCRIT
 .27408       .29115       .28473       .28463       .27748
 .27640       .26120       .22706       .20137              /
```

```
-- Acentric factors

ACF
 .22500      .04000      .01300      .09860      .15240
 .21575      .31230      .55670      .91692           /

-- Molecular Weights

MW
 44.01000    28.01300    16.04300    30.07000    44.09700
 66.86942   107.77943   198.56203   335.19790           /

-- Omega_A values

OMEGAA
 .4572355    .4572355    .5340210    .4572355    .4572355
 .4572355    .6373344    .6373344    .6373344           /

-- Omega_B values

OMEGAB
 .0777961    .0777961    .0777961    .0777961    .0777961
 .0777961    .0872878    .0872878    .0872878           /

-- Default fluid sample composition

ZMFVD
     1.00000      .01210      .01940      .65990      .08690
      .05910      .09670      .04745      .01515      .00330
  10000.00000      .01210      .01940      .65990      .08690
      .05910      .09670      .04745      .01515      .00330 /

-- Boiling point temperatures Deg R

TBOIL
   350.46000   139.32000   201.06000   332.10000   415.98000
   523.33222   689.67140   958.31604  1270.40061           /

-- Reference temperatures Deg R

TREF
   527.40000   140.58000   201.06000   329.40000   415.80000
   526.05233   519.67000   519.67000   519.67000           /

-- Reference densities LB/FT3

DREF
    48.50653    50.19209    26.53189    34.21053    36.33308
    37.87047    45.60035    50.88507    55.89861           /

-- Parachors (Dynes/cm)

PARACHOR
    78.00000    41.00000    77.00000   108.00000   150.30000
   213.52089   331.78241   516.45301   853.48860           /
```

```
-- Binary Interaction Coefficients

BIC
-.0200
 .1000  .0360
 .1300  .0500  .000000
 .1350  .0800  .000000  .000
 .1277  .1002  .092810  .000 .000
 .1000  .1000  .130663  .006 .006 .0
 .1000  .1000  .130663  .006 .006 .0 .0
 .1000  .1000  .130663  .006 .006 .0 .0 .0 /

-- Reservoir temperature in Deg F

RTEMP
200.0 /

--Water saturation functions

SWFN
0.16     0        0
0.18     0        0
0.2      0.002    0
0.24     0.01     0
0.28     0.02     0
0.32     0.033    0
0.36     0.049    0
0.4      0.066    0
0.44     0.09     0
0.48     0.119    0
0.52     0.15     0
0.56     0.186    0
0.6      0.227    0
0.64     0.277    0
0.68     0.33     0
0.72     0.39     0
0.76     0.462    0
0.8      0.54     0
0.84     0.62     0
0.88     0.71     0
0.92     0.8      0
0.96     0.9      0
1        1        0
/
   0.2 0 0
   1.0 1 0
/


--Gas saturation functions

SGFN
0        0        0
0.04     0.005    0
```

```
0.08      0.013    0
0.12      0.026    0
0.16      0.04     0
0.2       0.058    0
0.24      0.078    0
0.28      0.1      0
0.32      0.126    0
0.36      0.156    0
0.4       0.187    0
0.44      0.222    0
0.48      0.26     0
0.52      0.3      0
0.56      0.349    0
0.6       0.4      0
0.64      0.45     0
0.68      0.505    0
0.72      0.562    0
0.76      0.62     0
0.8       0.68     0
0.84      0.74     0
/
/

--Oil saturation functions

SOF3
   0.00  0.000  0.000
   0.04  0.000  0.000
   0.08  0.000  0.000
   0.12  0.000  0.000
   0.16  0.000  0.000
   0.20  0.000  0.000
   0.24  0.000  0.000
   0.28  0.005  0.005
   0.32  0.012  0.012
   0.36  0.024  0.024
   0.40  0.040  0.040
   0.44  0.060  0.060
   0.48  0.082  0.082
   0.52  0.112  0.112
   0.56  0.150  0.150
   0.60  0.196  0.196
   0.68  0.315  0.315
   0.72  0.400  0.400
   0.76  0.513  0.513
   0.80  0.650  0.650
   0.84  0.800  0.800
/
/

--Rock and water pressure data

ROCK
3550 0.000004 /
```

```
PVTW
3550 1.0 0.000003 0.31 0.0 /

--Surface density of water

DENSITY
1* 63.0 1* /

--SOLUTION section-----------------------------------------------
SOLUTION

--Equilibration data - initial pressure 3500 psi at 7500, which is
--the oil-water and the oil-gas contact depth

EQUIL
7500 3550 7500 0 7500 0 1 1 0  /

OUTSOL
PRESSURE SOIL VOIL ZMF/

RPTSOL
PRESSURE SOIL PCO PCG XMF /

FIELDSEP
 1   80 815 /
 2   80  65 /
 3   60 14.7 /
/

--SUMMARY section-----------------------------------------------
SUMMARY

ALL

RUNSUM

--Field oil production rate and total, GOR and field pressure

FOPR
FOPT
FGOR
FPR
--WXMF
--P 1 /
--/
--WXMF
--P 2 /
--/
--WXMF
--P 3 /
--/
--WXMF
--P 4 /
--/
```

```
--Producer block data

--BVOIL
--7 7 1 /
--/
--BSOIL
--5 5 1 /
--/
--BSWAT
--7 7 1 /
--/
--BSGAS
--7 7 1 /
--/
--BPRES
--5 5 1 /
--/
--BXMF
--5 5 1  9 /
--/
--BYMF
--5 5 1  9 /
--/

--BSSOLID
--7 7 1 /
--/
--BPRES
--7 7 1 /
--/

--saturation and composition history
INCLUDE
'BSOIL.txt'/

INCLUDE
'BSWAT.txt'/

INCLUDE
'BSGAS.txt'/

INCLUDE
'BXMF1.txt'/

INCLUDE
'BXMF9.txt'/

INCLUDE
'BYMF1.txt'/

INCLUDE
'BYMF9.txt'/

INCLUDE
```

```
'BVMF.txt'/

--SCHEDULE section-----------------------------------------------
SCHEDULE


RPTSCHED
PRESSURE SOIL PCO PCG  BSOL DENS SSOLID /

RPTRST
 PRESSURE SOIL SGAS SSOLID  /

--Define separator ; third stage represents stock tank

SEPCOND
SEP FIELD 1   80 815  /
SEP FIELD 2   80  65  /
SEP FIELD 3   60 14.7 /
/

--Define injection and production wells

--2000a WELLSPEC is used for back-compatibility, prefered keyword is WELSPECS
--WELLSPEC
--I FIELD 1 1 7330 /
--P FIELD 7 7 7400 SEP /
--/
WELSPECS
--I FIELD 1 1 7330 GAS/
P FIELD 5 5 7395 GAS/
/

--2000a uses WELSEPC to associate separator with wells
WSEPCOND
P SEP /
/

--2000a WELLCOMP is for back-compatibility, prefered keyword is COMPDAT
--WELLCOMP
--I 1 1 1 2 1 /
--P 7 7 3 4 1 /
--/
COMPDAT
--I 1 1 1 2 1* 1 /
P 5 5 1 1 'OPEN' 1 /
/

--Well P set to target gas rate of 6200, with min bhp of 500 psi

--2000a WELLPROD is for back-compatibility, prefered keyword is WCONPROD
--WELLPROD
--P GA 1* 1* 6200 1* 500 /
--WCONPROD
--P OPEN GRAT 1* 1* 6200 1* /
--/
```

```
--WELTARG
--P BHP 1500 /
--/
--ICP
-- Must come after COMPDAT
-- PI mult only used if NOCUT
-- <Well name> <CUT/NOCUT> <PI_Mult> <I> <J> <K> <C1> <C2>
WELLCF
 P CUT 1.0 5* /
/

WCONPROD
P    OPEN    BHP    1*  1*  1* 2* 500/
/

--Sales gas rate of 1500 MSCF/Day specified

--GRUPSALE
--Field 1500 /
--/

--Well I injects all unsold vapour

--2000a WELLINJE is for back-compatibility, prefered keyword is WCONINJE
--for reinjection, use GCONINJE
--WELLINJE
--I GV Field REINJE 3* 4000 3* 1 /

--GCONINJE
--Field GAS REIN 2* 1 /
--/
--GINJGAS
--Field GV Field /
--/

--WCONINJE
--I GAS OPEN GRUP 2* 4000 /
--/

--Set 15 day initial time step

--Time steps to 1600 days
TSTEP
10*160 /

SAVE

--Change separator conditions

--SEPCOND
--SEP FIELD 1 80 315 /
--/

--Time steps to 10 years : ten day step after separator modification
```

```
--TSTEP
--10*36.5 /

--2000a WELLSHUT is for back-compatibility, prefered keyword is WELOPEN
--WELLSHUT
--I /
--WELOPEN
--I SHUT/
--P SHUT /

--WELTARG
--P GRAT 0.0001 /
--/

--TUNING
--.000277 0.05  0.0000277 /

--TSTEP
--30*0.05 1000*1 /

END
```

Appendix F

F. Simulation Input File for Multicomponent Gas-Condensate Reservoirs with Gas Cycling

```
--                    ECLIPSE INPUT FILE
--
-----------------------------------------------------------------------
-->SPE third comparative problem
-- 9 components
-- Peng-Robinson EoS with correction
-- Grid dimensions 9x9x4
-- AIM solution method
-- FIELD units
-- 3-stage separator
-- GRUPSALE and gas reinjection of remaining gas
-----------------------------------------------------------------------

--RUNSPEC section-----------------------------------------------

RUNSPEC

--Request the FIELD unit set

FIELD

--Water is present

WATER

--AIM solution method

AIM

--Nine components in study ( plus water )

COMPS
9 /

--Peng-Robinson equation of state to be used

EOS
PR /

DIMENS
9 9 1 /
```

```
TABDIMS
1 1 40 40 /

--Is a gas condensate study
ISGAS

MULTSAVE
0 /

--Grid section-------------------------------------------------------

GRID

DX
81*293.3 /

DY
81*293.3 /

DZ
81*160 /

TOPS
81*7315 /

EQUALS
PORO 0.13 /
PERMX 130 /
PERMY 130 /
PERMZ 13 /
/

--Properties section---------------------------------------------

PROPS

NCOMPS
9 /

EOS
PR /

-- Peng-Robinson correction

PRCORR

-- Standard temperature and pressure in Deg F      and PSIA

STCOND
60.0 14.7 /

-- Component names

CNAMES
CO2 N2 C1 C2 C3 C4-6 C7+1 C7+2 C7+3 /
```

```
-- Critical temperatures Deg R

TCRIT
548.46000    227.16000    343.08000    549.77400    665.64000
806.54054    838.11282   1058.03863   1291.89071             /

-- Critical pressures PSIA

PCRIT
1071.33111    492.31265    667.78170    708.34238    618.69739
514.92549    410.74956    247.56341    160.41589             /

-- Critical Z-factors

ZCRIT
 .27408       .29115       .28473       .28463       .27748
 .27640       .26120       .22706       .20137             /

-- Acentric factors

ACF
 .22500       .04000       .01300       .09860       .15240
 .21575       .31230       .55670       .91692             /

-- Molecular Weights

MW
 44.01000     28.01300     16.04300     30.07000     44.09700
 66.86942    107.77943    198.56203    335.19790             /

-- Omega_A values

OMEGAA
 .4572355     .4572355     .5340210     .4572355     .4572355
 .4572355     .6373344     .6373344     .6373344             /

-- Omega_B values

OMEGAB
 .0777961     .0777961     .0777961     .0777961     .0777961
 .0777961     .0872878     .0872878     .0872878             /

-- Default fluid sample composition

ZMFVD
      1.00000       .01210       .01940       .65990       .08690
       .05910       .09670       .04745       .01515       .00330
  10000.00000       .01210       .01940       .65990       .08690
       .05910       .09670       .04745       .01515       .00330 /

-- Boiling point temperatures Deg R

TBOIL
   350.46000    139.32000    201.06000    332.10000    415.98000
```

```
   523.33222    689.67140    958.31604   1270.40061              /

-- Reference temperatures Deg R

TREF
   527.40000    140.58000    201.06000    329.40000    415.80000
   526.05233    519.67000    519.67000    519.67000              /

-- Reference densities LB/FT3

DREF
    48.50653     50.19209     26.53189     34.21053     36.33308
    37.87047     45.60035     50.88507     55.89861              /

-- Parachors (Dynes/cm)

PARACHOR
    78.00000     41.00000     77.00000    108.00000    150.30000
   213.52089    331.78241    516.45301    853.48860              /

-- Binary Interaction Coefficients

BIC
-.0200
 .1000  .0360
 .1300  .0500  .000000
 .1350  .0800  .000000  .000
 .1277  .1002  .092810  .000 .000
 .1000  .1000  .130663  .006 .006 .0
 .1000  .1000  .130663  .006 .006 .0 .0
 .1000  .1000  .130663  .006 .006 .0 .0 .0 /

-- Reservoir temperature in Deg F

RTEMP
200.0 /

--Water saturation functions

SWFN
0.16      0         0
0.18      0         0
0.2       0.002     0
0.24      0.01      0
0.28      0.02      0
0.32      0.033     0
0.36      0.049     0
0.4       0.066     0
0.44      0.09      0
0.48      0.119     0
0.52      0.15      0
0.56      0.186     0
0.6       0.227     0
0.64      0.277     0
0.68      0.33      0
```

```
0.72      0.39      0
0.76      0.462     0
0.8       0.54      0
0.84      0.62      0
0.88      0.71      0
0.92      0.8       0
0.96      0.9       0
1         1         0/

--Gas saturation functions

SGFN
0         0         0
0.04      0.005     0
0.08      0.013     0
0.12      0.026     0
0.16      0.04      0
0.2       0.058     0
0.24      0.078     0
0.28      0.1       0
0.32      0.126     0
0.36      0.156     0
0.4       0.187     0
0.44      0.222     0
0.48      0.26      0
0.52      0.3       0
0.56      0.349     0
0.6       0.4       0
0.64      0.45      0
0.68      0.505     0
0.72      0.562     0
0.76      0.62      0
0.8       0.68      0
0.84      0.74      0/

--Oil saturation functions

SOF3
   0.00  0.000  0.000
   0.04  0.000  0.000
   0.08  0.000  0.000
   0.12  0.000  0.000
   0.16  0.000  0.000
   0.20  0.000  0.000
   0.24  0.000  0.000
   0.28  0.005  0.005
   0.32  0.012  0.012
   0.36  0.024  0.024
   0.40  0.040  0.040
   0.44  0.060  0.060
   0.48  0.082  0.082
   0.52  0.112  0.112
   0.56  0.150  0.150
   0.60  0.196  0.196
   0.68  0.315  0.315
```

```
   0.72  0.400  0.400
   0.76  0.513  0.513
   0.80  0.650  0.650
   0.84  0.800  0.800 /

--Rock and water pressure data

ROCK
3550 0.000004 /

PVTW
3550 1.0 0.000003 0.31 0.0 /

--Surface density of water

DENSITY
1* 63.0 1* /

--Solution section-----------------------------------------------------

SOLUTION

--Equilibration data - initial pressure 3500 psi at 7500, which is
--the oil-water and the oil-gas contact depth

EQUIL
7500 3550 7500 0 7500 0 1 1 0  /

RPTRST
PRESSURE SOIL YMF VOIL /

RPTSOL
PRESSURE SOIL /

FIELDSEP
 1   80 815 /
 2   80  65 /
 3   60 14.7 /
/

SUMMARY    ==============================================================

ALL

RUNSUM

--Field oil production rate and total, GOR and field pressure

FOPR
FOPT
FGOR
FPR
WXMF
P 1 /
/
```

```
WXMF
P 2 /
/
WXMF
P 3 /
/
WXMF
P 4 /
/


--Producer block data

BVOIL
5 5 1 /
/
BSOIL
5 5 1 /
/
BSOIL
4 4 1 /
/
BSOIL
3 3 1 /
/
BSOIL
2 2 1 /
/
BSOIL
1 1 1 /
/

BSWAT
5 5 1 /
/
BSGAS
5 5 1 /
/
BPRES
1 1 1 /
/
BXMF
5 5 1 9 /
/
BXMF
4 4 1 9 /
/
BXMF
3 3 1 9 /
/
BXMF
2 2 1 9 /
/
BXMF
1 1 1 9 /
```

```
/
BYMF
5 5 1 9 /
/
BYMF
4 4 1 9 /
/
BYMF
3 3 1 9 /
/
BYMF
2 2 1 9 /
/
BYMF
1 1 1 9 /
/

--Schedule section-----------------------------------------------------

SCHEDULE

--Define separator ; third stage represents stock tank

SEPCOND
SEP FIELD 1   80 815  /
SEP FIELD 2   80  65  /
SEP FIELD 3   60 14.7 /
/

--Define injection and production wells

--2000a WELLSPEC is used for back-compatibility, prefered keyword is WELSPECS
--WELLSPEC
--I FIELD 1 1 7330 /
--P FIELD 7 7 7400 SEP /
--/
WELSPECS
I FIELD 1 1 7330 GAS/
P FIELD 5 5 7400 GAS/
/

--2000a uses WELSEPC to associate separator with wells
WSEPCOND
P SEP /
/

--2000a WELLCOMP is for back-compatibility, prefered keyword is COMPDAT
--WELLCOMP
--I 1 1 1 2 1 /
--P 7 7 3 4 1 /
--/
COMPDAT
I 1 1 1 1 1* 1 /
P 5 5 1 1 1* 1 /
/
```

```
--Well P set to target gas rate of 6200, with min bhp of 500 psi

--2000a WELLPROD is for back-compatibility, prefered keyword is WCONPROD
--WELLPROD
--P GA 1* 1* 6200 1* 500 /
WCONPROD
P OPEN GRAT 1* 1* 6200 2* 500 /
/

--Sales gas rate of 1500 MSCF/Day specified

GRUPSALE
Field 1500/
/

--Well I injects all unsold vapour

--2000a WELLINJE is for back-compatibility, prefered keyword is WCONINJE
--for reinjection, use GCONINJE
--WELLINJE
--I GV Field REINJE 3* 4000 3* 1 /
--Injection rate control
GCONINJE
Field GAS REIN 2* 1 /
/
--specify nature of injected gas
GINJGAS
Field GV Field /
/
--Control data for injection well
WCONINJE
I GAS OPEN GRUP 2* 4000 /
/

--Set 15 day initial time step

--Time steps to 9 years
TSTEP
3285 /

SAVE

--Change separator conditions

--SEPCOND
--SEP FIELD 1   80 315  /
--SEP FIELD 2   80  65  /
--SEP FIELD 3   60 14.7 /
--/

--Time steps to 10 years : ten day step after separator modification

TSTEP
365 /
```

```
--2000a WELLSHUT is for back-compatibility, prefered keyword is WELOPEN
--WELLSHUT
--I /
--WELOPEN
--I SHUT/
--/

TSTEP
1825 /

END
```

Appendix G

G. Simulation Input File for Multicomponent Gas-Condensate Reservoirs with Injection Gas

```
--                    ECLIPSE INPUT FILE
--

-----------------------------------------------------------------------
-->SPE third comparative problem
-- 9 components
-- Peng-Robinson EoS with correction
-- Grid dimensions 9x9x4
-- AIM solution method
-- FIELD units
-- 3-stage separator
-- GRUPSALE and gas reinjection of remaining gas
-----------------------------------------------------------------------

--RUNSPEC section-----------------------------------------------------

RUNSPEC

--Request the FIELD unit set

FIELD

--Water is present

WATER

--AIM solution method

AIM

--Nine components in study ( plus water )

COMPS
9 /

--Peng-Robinson equation of state to be used

EOS
PR /

DIMENS
```

```
9 9 1 /

TABDIMS
1 1 40 40 /

--Is a gas condensate study
ISGAS

MULTSAVE
0 /

--Grid section-------------------------------------------------------

GRID

DX
81*293.3 /

DY
81*293.3 /

DZ
81*160 /

TOPS
81*7315 /

EQUALS
PORO 0.13 /
PERMX 130 /
PERMY 130 /
PERMZ 13 /
/

--Properties section----------------------------------------------

PROPS

NCOMPS
9 /

EOS
PR /

-- Peng-Robinson correction

PRCORR

-- Standard temperature and pressure in Deg F      and PSIA

STCOND
60.0 14.7 /

-- Component names
```

```
CNAMES
CO2 N2 C1 C2 C3 C4-6 C7+1 C7+2 C7+3 /

-- Critical temperatures Deg R

TCRIT
548.46000    227.16000    343.08000    549.77400    665.64000
806.54054    838.11282   1058.03863   1291.89071              /

-- Critical pressures PSIA

PCRIT
1071.33111    492.31265    667.78170    708.34238    618.69739
514.92549    410.74956    247.56341    160.41589              /

-- Critical Z-factors

ZCRIT
 .27408       .29115       .28473       .28463       .27748
 .27640       .26120       .22706       .20137              /

-- Acentric factors

ACF
 .22500       .04000       .01300       .09860       .15240
 .21575       .31230       .55670       .91692              /

-- Molecular Weights

MW
 44.01000     28.01300     16.04300     30.07000     44.09700
 66.86942    107.77943    198.56203    335.19790              /

-- Omega_A values

OMEGAA
 .4572355     .4572355     .5340210     .4572355     .4572355
 .4572355     .6373344     .6373344     .6373344              /

-- Omega_B values

OMEGAB
 .0777961     .0777961     .0777961     .0777961     .0777961
 .0777961     .0872878     .0872878     .0872878              /

-- Default fluid sample composition

ZMFVD
      1.00000       .01210       .01940       .65990       .08690
       .05910       .09670       .04745       .01515       .00330
  10000.00000       .01210       .01940       .65990       .08690
       .05910       .09670       .04745       .01515       .00330 /

-- Boiling point temperatures Deg R
```

```
TBOIL
   350.46000    139.32000    201.06000    332.10000    415.98000
   523.33222    689.67140    958.31604   1270.40061            /

-- Reference temperatures Deg R

TREF
   527.40000    140.58000    201.06000    329.40000    415.80000
   526.05233    519.67000    519.67000    519.67000            /

-- Reference densities LB/FT3

DREF
    48.50653     50.19209     26.53189     34.21053     36.33308
    37.87047     45.60035     50.88507     55.89861            /

-- Parachors (Dynes/cm)

PARACHOR
    78.00000     41.00000     77.00000    108.00000    150.30000
   213.52089    331.78241    516.45301    853.48860            /

-- Binary Interaction Coefficients

BIC
-.0200
 .1000  .0360
 .1300  .0500  .000000
 .1350  .0800  .000000  .000
 .1277  .1002  .092810  .000 .000
 .1000  .1000  .130663  .006 .006 .0
 .1000  .1000  .130663  .006 .006 .0 .0
 .1000  .1000  .130663  .006 .006 .0 .0 .0 /

-- Reservoir temperature in Deg F

RTEMP
200.0 /

--Water saturation functions

SWFN
0.16     0        0
0.18     0        0
0.2      0.002    0
0.24     0.01     0
0.28     0.02     0
0.32     0.033    0
0.36     0.049    0
0.4      0.066    0
0.44     0.09     0
0.48     0.119    0
0.52     0.15     0
0.56     0.186    0
0.6      0.227    0
```

```
0.64      0.277     0
0.68      0.33      0
0.72      0.39      0
0.76      0.462     0
0.8       0.54      0
0.84      0.62      0
0.88      0.71      0
0.92      0.8       0
0.96      0.9       0
1         1         0/

--Gas saturation functions

SGFN
0         0         0
0.04      0.005     0
0.08      0.013     0
0.12      0.026     0
0.16      0.04      0
0.2       0.058     0
0.24      0.078     0
0.28      0.1       0
0.32      0.126     0
0.36      0.156     0
0.4       0.187     0
0.44      0.222     0
0.48      0.26      0
0.52      0.3       0
0.56      0.349     0
0.6       0.4       0
0.64      0.45      0
0.68      0.505     0
0.72      0.562     0
0.76      0.62      0
0.8       0.68      0
0.84      0.74      0/

--Oil saturation functions

SOF3
   0.00  0.000  0.000
   0.04  0.000  0.000
   0.08  0.000  0.000
   0.12  0.000  0.000
   0.16  0.000  0.000
   0.20  0.000  0.000
   0.24  0.000  0.000
   0.28  0.005  0.005
   0.32  0.012  0.012
   0.36  0.024  0.024
   0.40  0.040  0.040
   0.44  0.060  0.060
   0.48  0.082  0.082
   0.52  0.112  0.112
   0.56  0.150  0.150
```

```
   0.60  0.196  0.196
   0.68  0.315  0.315
   0.72  0.400  0.400
   0.76  0.513  0.513
   0.80  0.650  0.650
   0.84  0.800  0.800 /

--Rock and water pressure data

ROCK
3550 0.000004 /

PVTW
3550 1.0 0.000003 0.31 0.0 /

--Surface density of water

DENSITY
1* 63.0 1* /

--Solution section-----------------------------------------------------

SOLUTION

--Equilibration data - initial pressure 3500 psi at 7500, which is
--the oil-water and the oil-gas contact depth

EQUIL
7500 3550 7500 0 7500 0 1 1 0  /

RPTRST
PRESSURE SOIL YMF VOIL /

RPTSOL
PRESSURE SOIL /

FIELDSEP
 1   80 815 /
 2   80  65 /
 3   60 14.7 /
/

SUMMARY   ==============================================================

ALL

RUNSUM

--Field oil production rate and total, GOR and field pressure

FOPR
FOPT
FGOR
FPR
WXMF
```

```
P 1 /
/
WXMF
P 2 /
/
WXMF
P 3 /
/
WXMF
P 4 /
/


--Producer block data

BVOIL
5 5 1 /
/
BSOIL
5 5 1 /
/
BSOIL
4 4 1 /
/
BSOIL
3 3 1 /
/
BSOIL
2 2 1 /
/
BSOIL
1 1 1 /
/

BSWAT
5 5 1 /
/
BSGAS
5 5 1 /
/
BPRES
1 1 1 /
/
BXMF
5 5 1 9 /
/
BXMF
4 4 1 9 /
/
BXMF
3 3 1 9 /
/
BXMF
2 2 1 9 /
/
```

```
BXMF
1 1 1 9 /
/
BYMF
5 5 1 9 /
/
BYMF
4 4 1 9 /
/
BYMF
3 3 1 9 /
/
BYMF
2 2 1 9 /
/
BYMF
1 1 1 9 /
/

--Schedule section-----------------------------------------------------

SCHEDULE

--Define separator ; third stage represents stock tank

SEPCOND
SEP FIELD 1   80 815  /
SEP FIELD 2   80  65  /
SEP FIELD 3   60 14.7 /
/

--Define injection and production wells

--2000a WELLSPEC is used for back-compatibility, prefered keyword is WELSPECS
--WELLSPEC
--I FIELD 1 1 7330 /
--P FIELD 7 7 7400 SEP /
--/
WELSPECS
I FIELD 1 1 7330 GAS/
P FIELD 5 5 7400 GAS/
/

--2000a uses WELSEPC to associate separator with wells
WSEPCOND
P SEP /
/

--2000a WELLCOMP is for back-compatibility, prefered keyword is COMPDAT
--WELLCOMP
--I 1 1 1 2 1 /
--P 7 7 3 4 1 /
--/
COMPDAT
I 1 1 1 1 1* 1 /
```

```
P 5 5 1 1 1* 1 /
/

--Well P set to target gas rate of 6200, with min bhp of 500 psi

--2000a WELLPROD is for back-compatibility, prefered keyword is WCONPROD
--WELLPROD
--P GA 1* 1* 6200 1* 500 /
WCONPROD
P OPEN GRAT 1* 1* 6200 2* 500 /
/

--Sales gas rate of 1500 MSCF/Day specified

--GRUPSALE
--Field 1500/
--/

--Well I injects all unsold vapour

--2000a WELLINJE is for back-compatibility, prefered keyword is WCONINJE
--for reinjection, use GCONINJE
--WELLINJE
--I GV Field REINJE 3* 4000 3* 1 /
--Injection rate control
--GCONINJE
--Field GAS REINJ 2* 1 /
--/
--specify nature of injected gas
--GINJGAS
--Field STREAM Field /
--/
--Control data for injection well
WCONINJE
I GAS OPEN RATE  6200 1* 4000 /
/
WELLSTRE
METHANE 0 0 1 0 0 0 0 0 0                                    /
/
WINJGAS
I STREAM METHANE/
/
--Set 15 day initial time step

--Time steps to 9 years
TSTEP
3285 /

SAVE

--Change separator conditions

--SEPCOND
--SEP FIELD 1   80 315  /
--SEP FIELD 2   80  65  /
```

```
--SEP FIELD 3   60 14.7 /
--/

--Time steps to 10 years : ten day step after separator modification

TSTEP
365 /

--2000a WELLSHUT is for back-compatibility, prefered keyword is WELOPEN
--WELLSHUT
--I /
--WELOPEN
--I SHUT/
--/

TSTEP
1825 /

END
```

Appendix H

H. Optimization of Condensate Reservoirs with Gas Injection

```
--                    ECLIPSE INPUT FILE
--
--
-----------------------------------------------------------------------
--  Condensate field
--  Optimizing the oil production by adjusting the gas injection rate
--  Considering the cost of injecting Gas
-----------------------------------------------------------------------

RUNSPEC  ==============================================================

-- Phases present
OIL
WATER
GAS
ISGAS


FULLIMP

-- 2D model: x-z cross-section

DIMENS
--nx ny nz
  20  1  5 /


-- Unit: FIELD

FIELD

-- Number of components

COMPS
6 /


TABDIMS
-- sat pres - max rows in tables-
-- tab tab    sat    press
    1   1      40     40 /
```

```
WELLDIMS
-- max  max   max    max wells  max stages
--wells comps groups in group   per sep
   1*   10     2      1*       /

-- Starting date
START
1 Jan 1997 /

UNIFOUT

-- activate the reservoir optimization option

RESOPT

GRID

INIT

--  SPECIFY GRID BLOCK DIMENSIONS IN THE X DIRECTION
DXV
   20*200 /

--  SPECIFY GRID BLOCK DIMENSIONS IN THE y DIRECTION
DYV
    1000.0  /

-- SPECIFY CELL THICKNESSES ( DZ ), HORIZ. PERMEABILITIES ( PERMX )
-- AND POROSITIES ( PORO ) FOR EACH LAYER OF THE GRID. ALSO CELL TOP
-- DEPTHS ( TOPS ) FOR LAYER 1.

--     ARRAY    VALUE  ------ BOX ------
EQUALS

     'TOPS'    6100   1   1   1   1   1  1  /
     'TOPS'    6105   2   2   1   1   1  1  /
     'TOPS'    6110   3   3   1   1   1  1  /
     'TOPS'    6115   4   4   1   1   1  1  /
     'TOPS'    6120   5   5   1   1   1  1  /
     'TOPS'    6125   6   6   1   1   1  1  /
     'TOPS'    6130   7   7   1   1   1  1  /
     'TOPS'    6135   8   8   1   1   1  1  /
     'TOPS'    6140   9   9   1   1   1  1  /
     'TOPS'    6145   10  10  1   1   1  1  /
     'TOPS'    6150   11  11  1   1   1  1  /
     'TOPS'    6155   12  12  1   1   1  1  /
     'TOPS'    6160   13  13  1   1   1  1  /
     'TOPS'    6165   14  14  1   1   1  1  /
     'TOPS'    6170   15  15  1   1   1  1  /
     'TOPS'    6175   16  16  1   1   1  1  /
     'TOPS'    6180   17  17  1   1   1  1  /
     'TOPS'    6185   18  18  1   1   1  1  /
     'TOPS'    6190   19  19  1   1   1  1  /
     'TOPS'    6195   20  20  1   1   1  1  /
```

```
--     CONSTANT POROSITY AND NTG

    'PORO'   0.18   1  20    1  1   1  5   /
    'NTG'    1.00   1  20    1  1   1  5   /


    'DZ'     32.    1  20    1  1   1  1  /  LAYER 1
    'PERMX'  50.    1  20    1  1   1  1  /

    'DZ'     5.     1  20    1  1   2  2  /  LAYER 2
    'PERMX'  0.01   1  20    1  1   2  2  /

    'DZ'     20.    1  20    1  1   3  3  /  LAYER 3
    'PERMX'  20.    1  20    1  1   3  3  /

    'DZ'     41.    1  20    1  1   4  4  /  LAYER 4
    'PERMX'  80.    1  20    1  1   4  4  /

    'DZ'     32.    1  20    1  1   5  5  /  LAYER 5
    'PERMX'  150.   1  20    1  1   5  5  /


/   EQUALS IS TERMINATED BY A NULL RECORD

--  COPY X PERMEABILITIES ( PERMX ) INTO Y AND Z PERMEABILITIES
--  ( PERMZ ) FOR THE WHOLE GRID, AND THEN MULTIPLY PERMZ BY 0.2.
-------- SOURCE     DESTINATION
COPY
       'PERMX'     'PERMZ'     /
       'PERMX'     'PERMY'     /
/
-- set Kv/Kh ratio
MULTIPLY
--      array   factor i1  i2  j1 j2  k1 k2
      'PERMZ'     0.2  1  20   1  1   1  5  /
/


-- OUTPUT OF CELL DIMENSIONS, PERMEABILITIES, POROSITY AND TOPS
-- DATA IS REQUESTED, AND OF THE CALCULATED PORE VOLUMES, CELL
-- CENTRE DEPTHS AND X AND Z DIRECTION TRANSMISSIBILITIES

RPTGRID
 DX DY DZ PERMX PERMY PERMZ PORO NTG TOPS MIDS  /


PROPS    ==================================================================
-------- THE PROPS SECTION DEFINES THE REL. PERMEABILITIES, CAPILLARY
-------- PRESSURES, AND THE PVT PROPERTIES OF THE RESERVOIR FLUIDS
----------------------------------------------------------------------

-- include relative permeability and capillary pressure tables
-- saturation tables  THREE PHASE
```

```
SWFN
--  sw       krw      Pcwo
   0.15     0.       5
   0.2      0.       3
   0.25     0.01     1.9
   0.3      0.05     1
   0.35     0.1      0.7
   0.4      0.18     0.6
   0.45     0.28     0.5
   0.50     0.4      0.4
   1.00     1.       0.
/

SOF3
--  so      krow      krog
   0.       0.        0.
   0.1      0.        0.
   0.15     0.        0.01
   0.2      0.05      0.03
   0.25     0.1       0.05
   0.3      0.15      0.08
   0.35     0.2       0.11
   0.4      0.25      0.15
   0.45     0.3       0.19
   0.5      0.35      0.23
   0.55     0.4       0.28
   0.6      0.45      0.34
   0.65     0.5       0.4
   0.7      0.55      0.47
   0.75     0.6       0.54
   0.85     0.7       0.7
/

SGFN
--  sg       krg      Pcgo
   0.       0.        0.
   0.05     0.        0.
   0.1      0.03      0.
   0.15     0.06      0.
   0.2      0.1       0.
   0.25     0.15      0.
   0.3      0.2       0.
   0.35     0.25      0.
   0.4      0.3       0.
   0.45     0.36      0.
   0.5      0.42      0.
   0.55     0.5       0.
   0.850    1.000     0.
/

--    'RELPFCON.DAT'  / special for water injection into condensates
--
--  'relpfld.dat'  / file name depends on machine
```

```
-- Properties section: PVT data

NCOMPS
       6 /

EOS
 PR   /

-- Peng-Robinson correction

PRCORR

-- Standard temperature and pressure in Deg F      and PSIA

STCOND
    60.00001     14.69590 /

-- Component names

CNAMES
 CO2
 N2
 C1
 C3
 C10
 C15
 /

-- Critical temperatures Deg R

TCRIT
  5.484599855E+02  2.271599940E+02  3.430799909E+02  6.656399824E+02
  1.126799970E+03  1.303199965E+03                                  /

-- Critical pressures PSIA

PCRIT
  1.071331110E+03  4.923126500E+02  6.677816960E+02  6.186973900E+02
  3.509380920E+02  2.552677830E+02                                  /

-- Critical volumes

VCRIT
  1.505735240E+00  1.441661400E+00  1.569809080E+00  3.203692000E+00
  8.553857640E+00  1.247838034E+01                                  /

-- Critical Z-factors

ZCRIT
  2.740777974E-01  2.911514044E-01  2.847294766E-01  2.774828283E-01
  2.482516673E-01  2.277663896E-01                                  /

-- Critical volumes for LBC Viscosities

VCRITVIS
```

```
  1.505735240E+00  1.441661400E+00  1.569809080E+00  3.203692000E+00
  8.553857640E+00  1.247838034E+01                                   /

-- Critical Z-factors for LBC Viscosities

ZCRITVIS
  2.740777974E-01  2.911514044E-01  2.847294766E-01  2.774828283E-01
  2.482516673E-01  2.277663896E-01                                   /

-- Reference 3-Parameter PR   EoS Shift Coefficients

SSHIFT
 -4.273033674E-02 -1.313342386E-01 -1.442656189E-01 -7.750138148E-02
  9.246642050E-02  1.524746377E-01                                   /

-- Acentric factors

ACF
  2.250000000E-01  4.000000000E-02  1.300000000E-02  1.524000000E-01
  3.850000000E-01  5.500000119E-01                                   /

-- Molecular Weights

MW
  4.401000000E+01  2.801300000E+01  1.604300000E+01  4.409700000E+01
  1.340000000E+02  2.060000000E+02                                   /

-- Default fluid sample composition

ZMFVD
  1.000000000E+00  1.000000000E-02  1.000000000E-02  7.500000000E-01
  1.700000000E-01  4.000000000E-02  2.000000000E-02
  1.000000000E+04  1.000000000E-02  1.000000000E-02  7.500000000E-01
  1.700000000E-01  4.000000000E-02  2.000000000E-02                 /

-- Boiling point temperatures Deg R

TBOIL
  3.504599852E+02  1.393199991E+02  2.010599892E+02  4.159800000E+02
  7.901999791E+02  9.701999743E+02                                   /

-- Reference temperatures Deg R

TREF
  5.273999860E+02  1.405799935E+02  2.010599892E+02  4.157999890E+02
  5.201999862E+02  5.201999862E+02                                   /

-- Reference densities LB/FT3

DREF
  4.850653269E+01  5.019208788E+01  2.653188725E+01  3.633307854E+01
  4.888110051E+01  5.225221089E+01                                   /

-- Parachors (Dynes/cm)
```

```
PARACHOR
  7.800000000E+01  4.100000000E+01  7.700000000E+01  1.503000031E+02
  4.048999939E+02  5.505999756E+02                                  /

-- Binary Interaction Coefficients

BIC
  -.01200000
  0.10000000  0.10000000
  0.10000000  0.10000000  0.00000000
  0.10000000  0.10000000  0.04162000  0.01000000
  0.10000000  0.10000000  0.04918000  0.01000000  0.00000000
/

-- Units are: FIELD


RTEMP
   180.00000 /


-- Compositional run only water density required
DENSITY
--  lb/ft^3 ---- (surface conditions)
1*  64.0    1* /


-- Rock and water properties

ROCK
-- ref pres  compressibility (1/psi)
     3000.0    0.000004  /

PVTW
--     Pref          Bw            Cw            Vw           Cvw
--  PSIA          RB/STB        1/PSI         CPOISE        1/PSI
    3000.00000       1.00528   3.27915E-06       0.55730   5.89998E-06
/


SOLUTION ==============================================================

-- set reservior initial conditions
EQUIL
-- datum pressure   depth  Pc@ depth  Pc@ init init init  comp
-- depth at datum    woc   woc  goc   goc type type accur case
   6100    4700      8000   0   8000   0  1*    1*   1*    1   / class problem

-- set field separator conditions
FIELDSEP
--stage  temp  press
--       deg F psia
    1    100.  815.  /
    2     70.  500.  /
    3     60.  14.7  /
```

```
/
-- set variables to be printed in the .PRT file
RPTSOL
PRES  SOIL  SGAS XMF YMF /

-- set variable to be put into .X00  files
OUTSOL
PRES SOIL SGAS SWAT XMF YMF /

SUMMARY  ============================================================

-- set summary variable to be stored to be available for line plots

FOPT
FGOR
FGPT
FOPR
FGIR
FGIT
FPR
-- FIOP is field oil in place, oil recovery efficiency is determined
-- by looking up the initial FOIP after the first small time step
-- in the .RSM file and subtracting the final FOIP (last FOIP value
-- in the .RSM file) and then dividing the difference by the inital FOIP.
FOIP

WGIR
 IN
/

WGPR
 P1
 P2
/

WOPR
 P1
 P2
/

WBHP
 P1
 P2
/

WYMF
 P1  2  /
 P2  2  /
 P1  3  /
 P2  3  /
 P1  1  /
 P2  1  /
 P1   4  /
 P2   4  /
/
```

```
RPTONLY
-- create a .RSM file of summary results
RUNSUM

SCHEDULE ==============================================================

--Define injection and production wells

WELSPECS
--well group   i  j  bhp    Phase
--name name          depth
  IN   Field   1  1  1*     GAS /
  P1   Field  10  1  1*     OIL /
  P2   Field  20  1  1*     OIL /

/

COMPDAT
--name     i  j k1 k2 status  sat_table Con_fact w-diam
IN         1  1  1  1    1*      1*       1*      .6      /
P1        10  1  4  5    1*      1*       1*      .6      /
P2        20  1  3  5    1*      1*       1*      .6      /
/

-- set injectior well stream mole fractions
WELLSTRE
--       CO2  N2   C1   C3   C10  C15
CO2      1.0  0.0  0.0  0.0  0.0  0.0  /
N2       0.0  1.0  0.0  0.0  0.0  0.0  /
SOLVENT  0.0  0.0  .60  .40  0.0  0.0  /
C1       0.0  0.0  1.0  0.0  0.0  0.0  /
/

--
-- set injection well specifications
WELLINJE
--name  inj      name   cntl oil  water gas  bhp  thp   rv   wg   re-in
--well  fluid           mode rate rate  rate           rate rate  frac
    IN  STREAM    C1     GAS   1*   1*   4500 6000  1*   1*    1*    1*  /
/


-- set production well specifications
WCONPROD
--name Status cntl oil  water  gas   liq  resv  bhp
--well       mode rate  rate  rate  rate  rate
   P1   OPEN  BHP   1*    1*   4500   1*   1*  300. /
   P2   OPEN  BHP   1*    1*   4500   1*   1*  300. /
/




--Specify solution maps of pressure and saturations
```

```
RPTSCHED
PRESSURE SGAS   /

RPTRST
BASIC=2 /

--Initial step of 0.1 days

TSCRIT
0.1  0.1 50.         /


-- run for 20 years max
TSTEP
 0.1 365.15  19*365.25  /

-----------------------------------------------
OPTIMIZE
-----------------------------------------------
-- output separate summary files for each iteration
RPTOPT
  SEPARATE /
-- optimize, say
-- Income = FOPT*80($/stb) (discount factor=0.0)+ FGIT*4 - FGIT*6($/Mscf cost for injecting gas)
OPTFUNC
  FOPT  FIELD 80.0  0.0  /
  FGPT  FIELD 4  0.0  /
  FGIT  FIELD -6  0.0  /
/
-- Max_outer_iter   Max_runs
OPTDIMS
  40 200 /
-- Change gas injection rate for the optimization
OPTPARS
'WGIR' 'IN'  0  10000 /
/

-- re-set the convergence criteria for the objective function
OPTTUNE
3* 1e-4 1e-4 /

--No constraints in theis case
--OPTCONS
--'WWCT' 'P' '<' 0.99  /
--/

END
```